PEROXIDASIN IS A NOVEL TARGET OF NRF2 AND INFLUENCES EPITHELIAL–TO–MESENCHYMAL TRANSITION DURING OXIDATIVE STRESS

Kerry Leigh Hanmer

Supervisor: Dr D. Mavri-Damelin

A Thesis submitted to the Faculty of Science, University of the Witwatersrand, in fulfilment of the requirements for the degree of Doctor of Philosophy

Johannesburg, 2018

Declaration

I, **Kerry Leigh Hanmer (459343)**, am a student registered for the degree of Doctor of Philosophy in the academic year 2018.

I hereby declare the following:

I am aware that plagiarism (the use of someone else's work without their permission and/or without acknowledging the original source) is wrong.

I confirm that the work submitted for assessment for the above degree is my own unaided work except where explicitly indicated otherwise and acknowledged.

I have not submitted this work before for any other degree or examination at this or any other University.

The information used in the thesis has not been obtained by me while employed by, or working under the aegis of, any person or organisation other than the University.

I have followed the required conventions in referencing the thoughts and ideas of others.

I understand that the University of the Witwatersrand may take disciplinary action against me if there is a belief that this is not my own unaided work or that I have failed to acknowledge the source of the ideas or words in my writing.

Signature 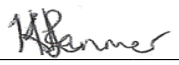 17/08/2018

To my Husband

And my Family

Abstract

Peroxidasin (PXDN) is a member of the haem-peroxidase protein family that contains a conserved peroxidase domain and additional extracellular matrix (ECM) protein binding domains. The functions of PXDN are still being identified although it has been shown to i) oxidise molecules by utilising hydrogen peroxide (H_2O_2), ii) facilitate formation of dityrosine cross-links and iii) catalyse sulfilimine bond formation within the basement membrane. PXDN expression is altered in various diseases such as cancer and therefore it is important to determine the regulators and functions of PXDN so as to identify new therapeutic targets.

Since PXDN utilises H_2O_2, and previous studies have shown PXDN expression changes in response to H_2O_2, we hypothesised that the nuclear factor erythroid 2-related factor 2 (Nrf2) transcription factor is involved in *PXDN* regulation. Western blot analyses and immunofluorescence microscopy confirmed an increase in Nrf2 and PXDN expression during oxidative stress and upon treatment with Nrf2-specific inducers. Chromatin immunoprecipitation confirmed binding of Nrf2 to the *PXDN* promoter and luciferase assays indicated that Nrf2 binding to the *PXDN* promoter increases luciferase reporter gene expression. Mutagenesis of the potential Nrf2 binding site within the *PXDN* promoter significantly decreased gene expression thus confirming that Nrf2 regulates *PXDN*.

A role for PXDN in cancer was then investigated and it was hypothesised that PXDN is potentially involved in epithelial-to-mesenchymal transition (EMT) during oxidative stress. Knockdown of PXDN expression (siRNA-mediated) was quantified by ELISA and preliminary assays were performed on wild type HeLa and SiHa cervical carcinoma cells in comparison to knockdown cells. PXDN knockdown in both cell lines resulted in decreased cell attachment. In HeLa cells, oxidative stress resulted in increased migration but PXDN knockdown abolished this effect. Oxidative stress in HeLa cells decreased invasion with PXDN knockdown resulting in a further decrease. PXDN knockdown in SiHa cells decreased cell migration and SiHa cells under oxidative stress exhibited increased invasion, which was reversed by PXDN knockdown. Reduced PXDN expression decreased the size and formation of 3D spheroids in both cell lines.

In summary, Nrf2 binds the sequence, TGAATCTGGC, within the *PXDN* promoter and increases PXDN expression. Our preliminary findings also implicate PXDN in redox related EMT since PXDN knockdown caused significant alterations to key EMT features.

Research Outputs

Original Publications:

Hanmer, K.L. and Mavri-Damelin, D. (2018) Peroxidasin is a novel target of the redox-sensitive transcription factor Nrf2. *Gene*, **674**, 104–114

National Conferences:

Poster presentation: McGowan, K.L. and Mavri-Damelin, D. Investigating Nrf2 as a candidate transcription factor in the regulation of *peroxidasin* gene expression. 16th Biennial Congress of the Southern African Society for Human Genetics (SASHG), Centurion, 2015.

Poster presentation: McGowan, K.L. and Mavri-Damelin, D. Investigating Nrf2 as a candidate transcription factor in the regulation of *peroxidasin* gene expression. Young Researchers Forum, University of Pretoria, 2015.

Internal Conferences:

Second prize poster presentation: McGowan, K.L. and Mavri-Damelin, D. Identifying the gene regulatory factors of peroxidasin. University of the Witwatersrand Molecular Biosciences Research Thrust (MBRT) Annual Research Day, Johannesburg, 2014.

Poster presentation: McGowan, K.L., Moleya, B., Mavri-Damelin, D. and Nikitina, N. Identifying the gene expression patterns of peroxidasin and peroxidasin-like during embryonic development using the chick model organism. University of the Witwatersrand 6th Cross-Faculty Graduate Symposium, Johannesburg, 2014.

Poster presentation: Hanmer, K.L., Sitole, B.N. and Mavri-Damelin, D. Peroxidasin is involved in mediating cell attachment, migration and invasion in cervical carcinoma cells under oxidative stress. University of the Witwatersrand Molecular Biosciences Research Thrust (MBRT) Annual Research Day, Johannesburg, 2017.

Oral presentation: Hanmer, K.L. and Mavri-Damelin, D. Investigating Nrf2 as a candidate transcription factor in the regulation of *peroxidasin* gene expression. University of the Witwatersrand Life Sciences Imaging Facility Users Meeting, Johannesburg, 2017.

Acknowledgements

I would first like to acknowledge and thank my supervisor, Dr. Demetra Mavri-Damelin, as this project was her idea and design. I would like to thank you for helping me to become the researcher I am today. I have learnt many, many, many skills from this project and although it has been one of the most challenging stages of life, I am so glad that I joined the lab back in 2013. Not only have I been exposed to so many techniques but I also gained a wonderful mentor and friend. Thank you for all of your guidance throughout these years.

Thank you to the many people who have helped me to achieve my goal. To Dr. Leonard Damelin, thank you for assisting with a few of my experiments by providing me with sound advice and encouragement and for kindly offering me a cup of tea when experiments did not work! Thank you to Prof. Robin Veale for allowing me to access the tissue culture facilities and to Ms. Sabeeha Mahomed for providing assistance with tissue culture over the years. Thank you to Dr. Clement Penny, Ms. Pamela Sharp and Dr. Aurelie Deroubaix for so much assistance with the Carl Zeiss LSM 780 confocal microscope at the Life Sciences Imaging Facility at the University of the Witwatersrand Medical School. I would also like to acknowledge the Microscopy and Microanalysis Unit at the University of the Witwatersrand for granting me access to and providing assistance with the Olympus BX63 microscope.

I would like to thank all of my wonderful colleagues from the Functional Genetics Research Laboratory, who have become very close and precious friends, for their support and advice throughout the years. Nonie Sitole (my PXDN partner), Rupal Jivan, Charissa Mynhardt and Sabeeha Mahomed, thank you for all of the laughs and wonderful memories that you have given me.

I would like to acknowledge the National Research Foundation (NRF) for funding me throughout my PhD degree by providing me with the PhD Innovations scholarship. I would also like to thank the University of the Witwatersrand for funding me through the Postgraduate Merit Award. I sincerely appreciate the generous financial support.

I especially thank my family, Kevin, Carol and Lauren McGowan, for their love and support over the years. I also need to acknowledge my extended family: Ian, Victoria and Sharon Pettigrew; Edward and Doreen McGowan; Thomas, Julienne and Jenna Hanmer; Kevin Gamble and Samantha Gladysek. Not only have you all encouraged me so much but you have also been so very understanding. My degree was very challenging and oftentimes I would not

get to spend as much time around you all as I would have liked. Luckily, you all stuck by my side and for that I am eternally grateful.

Lastly, I have to thank my husband, Jeffrey Hanmer. A thank you from the bottom of my heart is simply not enough. Your love, support and comforting words have helped me through the most difficult times during my degree. You have always provided me with encouraging words. I would not have had the courage to keep working so hard without you. Thank you for never giving up on me and having such an undying faith in my capabilities even when I doubted myself. I love you, always, all ways.

Contents

List of Figures

List of Tables

List of Abbreviations

A	-	Adenine
Ang II	-	Angiotensin II
APC	-	Allophycocyanin
APS	-	Ammonium persulfate
ARE	-	Antioxidant response elements
BM	-	Basement membrane
bp	-	Base pairs
BSA	-	Bovine serum albumin
cDNA	-	Complementary DNA
ChIP	-	Chromatin immunoprecipitation
C	-	Cytosine
DAPI	-	4', 6-Diamidino-2-phenylindole dihydrochloride
dH_2O	-	Distilled water
DIC	-	Differential interference contrast
DMEM	-	Dulbecco’s Modified Eagle’s Medium
DNA	-	Deoxyribonucleic acid
ECM	-	Extracellular matrix
EDTA	-	Ethylenediaminetetraacetic acid
ELISA	-	Enzyme linked immunosorbent assay
em	-	Emission
EMT	-	Epithelial-to-mesenchymal transition
eNOS	-	Endothelial nitric oxide synthase

ERK	-	Extracellular regulated kinase
ex	-	Excitation
FBS	-	Foetal bovine serum
FITC	-	Fluorescein isothiocyanate
GAPDH	-	Glyceraldehyde 3-phosphate dehydrogenase
G	-	Guanine
H_2O_2	-	Hydrogen peroxide
HCl	-	Hydrochloric acid
HOBr	-	Hypobromous acid
HOCl	-	Hypochlorous acid
HEK293	-	Human embryonic kidney cells 293
HO-1	-	Haem oxygenase-1
IF	-	Immunofluorescence
IP	-	Immunoprecipitation
IR	-	Ischemia reperfusion
kDa	-	Kilodaltons
Keap1	-	Kelch-like ECH-associated protein 1
KO	-	Knock-out
M	-	Molecular weight marker
MAPK	-	Mitogen-activated protein kinase
MET	-	Mesenchymal-to-epithelial transition
MMPs	-	Matrix metalloproteinases
MPO	-	Myeloperoxidase

mRNA	-	Messenger RNA
MTT	-	3-(4,5-dimethylthiazol-2-yl)-2,5 diphenyltetrazolium bromide
NAC	-	*N*-acetylcysteine
Neh	-	Nrf2-ECH homology
NO	-	Nitric oxide
Nox	-	NADPH-oxidases
NQO1	-	NAD(P)H quinone oxidoreductase 1
Nrf2	-	Nuclear factor erythroid 2-related factor 2
NTC	-	No template control
ox-LDL	-	Oxidised-low density lipoprotein
PBS	-	Phosphate buffered saline
PCR	-	Polymerase chain reactions
PMSF	-	Phenylmethanesulfonyl fluoride
PXDN	-	Peroxidasin
Redox	-	Reduction-oxidation
RIPA	-	Radioimmunoprecipitation assay
RNA	-	Ribonucleic acid
ROS	-	Reactive oxygen species
RT-PCR	-	Reverse transcription PCR
RT	-	Room temperature
SD	-	Standard deviation
SDS	-	Sodium dodecyl sulphate
SDS-PAGE	-	Sodium dodecyl sulphate polyacrylamide gel electrophoresis

SFM	-	Serum-free medium
SFN	-	Sulforaphane
TAE	-	Tris acetate EDTA
tBHQ	-	*tert*-butylhydroquinone
TBS/T	-	Tris buffered saline/Tween-20
TCA	-	Trichloroacetic acid
TEMED	-	Tetramethylenediamine
TF	-	Transcription factor
TGF-β	-	Transforming growth factor-β
T	-	Thymine
UV	-	Ultraviolet

Chapter 1: Introduction

1.1. Peroxidasin

1.1.1. PXDN structure

Peroxidasin (PXDN) is a human homologue of *Drosophila* PXDN and has been classified as a member of the haem-containing peroxidase protein family, a group of oxidoreductases that utilise haem as a co-factor, as it contains a conserved peroxidase domain (Cheng *et al*., 2008; Péterfi *et al*., 2009; Ma *et al*., 2013). The *PXDN* gene is located on chromosome 2p25.3 (reverse strand) and encodes a 7.5 kb transcript that gives a 165 kilodaltons (kDa) protein (Nelson *et al*., 1994; Horikoshi *et al*., 1999; Cheng *et al*., 2011). As well as the peroxidase domain, PXDN also has an extracellular secretory signal and additional domains that allow it to interact with proteins of the extracellular matrix (ECM), which are not found in other protein members of this family (Figure 1.1) (Shi *et al*., 2011). The leucine rich repeats suggest that PXDN may be involved in protein-protein interactions while the immunoglobulin loops and von Willebrand factor C-type domains indicate PXDN involvement in cell adhesion and protein complex formation (Horikoshi *et al*., 1999; Cheng *et al*., 2008; Péterfi *et al*., 2009). The exact functions of PXDN are still relatively unclear but since PXDN has a 42% identity to myeloperoxidase (MPO), a well-known member of this protein family, initial insight into these functions were provided by those of MPO (Cheng *et al*., 2008).

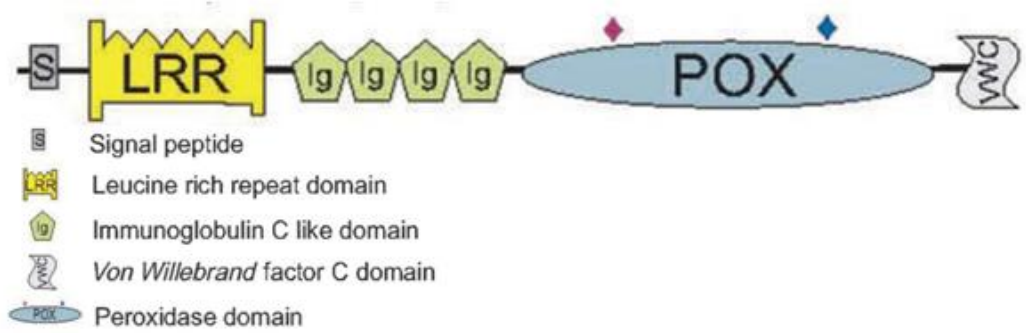

Figure 1.1: The domains of the human PXDN protein. The domains of the PXDN protein include: an extracellular secretory signal peptide, leucine rich repeats, an immunoglobulin C like domain, a conserved peroxidase domain and a von Willebrand factor C domain. All domains, except for the peroxidase domain, are unique to PXDN only, within this protein family, and indicate potential interactions with ECM proteins (Soudi *et al*., 2012).

1.1.2. Functions of PXDN

The functions of PXDN are slowly being elucidated with most being hypothesised based on the abovementioned domains. The potential functions of PXDN have further been refined by the locations in which it is found. PXDN mRNA is expressed in most regions of the body in normal tissue but protein expression seems to be restricted to the cardiovascular system where it is secreted from vascular endothelial cells, circulates in plasma and associates with other proteins of the ECM (Cheng *et al.,* 2008; Gueron *et al*., 2009; Cheng *et al.,* 2011; Ma *et al*., 2013).

The most notable function of PXDN stems from its conserved peroxidase domain which allows it to catalyse the oxidation of other molecules. PXDN utilises hydrogen peroxide (H_2O_2), produced predominantly by NADPH-oxidases (Nox) expressed in vascular smooth muscle cells, as an electron acceptor during these reactions (Cheng *et al*., 2008; Zhang *et al*., 2012). The H_2O_2 from these Nox enzymes is produced from the rapid dismutation of superoxide anions (Zhang *et al*., 2012). Since PXDN is similar to MPO, it is also potentially capable of performing similar functions. MPO is able to form hypochlorous acid (HOCl) when in the presence of H_2O_2 and chloride (Wang *et al*., 2007). Indeed, PXDN has been shown to produce hypohalous acids in the presence of H_2O_2 and halides, although the exact reasons for this, and the actual ability of PXDN to produce HOCl, are still under investigation (Bhave *et al*., 2012; Li *et al*., 2012; Jones-Paris *et al*., 2017).

MPO is known to be produced specifically in neutrophils and the HOCl that it produces is able to induce apoptosis through the p38 mitogen-activated protein kinase (MAPK) pathway (Midwinter *et al*., 2001; Cheng *et al*., 2008). Interestingly, PXDN has also been detected in cells undergoing oxidised-low density lipoprotein (ox-LDL)-induced endothelial cell apoptosis where it is indicated that HOCl produced by PXDN activates the p38 MAPK/caspase-3 pathway (Bai *et al*., 2011; Zhang *et al*, 2012). MPO also releases HOCl in a respiratory burst to destroy foreign microorganisms during an immune response and HOCl produced by PXDN has also been found to destroy *Escherichia coli* (*E.coli*) in culture (Li *et al*., 2012). PXDN is also secreted into circulating plasma and so is likely to perform similar antimicrobial functions to that of MPO during an immune response (Cheng *et al*., 2011). In contrast to the apoptotic functions of PXDN, PXDN may also be involved in promoting cell proliferation and survival. One study found that PXDN expression promoted vascular smooth muscle cell proliferation as PXDN utilised H_2O_2, supplied from Nox, to produce HOCl that

activated the extracellular regulated kinase (ERK) 1/2 pathway responsible for promoting cell proliferation (Midwinter *et al*., 2001; Blanc *et al*., 2003; Shi *et al*., 2011). The observations made in those studies, as well as the similarities between MPO and PXDN, indicate a potential role for PXDN in the regulation of cell survival within the cardiovascular system.

PXDN contains additional domains that allow it to interact with other proteins associated with the ECM and it has since been found that PXDN is able to both form and strengthen the basement membrane (BM)– a specialised ECM underlying epithelial cells (Bhave *et al*., 2012; Soudi *et al*., 2012; Fidler *et al*., 2014). This function of PXDN was discovered when the first PXDN studies established that *Drosophila* PXDN and collagen IV were both secreted from haemocytes into the ECM (Nelson *et al*., 1994). Human PXDN was then shown to consolidate the BM by producing hypohalous acid intermediates (bromide or chloride ions are mainly used to produce hypobromous acid (HOBr) and HOCl respectively) for cross-linking reactions within the collagen IV network in the BM (Bhave *et al*., 2012; McCall *et al*., 2014; Lázár *et al*., 2015; Paumann-Page *et al*., 2017). PXDN utilises these hypohalous acid intermediates to catalyse the formation of a covalent bond between a methionine sulphur and a hydroxylysine nitrogen, known as a sulfilimine bond, at the C-termini of collagen type IV protomers (Figure 1.2) (Bhave *et al*., 2012; Weiss, 2012; Fidler *et al*., 2014). PXDN is also able to strengthen the BM through its ability to catalyse the formation of dityrosine bridges– covalent bonds formed by the oxidation of tyrosine residues using H_2O_2 (Péterfi *et al*., 2009; Cheng *et al*., 2011; Weiss, 2012). In addition to the enzymatic contributions of PXDN in strengthening the BM, PXDN itself has been found to organise into fibrillar-like structures that form a network within the ECM; these networks have also been shown to colocalise with fibronectin– an abundant ECM glycoprotein (Péterfi *et al*., 2009; Cheng *et al*., 2011; Bhave *et al*., 2012).

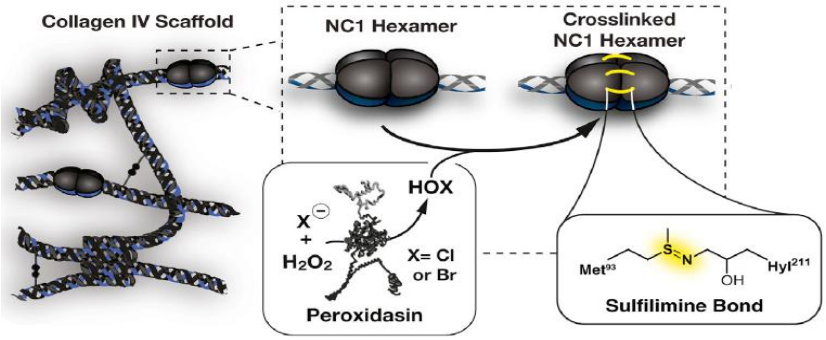

Figure 1.2: Sulfilimine bond formation within the collagen IV network. PXDN catalyses the formation of covalent sulfilimine bonds using hypohalous acid intermediates, to strengthen the basement membrane (McCall *et al*., 2014).

It is clear from its unique structure that PXDN may be involved in many different aspects of cellular functioning including: determining cell death and survival, altering cellular environments through ECM modifications and cell signalling. By examining all of these potential functions of PXDN, it is clear that an alteration in PXDN expression may have a great impact on the development of multiple diseases that arise when one or more of the above functions is altered. Therefore, it is important that PXDN expression and function be investigated not only in normal tissues but also in disease states.

1.1.3. PXDN in disease

Research into PXDN has been slowly gaining momentum over the past few years due to its potential roles in an array of cellular functions. Altered PXDN expression has already been observed in multiple diseases although its exact role in these processes remains unclear. Since PXDN is involved in reactive oxygen species (ROS) production and regulation (namely H_2O_2 and HOBr/HOCl) and has the ability to alter the ECM, PXDN would be an interesting therapeutic target for the treatment of diseases influenced by alterations in these functions such as fibrosis and cancer.

For instance, PXDN has been found to colocalise with the ECM protein fibronectin during kidney fibrosis (Péterfi *et al*., 2009). Another recent study also found that PXDN knock-out (KO) mice exhibited decreased collagen IV cross-links, accompanied by reduced stiffness in the renal tubular BM; thus implicating that over-expression of PXDN may result in enhanced BM stiffness observed during fibrosis (Bhave *et al*., 2017). PXDN expression has also been found to be upregulated in the lung tissue of patients suffering with pulmonary fibrosis (Tahmasbpour *et al*., 2016). A rat animal study also showed elevated PXDN expression during induced liver fibrosis (Liu, X. *et al*., 2017). Although elevated PXDN expression has been shown in a number of cases of fibrosis, the exact role of PXDN in fibrosis is not entirely clear. Since PXDN is involved in modifying the ECM, it seems reasonable to assume that an alteration in its regulation, that possibly results in PXDN over-expression, may result in excessive deposition of PXDN fibril networks and extensive cross-linking of ECM proteins; thus resulting in ECM hardening and the development of fibrosis (Péterfi *et al*., 2009; Shin *et al*., 2010). Further research will be required to determine the involvement of PXDN in the disease.

PXDN has also been thought to be responsible for the occurrence of myocardial ischemia reperfusion (IR) injury which occurs once oxygenated blood is restored to previously

deprived cells and results in the oxidative damage of tissue (Zhang *et al*., 2012). It is hypothesised that since PXDN is secreted into the vascular system, it may induce oxidative stress by producing excessive amounts of HOCl, a strong oxidant, thus resulting in the cellular apoptosis and inflammation that characterises IR injury (Cheng *et al*., 2011; Zhang *et al*., 2012). Therefore, it would also be worth investigating whether PXDN is a potential therapeutic target for preventing IR injury.

There have also been a few studies indicating a potential link between PXDN expression and cancer. PXDN has been found to be expressed, and is often upregulated, in breast, colon, renal, prostate, cervical and ovarian carcinomas, skin melanomas as well as in primary and metastatic brain tumours (Mitchell *et al*., 2000; Liu *et al*., 2010; Tauber *et al*., 2010; Barnett *et al*., 2011; Jayachandran *et al*., 2016; Sitole and Mavri-Damelin, 2018). A PXDN KO study found decreased invasion and attachment of choriocarcinoma cells to laminin and fibronectin-coated wells, while another recent study found that silencing PXDN expression reduced both the invasion and migration of metastatic melanoma cells (Tauber *et al*., 2010; Jayachandran *et al*., 2016). Metastatic gliomas have also been shown to exhibit slightly higher PXDN expression levels, although the role of PXDN in this case is still unclear (Liu *et al*., 2010). Another study that focussed on breast cancer found PXDN knockdown to decrease cancer cell proliferation; curiously, levels of PXDN expression varied even among basal and luminal breast cancer subtypes with PXDN knockdown affecting cellular proliferation of the subtypes by varying degrees (Young *et al*., 2015). Although PXDN expression has been shown to be altered across multiple cancer types, even among subtypes, the exact function of PXDN in cancer is still not well understood.

One major interest of our laboratory is the effect of reduction-oxidation (redox) on cancer initiation and progression. If PXDN is to be treated as a potential therapeutic target for cancer, it would be important to determine how PXDN is regulated and to determine its potential roles in cancer. Considering that PXDN is able to respond to ROS and modify the ECM, and that the apparent dysregulation of PXDN expression contributes to features of the cancer phenotype, we hypothesised that PXDN may be regulated by nuclear factor erythroid 2-related factor 2 (Nrf2), a master regulator of the redox response.

1.2. Nrf2

1.2.1. Nrf2 Activation

ROS are molecules, radicals or ions that are often by-products of metabolic redox reactions that occur within cells (Giannoni *et al*., 2012). Physiological ROS may be further classified as free oxygen radicals that have an unpaired electron in the outermost orbital of electrons (such as nitric oxide (NO)), or classified as non-radical ROS (such as H_2O_2 or HOCl) and both forms are involved in important processes such as cell signalling (Holmström and Finkel, 2014; Gill *et al*., 2016). ROS have been shown to oxidise cysteine residues of proteins that alter both protein conformation and expression, and ROS also influence molecular pathways such as those involved in proliferation and apoptosis (Holmström and Finkel, 2014). ROS levels are constantly monitored and kept under control by various proteins that can neutralise ROS. However, oxidative stress may occur when there is an imbalance between the production and clearance of ROS often resulting in the accumulation of ROS (Reuter *et al*., 2010; Gill *et al*., 2016). Oxidative stress can cause damage or mutations to DNA often resulting in cell death and/or inflammation, and the persistence of these conditions eventually leads to the onset of diseases such as fibrosis and cancer (Reuter *et al*., 2010). Persistent oxidative stress has been shown to promote fibrosis due to excessive ROS levels altering and enhancing the expression of genes that promote proliferation and ECM deposition (Morry *et al*., 2017). Oxidative stress can also initiate cancer in multiple ways: ROS can alter and mutate DNA which affects transcription factor (TF) binding sites and gene expression, ROS interfere with normal protein expression by changing protein conformation and ROS can also potentiate cell survival and proliferation pathways (Gill *et al*., 2016; Morry *et al*., 2017).

Nrf2 is a notable basic leucine zipper TF that belongs to the cap ‘n’ collar family of proteins and is known to be activated in response to oxidative stress (McMahon *et al*., 2001; Sykiotis and Bohmann, 2010). Nrf2 is found throughout the body and is normally found in an inactive state as it is sequestered within the cytosol by the Kelch-like ECH-associated protein 1 (Keap1)-E3 ubiquitin ligase complex (Figure 1.3A) (Jung *et al*., 2018). Keap1 interacts with the Neh2 domain and ubiquitously marks Nrf2 for proteasomal degradation until changes in levels of ROS, such as H_2O_2, or electrophiles induce conformational changes to Keap1 thus allowing for the release, and subsequent nuclear translocation, of Nrf2 (Figure 1.3B) (Lee and Johnson, 2004; Imhoff and Hansen, 2010; Taguchi *et al*., 2011). Keap1 has a specific redox-

sensitive protein domain, known as the intervening region, which is rich in cysteine residues (Dinkova-Kostova *et al*, 2002; Jung *et al*., 2018). During oxidative stress, the thiol groups (SH) of the cysteine residues (specifically the cysteine residues at positions 257, 273, 288 and 297) are oxidised resulting in the formation of disulphide bonds; these disulphide bonds alter the conformation of Keap1 and result in the release of Nrf2 (Dinkova-Kostova *et al*, 2002). Once inside the nucleus, Nrf2 locates and binds to specific antioxidant response elements (ARE) within the promoters of antioxidant genes (Figure 1.3C). The antioxidant genes activated by Nrf2 encode different proteins that will assist the cell in lowering the levels ROS in an attempt to promote cell survival (Kuosmanen *et al*., 2016).

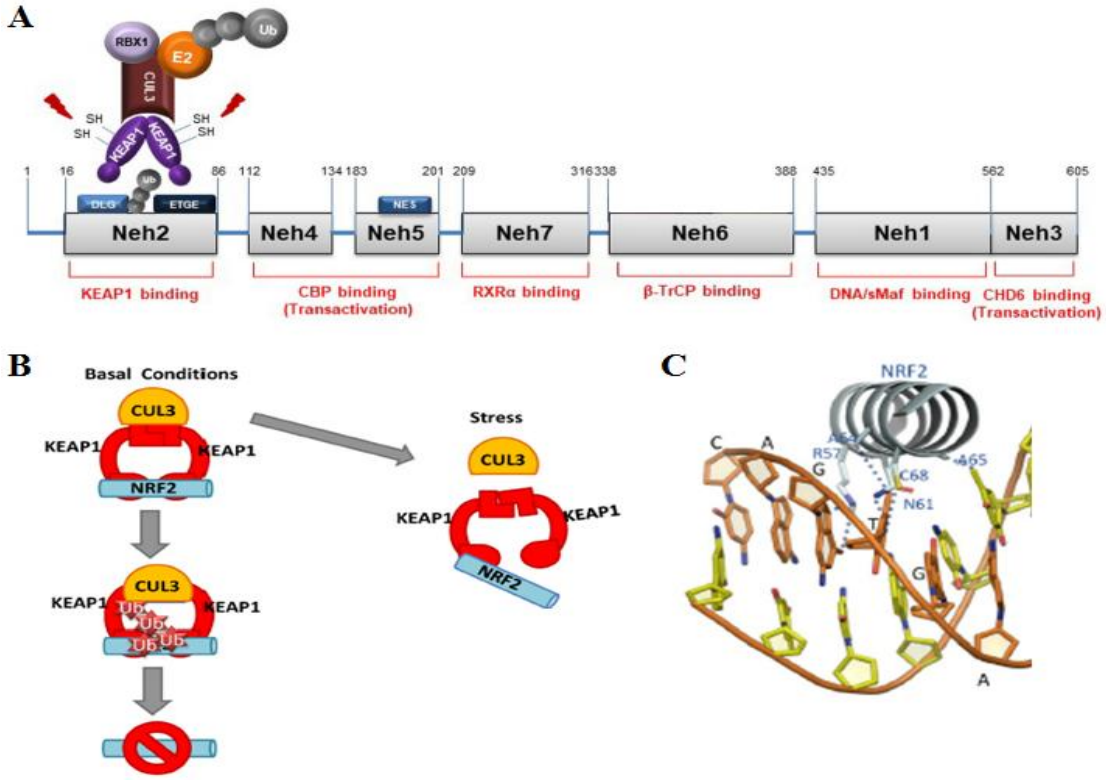

Figure 1.3: Nrf2 structure, activation and binding. A) Nrf2 has seven conserved Nrf2-ECH homology (Neh) domains: Neh1, 3, 4, and 5 facilitate Nrf2 activation and DNA binding while Neh2, 6 and 7 are responsible for Nrf2 degradation (Adapted from Jung *et al*., 2018). **B)** Nrf2 is constantly marked for ubiquitinated degradation by Keap1 until oxidative stress causes the release of Nrf2 and allows its subsequent nuclear translocation (Kuosmanen *et al*., 2016). **C)** Once in the nucleus, Nrf2 binds to antioxidant response elements in promoters of genes encoding antioxidant proteins (Kuosmanen *et al*., 2016).

1.2.2. Nrf2: functions and role in cancer

Nrf2 is expressed in most tissues and is involved in activating an antioxidant cellular response against oxidative stress that can result from ionizing radiation, microbial infections, pollutants or diet (Osburn and Kensler, 2008; Surh *et al*., 2008). When oxidative stress triggers the nuclear translocation of Nrf2, Nrf2 will bind to a specific ARE that usually follows the consensus sequence of TGAnTCnGCn, where 'n' represents either of the four DNA nucleotides: thymine (T), guanine (G), adenine (A) and cytosine (C) (Chorley *et al*., 2012; Kuosmanen *et al*., 2016). The ARE is a *cis*-acting enhancer sequence that is found within the promoter regions of genes that usually encode antioxidant enzymes– such as haem oxygenase-1 (HO-1), glutathione *S*-transferases and NAD(P)H: quinoneoxidoreductase-1 (NQO1) (Kwak *et al*., 2001; Lee and Johnson, 2004; Pi *et al*., 2008; Surh *et al*., 2008; Lin *et al*., 2011). Since excessive ROS may result in DNA damage that could lead to uncontrolled cell proliferation and an enhanced probability of cancer metastasis, it was originally thought that the genes activated by Nrf2 would only encode antioxidant enzymes (Lee and Johnson, 2004). However, it has been discovered that multiple gene families contain the Nrf2 ARE sequence including those responsible for: promoting toxin export through transporters, promoting the repair or degradation of damaged proteins, regulating the expression of other TFs and receptors, and preventing ECM degradation (Wakabayashi *et al*., 2010; Saw *et al*., 2014). A comprehensive list of genes currently known to be regulated by Nrf2 has been reviewed by Hayes and Dinkova-Kostova (2014). One of the most commonly used positive controls for Nrf2-related studies is NQO1. This enzyme is a quinone reductase that uses NADH/NADPH co-factor to catalyse the two electron reduction of quinones, which are a class of toxic intermediates that can lead to ROS formation, into less harmful hydroquinones (Lin *et al*., 2011; Cuff *et al*., 2018). The *NQO1* promoter is known to contain AREs and Nrf2 activation and binding greatly increases NQO1 expression; NQO1 is thus included as a positive control in the Nrf2 regulation studies of PXDN (Surh *et al*., 2008).

Nrf2 activation is responsible for the protection of cells against oxidative stress; however, in some human cancers, Nrf2 is constitutively activated due to mutations in either the *Keap1* or *Nrf2* genes that prevent the interaction of Keap1 with Nrf2 and ultimately the degradation of Nrf2 (Taguchi *et al*., 2011). Missense mutations have been found to occur in the *Keap1* gene in non-small-cell lung cancer and somatic mutations, that result in amino acid changes, have been found to occur in gall, lung and liver cancer (Singh *et al*., 2006; Ohta *et al*., 2008; Homma *et al*., 2009; Jeong *et al*., 2017). Keap1 expression was also found to be repressed in

renal cell carcinoma due to hypermethylation of the *Keap1* promoter (Fabrizio *et al*., 2017). These mutations/changes in expression of Keap1 affect the ability of Keap1 to bind to Nrf2 thus resulting in the constitutive nuclear translocation of Nrf2 and activation of downstream genes (Singh *et al*., 2006; Jeong *et al*., 2017). Somatic mutations of the *Nrf2* gene that affect the Neh2 Keap1 binding site, causing a disruption of Keap1 facilitated degradation of Nrf2, have also been detected in lung, head/neck cancer and squamous cell carcinomas of the skin, oesophagus and larynx (Kim *et al*., 2010; Taguchi *et al*., 2011). The constitutive activation of Nrf2, and subsequent constant expression of downstream genes, allows cancer cells to survive and be protected against certain anti-cancer drugs that induce oxidative stress in order to destroy the cancer cell; and in the case of lung squamous cell carcinoma, enhanced Nrf2 activation promotes tumour progression and metastasis (Taguchi *et al*., 2011; Jeong *et al*., 2017). However, there are also human cancer cases, such as lung adenocarcinoma and hepatocellular carcinoma, where Nrf2 expression is suppressed, and one study that involved silencing Nrf2 in cancerous cell lines found enhanced ROS production accompanied by increased motility and cell survival (Rachakonda *et al*., 2010; Taguchi and Yamamoto, 2017).

Nrf2 is an important TF that is essential for the regulation of ROS in normal cells and mutations affecting Nrf2 degradation influence the development and progression of many cancer types. The exact mechanisms of how Nrf2 may potentiate a metastatic phenotype or influence tumour cells are still being identified and since PXDN is able to utilise H_2O_2 and also has altered expression in cancer, it would be interesting to determine whether there is a link between the two proteins as identifying a connection between the two proteins could potentially provide new cancer therapy targets.

1.3. EMT

1.3.1. Types of EMT

Epithelial-to-mesenchymal transition (EMT) is defined as the process whereby epithelial cells alter their cell-cell and cell-ECM interactions in order to free themselves from surrounding tissue and take on more motile properties (Giannoni *et al*., 2012; Mitra *et al*., 2015). Cells undergoing the process of EMT often exhibit alterations in behaviour and visible morphology, such as having decreased proliferation, increased migration and invasion as well as becoming elongated and tapered in appearance (Jordan *et al*., 2011; Nieto *et al*., 2016; Jiang *et al*., 2017). However, it is slowly becoming apparent that not all of these above changes occur during EMT and EMT is actually a far more complicated process than what was originally perceived (Huang *et al*., 2012; Nieto *et al*., 2016). There is also the added fact that transitioned cells have the ability to revert back to the epithelial phenotype in a process known as mesenchymal-to-epithelial transition (MET) (Thiery *et al*., 2009). The ability of cells to alter their surroundings introduces the potential for cells to migrate and survive in an abnormal manner as observed in diseases such as fibrosis and cancer (Kalluri and Weinberg, 2009). However, there are multiple instances where EMT is essential for normal physiological processes; it is therefore necessary to categorise the different types of EMT based on occurrence and purpose. There are three different types of EMT: Type I, Type II and Type III (Kalluri and Weinberg, 2009; Giannoni *et al*., 2012).

Type I EMT is an important process that is activated during early development and gastrulation and is not able to result in fibrosis or promote the invasive abilities of metastatic tumour cells (Thiery *et al*., 2009; Jordan *et al*., 2011). Cells undergo Type I EMT during: embryo implantation into the uterus, placenta formation and in early organ formation and also undergo the process of MET since early embryonic cells need to become specific and differentiated cell types (Kalluri and Weinberg, 2009).

Type II EMT specifically refers to the process required during wound healing and tissue regeneration. Cells need to be able to move to sites of injury in order to repair damage that results from inflammation or physical trauma (Yan, C. *et al*., 2014). This type of EMT has the potential to cause fibrosis since the deposition of cells may become uncontrolled and excessive thus resulting in the tissue hardening associated with the condition (Shin *et al*., 2010). It has also been established that Type II EMT is influenced by the level of

inflammation and constant inflammation has been shown to induce fibrosis of organs such as the kidney and lung (Willis and Borok, 2007; Kalluri and Weinberg, 2009; Yan, C. *et al*., 2014).

The last form of EMT is a category named Type III. Type III EMT occurs when cells with altered genetic capacities, most commonly cancer cells, alter their interactions with neighbouring cells and the ECM in order to allow migration and invasion into surrounding tissues (Nieto *et al*., 2016). Cancerous tumour cells are able to migrate around the body through the blood stream and produce secondary tumours at other locations; this phenomenon, known as cancer metastasis, is a result of Type III EMT. Type III EMT is often activated by extracellular signals which then alter the protein expression of the cancerous cell allowing it to move (Radisky, 2005). A well known trigger for Type III EMT is the transforming growth factor beta (TGF-β) family of growth factors and multiple studies have shown that TGF-β1 treatment activates TFs involved in EMT, such as Snai1, that alter the expression of genes and proteins in order to gain the mesenchymal phenotype (Peinado *et al*., 2003; Zavadil and Böttinger, 2005). Snai1 is a zinc finger TF that is commonly activated during EMT as it binds to a multitude of gene promoters and alters the expression of proteins involved in maintaining cell-cell and cell-ECM interactions (Nieto, 2002). One such Snai1-binding promoter is that of E-cadherin– an important protein that is involved in maintaining cell-cell adherens junctions (Zavadil and Böttinger, 2005). Snai1 has been shown to bind to the *E-cadherin* promoter and downregulate its expression in multiple cancer types and this decrease in E-cadherin expression has become one of the apparent indicators of Type III EMT (Cano *et al*., 2000; Jordan *et al*., 2011).

Although all three types of EMT occur at different stages and serve various purposes, it is established that all forms of EMT are activated by a variety of different proteins and signalling molecules/factors (Nieto *et al*., 2016). Many of the triggers, genes and regulatory proteins involved in EMT are still being investigated; however, it is becoming increasingly apparent that ROS have a major influence on both the initiation and progression of EMT, especially when it comes to disease (Mori *et al*., 2004).

1.3.2. Influence of ROS on EMT

As mentioned, ROS are molecules that have recently been found to be prominently involved in many cellular processes such as cell signalling (Holmström and Finkel, 2014; Gill *et al*.,

2016). Within normal physiological environments, the levels of ROS are low and are usually carefully controlled; irregularities in ROS levels, especially in the instance of unusually high levels of ROS or oxidative stress, may contribute to the initiation of many diseases (Reuter *et al*., 2010). ROS have the ability to alter protein function either directly, such as by altering the cysteine residues of enzymes, or indirectly by altering the activation of TFs and therefore controlling downstream gene expression; ROS can therefore influence a wide variety of proteins that may be involved in cell fate determination or cell-cell and cell-ECM interactions (Cannito *et al*., 2010). For example, ROS have been shown to alter proteins expressed within the ECM, such as to enhance the production of collagen IV, as well as alter the conformation and functioning of various integrins which are important cell adhesion molecules (Eble and de Rezende, 2014). Additionally, in order for EMT to occur, alterations to TF activation is required which is also influenced by ROS (Peinado *et al*., 2003; Radisky, 2005). Due to the involvement of ROS in all forms of cellular functioning, ROS are able to influence the processes that take place during EMT (Gill *et al*., 2016). The mechanisms of how ROS influences EMT are still being investigated and current research is mostly focused on the effects of ROS on Type II and III EMT since these types are responsible for the pathogenesis of diseases such as fibrosis and metastatic cancer respectively (Kalluri and Weinberg, 2009). For the purpose of this thesis, the effects of ROS on Type III EMT will be the main focus of discussion.

The influence of ROS on Type III EMT is complex; this is because there are multiple cellular alterations that occur in order for cancerous cells to gain the ability to migrate and metastasise (Mori *et al*., 2004; Cannito *et al*., 2010). What has also become apparent is that cancerous cells can develop the ability to carefully control the level of ROS experienced by the cells by altering TF and protein expression (Giannoni *et al*., 2012). In normal cellular environments, oxidative stress can result in extensive DNA damage that usually results in cell death or apoptosis (Reuter *et al*., 2010; Gill *et al*., 2016). Cancerous cells develop DNA mutations, often as a result of excessive ROS, that lead to an upregulation of antioxidant proteins usually through the activation of TFs such as Nrf2, which prevents cell death caused by oxidative stress (Taguchi and Yamamoto, 2017; Jung *et al*., 2018). As mentioned, mutations have been found in both the *Keap1* and *Nrf2* genes in multiple cancer types, all of which result in the over-expression and nuclear accumulation of Nrf2 (Jung *et al*., 2018). Due to genetic mutations, cancerous cells are able to manage oxidative stress thus allowing cells to survive and promote tumorigenesis.

Cancer cells are able to modify genes and protein expression in order to survive oxidative stress and promote the initiation/growth of tumours. An instance where cancerous cells undergoing Type III EMT need protection against oxidative stress is when the cells initially detach from the ECM (Giannoni *et al*., 2012; Gill *et al*., 2016). When normal cells detach from the ECM they will undergo anoikis, which is a form of apoptosis that occurs when cells are no longer correctly attached to substrate/ECM (Paoli *et al*., 2013). The initiation of anoikis produces excessive levels of ROS and in order to prevent inevitable cell death, cancerous cells may upregulate: oncogene expression, TFs such as Nrf2, and antioxidant detoxification proteins (Gill *et al*., 2016). ROS may thus promote Type III EMT initiation by eliciting strong antioxidant responses in transitioning cancer cells (Paoli *et al*., 2013; Poillet-Perez *et al*., 2015). Studies have observed increased ROS in many cancer types, such as cervical and gastric cancer, and it was hypothesised that treatment with antioxidants, such as selenium or vitamin E, would help to destroy or prevent cancer cells as theoretically, decreasing ROS would decrease the instance of DNA mutations (Gill *et al*., 2016; Milkovic *et al*., 2017). Instead, clinical trials established that additional treatment/supplements with antioxidants either had no beneficial effect with successfully preventing cancer, as observed with men receiving selenium or vitamin E to prevent prostate cancer, or as in the case of non-small cell lung cancer, actually promoted secondary tumour formation in patients receiving selenium (Lippman *et al*., 2009; Karp *et al*., 2013). The failure of the clinical trials involving prevention/treatment of cancer with antioxidants was most likely due to the fact that cancerous cells already have increased antioxidant protein expression, and treatment with additional antioxidants only helped the cells to survive and manage the oxidative stress (Gill *et al*., 2016).

So far, studies have clarified that ROS promote Type III EMT initiation; however, emerging research has also found that ROS also influence the progression of Type III EMT at various stages (Giannoni *et al*., 2012; Gill *et al*., 2016). One study involving human melanoma mouse xenograft models highlighted that oxidative stress restricted the establishment of secondary tumours; however, treatment with the antioxidant, *N*-acetylcysteine (NAC), increased the number of invading circulating melanoma cells and therefore, metastatic occurrence (Piskounova *et al*., 2015). Another study revealed that treatment with the antidiabetic and antioxidant drugs, saxagliptin and sitagliptin, specifically increased Nrf2 activation and promoted metastasis in xenograft mouse models, and elevated Nrf2 expression correlated with increased metastasis in human liver cancer samples (Wang *et al*., 2016). Since additional

antioxidant treatment and enhanced Nrf2 activation promoted cancer metastasis, it would seem that uncontrollable levels of oxidative stress prevent Type III EMT progression (Gill *et al*., 2016). However, one study found that mouse melanoma tumour cells had increased metastatic potential when cancer cell mitochondria, organelles that produce ROS during aerobic cellular respiration, elevated ROS production (Porporato *et al*., 2014). In another study, Lewis lung carcinoma was used to develop two metastatic tumour types in mice and the mice that had enhanced ROS production, from cancer cells containing mutated mitochondria, displayed higher incidences of cancer metastasis; this metastatic potential was reduced in mice treated with NAC (Ishikawa *et al*., 2008). Indeed, when Nrf2-deficient mice were implanted with Lewis lung carcinoma, the Nrf2 deficiency resulted in mice experiencing increased pulmonary metastasis and elevated ROS levels compared to wild type mice (Satoh *et al*., 2010). These findings suggest that elevated ROS is actually necessary to promote the end stages of EMT progression and metastasis in certain cancer types and treatment with antioxidants may prevent cancer progression.

What can be deduced from the above is that the involvement of ROS in Type III EMT is complex and still not well understood. ROS have the ability to influence each of the many stages of EMT from initiation to progression and even the degree of ROS influence varies with cancer type (Piskounova *et al*., 2015; Gill *et al*., 2016). Understanding the influence of ROS on Type III EMT may help to provide therapeutic options for treating cancer metastasis and since PXDN is involved with H_2O_2 and may also be involved during various stages of Type III EMT due to the involvement of PXDN with ECM modifications, examining the role of PXDN in this process may provide insight into potentially utilizing PXDN expression as a therapeutic target.

Due to the involvement of ROS in currently known PXDN functions, we hypothesised that the master redox-response TF, Nrf2, regulates PXDN expression. We also hypothesised that PXDN is involved in influencing EMT in cancer cells due to the interaction of PXDN with the ECM and that this involvement could be altered depending on the oxidative state of the cell environment.

1.4. Aims and Objectives

Aim 1: To investigate Nrf2 as a candidate TF in the regulation of *PXDN* gene expression.

Objectives:

1. Establish PXDN mRNA expression in human embryonic kidney cells 293 (HEK293) and HeLa cervical carcinoma cell lines using RT-PCR.
2. Establish PXDN and Nrf2 protein expression in cells, with or without the treatment of H_2O_2, using SDS-PAGE and western blot analysis.
3. Observe Nrf2 nuclear translocation and PXDN expression levels in cells experiencing oxidative stress, after treatment with H_2O_2, using Immunofluorescence (IF) microscopy.
4. Establish PXDN and Nrf2 protein expression in cells, with or without the treatment of Nrf2 inducers, SFN and tBHQ, using SDS-PAGE and western blot analysis.
5. Observe Nrf2 nuclear translocation and PXDN expression levels upon treatment with Nrf2 inducers using IF.
6. Determine whether Nrf2 interacts with the *PXDN* promoter using Chromatin Immunoprecipitation (ChIP).
7. Quantify the contribution of Nrf2 to *PXDN* gene expression regulation using luciferase reporter assays on the *PXDN* promoter.

Aim 2: To investigate the role of PXDN in EMT during oxidative stress in HeLa and SiHa cervical carcinoma cells.

Objectives:

1. Quantify PXDN expression upon knockdown of PXDN using siRNA by ELISA.
2. Observe changes to cell morphology upon silencing of PXDN using differential interference contrast (DIC) microscopy.
3. Observe pattern of PXDN, Snai1 and E-cadherin expression upon oxidative stress with PXDN knockdown using IF microscopy.
4. Determine the role of PXDN in cellular proliferation through MTT cell proliferation assays.
5. Investigate the role of PXDN in cell attachment using cell adhesion assays.
6. Investigate PXDN in cell migration by performing scratch assays.
7. Determine the contribution of PXDN in cellular invasion through invasion assays.
8. Identify the involvement of PXDN in 3D spheroid formation using soft agar colony formation assays.

Chapter 2: Nrf2 is involved in the regulation of *PXDN* gene expression

2.1. Introduction

2.1.1. Nrf2: the master regulator of redox response

The Nrf2 TF is involved in eliciting an antioxidant response in cells that are under oxidative stress that may occur from the accumulation of ROS such as H_2O_2 or HOCl (McMahon *et al*., 2001). In regular circumstances, Nrf2 is sequestered within the cytosol and bound to Keap1, where Keap1 ensures that Nrf2 is constantly ubiquitinated for proteasomal degradation (Lee and Johnson, 2004; Imhoff and Hansen, 2010; Taguchi *et al*., 2011). During oxidative stress, Nrf2 is de-repressed due to release from Keap1 and allowed to accumulate and translocate into the nucleus, where Nrf2 will bind to ARE within antioxidant response gene promoters (Chorley *et al*., 2012). Since Nrf2 responds to oxidative stress, we used H_2O_2 treatment in this study to induce Nrf2 nuclear translocation thus allowing us to determine the effects of Nrf2 activation on PXDN expression.

ROS cause alterations to Keap1 conformation which results in the release of Nrf2; however, xenobiotics can also promote the activation of Nrf2 and increase transcription of Nrf2 mRNA (Imhoff and Hansen, 2010; Lin *et al*., 2011). Two well-established inducers of Nrf2 nuclear translocation were used in this chapter: sulforaphane (SFN) and *tert*-butylhydroquinone (tBHQ). SFN is an isothiocyanate compound found in broccoli and other cruciferous vegetables and activates Nrf2 by interacting with the cysteine residues of Keap1 thereby forming thionoacyl adducts, mainly with the Keap1 Kelch (Nrf2 binding) domain (Hong *et al*., 2005). These adducts disrupt the interaction of Keap1 with Nrf2 thus allowing Nrf2 to avoid degradation and to accumulate within the nucleus and induce an antioxidant response (Fahey *et al*., 2002; Hong *et al*., 2005; Kensler *et al*., 2013). tBHQ belongs to the class of quinone compounds and induces Nrf2 activation by promoting phosphorylation of Nrf2 residues, such as serine-40, by protein kinase C, thus allowing Nrf2 to stabilise and dissociate from Keap1 (Huang *et al*., 2002; Nguyen *et al*., 2003; Bryan *et al*., 2013). Ubiquitinated Nrf2 is also stabilised by tBHQ thus preventing Nrf2 proteasomal degradation and allowing nuclear translocation (Li *et al*., 2005). Treatment of cells with either SFN or tBHQ will increase Nrf2 activation as well as antioxidant response proteins, thus allowing us to

determine whether the level of PXDN expression is altered by the Nrf2 inducers as this will indicate a potential link between Nrf2 and PXDN expression.

Upon activation, Nrf2 will translocate into the nucleus and bind to ARE in gene promoters. The consensus binding sequence of Nrf2 has been altered multiple times over the years since Nrf2 was continually being found to interact with sequences that differed greatly from the consensus sequence (Kuosmanen *et al*., 2016). Presently, the Nrf2 consensus sequence is taken as TGAnTCnGCn, where 'n' represents any of the four DNA nucleotides and the given nucleotides occur most frequently among experimentally determined Nrf2 binding sequences (Chorley *et al*., 2012; Kuosmanen *et al*., 2016). As previously mentioned, the *NQO1* promoter region contains ARE sequences that Nrf2 is known to bind to and Nrf2 has been shown to increase NQO1 expression in multiple studies (Surh *et al*., 2008; Lin *et al*., 2011; Cuff *et al*., 2018). The ARE within *NQO1* has even been used as a basis for the determination of the Nrf2 consensus binding sequence (Chorley *et al*., 2012). NQO1 expression has also been shown to increase upon treatment with the Nrf2 specific inducers SFN and tBHQ (Lee *et al*., 2001; Wu *et al*., 2016). For these reasons, NQO1 was used as the positive control in all experiments of Chapter 2; any alterations to PXDN expression upon Nrf2 induction together with any potential Nrf2 binding to the *PXDN* promoter can be validated if NQO1 responds to Nrf2 as expected.

Nrf2 is regarded as a master regulator due to its ability to recognise and bind to multiple ARE sequences that may contain many variations to that regarded as the Nrf2 consensus sequence. Nrf2 is also responsible for driving a strong cell response against oxidative stress, which helps to protect cells from oxidative damage, and has been shown to activate a variety of proteins ranging from antioxidant enzymes to proteins that prevent ECM degradation, to aid in the antioxidant response (Wakabayashi *et al*., 2010; Saw *et al*., 2014). For example, Nrf2 activates HO-1 expression during oxidative stress; HO-1 catalyses the degradation of harmful haem, produces antioxidants (such as biliverdin) and generates other molecular products that regulate multiple processes such as proliferation and fibrosis (Loboda *et al*., 2016). However, as already mentioned, Nrf2 mutations that result in constitutive Nrf2 expression have been detected in multiple cancer types such gall, lung, renal and liver cancer (Singh *et al*., 2006; Ohta *et al*., 2008; Homma *et al*., 2009; Fabrizio *et al*., 2017; Jeong *et al*., 2017). The exact mechanisms, pathways and proteins involved in disease progression, through aberrant Nrf2 activation, still need to be determined and this greatly limits therapeutic potential. Since PXDN has altered expression in diseases such as cancer and is involved with ROS

production, it would be worth investigating whether there is a link between Nrf2 and PXDN as this potential interaction may be suitable to target for new therapeutic options.

2.1.2. Role of PXDN in redox-based disease progression

As already mentioned, PXDN is able to utilise H_2O_2 produced by Nox and hypohalous ions to form hypohalous acids that are used to strengthen the BM, activate various cell signalling pathways and participate in immune defence (Cheng *et al*., 2008; Zhang *et al*., 2012; McCall *et al*., 2014). PXDN expression has been shown to increase with H_2O_2 treatment in multiple cell types including: human umbilical vein endothelial cells, HEK293 cells and rat aortic smooth muscle cells and PXDN over-expression has been detected in human blood samples of individuals with hyperbaric oxygen-induced oxidative stress (Cheng *et al*., 2011; Shi *et al*., 2011; Alleva *et al*., 2012; Li *et al*., 2014). Based on the involvement of PXDN with ROS, PXDN can be classified as a redox-responsive protein.

Since PXDN seems to respond to a changing redox environment, we hypothesised that PXDN may be regulated by the master redox regulator Nrf2. This may have relevance for a variety of disease states, such as fibrosis and cancer, which could result from prolonged oxidative stress.

Excessive conversion of epithelial cells into myofibroblasts can result in tissue fibrosis due to the excessive production of components of the ECM by the myofibroblasts (Radisky, 2005; Shin *et al*., 2010). Nrf2 has been demonstrated to prevent fibrosis by preventing EMT induction caused by oxidative stress (Shin *et al*., 2010). Since PXDN utilises ROS to help stabilise and form the ECM, Nrf2 could activate PXDN under oxidative stress in order to help prevent EMT and restrict cell mobility (Bhave *et al*., 2012). PXDN over-expression has been seen as a feature of kidney fibrosis, thus over-activation of Nrf2 could cause greater deposition of PXDN and may be a feature of fibrosis in other organs (Péterfi *et al*., 2009). Indeed, aberrant activation of Nrf2 was shown to promote liver inflammation and fibrosis in mouse models and a separate study found upregulated PXDN expression in dimethylnitrosamine-induced liver fibrosis in rats; it may be worth investigating a potential interaction between these two proteins in fibrosis (Ni *et al*., 2014; Liu, X. *et al*., 2017).

In terms of cancer, a study found that Nrf2-deficient mice have increased lung metastasis, and another study on various cancer cell lines found Nrf2 knockdown enhanced cell motility (Rachakonda *et al*., 2010; Satoh *et al*., 2010). Nrf2 binds to and activates HO-1, an important

indicator of oxidative stress that has also been implicated in promoting cancer cell survival (Tauber *et al*., 2010; Pronk *et al*., 2014). HO-1 has been shown to be upregulated in cancer and has a role in cell adhesion. One study found that PXDN colocalises with HO-1 in invasive cells and HO-1 mediated adhesion is greatly reduced with PXDN knockdown (Tauber *et al*., 2010). Due to this close interaction between PXDN and HO-1, as well as Nrf2 binding the *HO-1* promoter, it would be worthwhile to investigate whether Nrf2 has a role in PXDN regulation.

Based on the fact that PXDN has both a peroxidase function and role in ECM formation and stabilisation, and that Nrf2 is involved in regulating proteins with either of these functions, the aim for this chapter was focused on identifying and establishing whether Nrf2 is involved in the regulation of PXDN expression.

2.2. Methods

2.2.1. Cell culture

HEK293 (a gift from Dr. Clement Penny) and cervical carcinoma cell lines, HeLa (Cellonex) and SiHa (ATCC), were maintained in Dulbecco's Modified Eagles Medium/Hams F12 Glutamax (Gibco), supplemented with 10% (v/v) foetal bovine serum (FBS) (Gibco) and 100 U/ml penicillin/0.1 mg/ml streptomycin, at 37 °C with 5% carbon dioxide. Cell cultures were routinely sub-cultured at 70–90% confluence at which time old medium was first aspirated from the culture dishes and cells washed twice with 1X phosphate buffered saline (PBS) (Table A1). To detach cells, 500 µl Trypsin-ethylenediaminetetraacetic acid (EDTA) (Gibco) diluted in 1 700 µl 1X PBS was added, followed by incubation at 37 °C for 2–4 min. Detached cells (300 µl) were re-suspended in 8 ml of fresh culture medium, returned to the culture dish and placed back into the 37 °C incubator. Every two days, the medium was replaced with 8 ml of fresh culture medium. For experiments that required a specific number of cells, 10 µl of detached cells was mixed with an equal volume of 0.2% (w/v) trypan blue (Table A1) then counted on a haemocytometer. Specific cell densities and tissue culture plates used varied between experiments; these details are provided when necessary. Unless otherwise stated, cells were left to settle for 24 h after seeding and were incubated after treatment and/or transfection at 37 °C for the specified time.

HEK293 and HeLa cells were used for all of the experiments in this chapter. HEK293 cells were selected for experiments since HEK293 cells have been shown to express PXDN in previous studies, and aberrant PXDN expression has been observed in the fibrotic kidney (Péterfi *et al*., 2009; Cheng *et al*., 2011; Bhave *et al*., 2012). In this chapter, HEK293 cells were used to represent a 'normal' cell type and HeLa cells were selected in order to determine PXDN expression in a cancerous cell line since PXDN expression in HeLa cells has not been thoroughly investigated. Since Nrf2 is known to bind to and activate the *NQO1* promoter, this gene was used as a positive control for all experiments presented in this chapter (Chorley *et al*., 2012).

2.2.2. Establish PXDN mRNA expression using RT-PCR

Reverse transcription polymerase chain reactions (RT-PCR) were performed on HEK293 and HeLa cells in order to establish PXDN messenger ribonucleic acid (mRNA) expression. This was accomplished by first extracting total RNA using the TRI-Reagent® protocol, followed

by complementary deoxyribonucleic acid (cDNA) synthesis and then amplification of specific regions of mRNA using polymerase chain reactions (PCR).

2.2.2.1. RNA extraction

Cells were seeded into 10 cm dishes and left to settle for 48 h. The cells were washed twice with cold 1X PBS, then 1 ml of TRI-Reagent® (Sigma-Aldrich) added to lyse the cells. A 500 µl aliquot was incubated for 5 min at RT, in order to allow phase separation of the cellular components to occur, followed by the addition of 100 µl of chloroform (Sigma-Aldrich). The sample was shaken vigorously for 15 s, left to stand at RT for 5 min, then centrifuged at 13 000 rpm at 4 °C for 15 min in order to separate the phases. The clear upper aqueous phase, that contained RNA, was transferred into a new microcentrifuge tube and 250 µl of 2-propanol (Sigma-Aldrich) was added and left to stand for 10 min at RT. The sample was centrifuged at 13 000 rpm for 10 min at 4 °C to pellet the RNA. The RNA pellet was washed with 75% (v/v) ethanol, followed by centrifugation at 13 000 rpm at 4 °C, then allowed to air-dry. RNA was re-suspended in an appropriate volume of RNase-free water and the concentration determined at 260 nm and 280 nm using a NanoDrop ND-1000 Spectrophotometer (ThermoFisher Scientific). Samples of the RNA were resolved on a 1% (w/v) agarose gel to confirm RNA quality and integrity.

2.2.2.2. Agarose gel electrophoresis

A 1% (w/v) agarose gel was prepared by mixing 0.5 g of agarose with 50 ml of 1X Tris acetate EDTA (TAE) buffer (Table A1) followed by heating to dissolve the agarose. Once cooled, 1 µl of ethidium bromide (10 mg/ml stock) was added to visualise the RNA. The liquid agarose gel was poured and allowed to solidify, then placed into a gel electrophoresis tank filled with 1X TAE buffer. RNA samples were loaded into the gel after being mixed with 6X DNA loading dye (Table A1) and the GeneRuler™ 1 kb DNA ladder was used to determine band size. The gel was resolved at a constant 100 V for 40 min and RNA visualised under ultraviolet (UV) light with the Bio-Rad Gel Doc XR system and Image Lab 6.0 software (Bio-Rad).

2.2.2.3. cDNA synthesis

Once it was clear that the RNA was of good quality, cDNA was synthesised using the RevertAid™ first strand cDNA synthesis kit (ThermoFisher Scientific) according to the manufacturer's instructions. Briefly, a template-primer mixture was first prepared in a

nuclease-free PCR tube (2 µg template RNA, 1 µl oligo $(dT)_{18}$ primer, up to 12 µl RNase free water) and then heated at 65 °C for 5 min followed by immediate cooling on ice. The reaction mixture was then prepared (12 µl template-primer mixture, 4 µl 5X reaction buffer, 1 µl RiboLock™ RNase Inhibitor (20 U/µl), 2 µl 10 mM dNTP mix, 1 µl RevertAid M-MuLV RT (200 U/µl), RNase free dH_2O up to 20 µl) and incubated at 42 °C for 1 h for cDNA synthesis, heated at 70 °C for 5 min for enzyme inactivation and then cooled on ice.

2.2.2.4. PCR

PCR was performed on prepared cDNA in order to determine whether PXDN mRNA was originally present in the cells tested. KAPA Taq ReadyMix DNA Polymerase (KAPA Biosystems) was used for the PCR (2–3 µg cDNA template, 10 µl 2X ReadyMix with Mg^{2+}, 0.5 µM each of forward and reverse primers, nuclease-free dH_2O up to 20 µl). A control PCR was first conducted using glyceraldehyde 3-phosphate dehydrogenase (GAPDH) primers ($GAPDH^{mRNA}$, Table A2) to confirm the successful synthesis of cDNA. PXDN expression primers ($PXDN^{mRNA}$, Table A2) were then tested on the cDNA from HEK293 and HeLa cells. PCR was conducted using a GeneAmp® PCR System 2700 (Applied Biosystems) according to the PCR conditions in Table A2. All PCR products were visualised on a 1% (w/v) agarose gel in 1X TAE, prepared and visualised as described previously in Chapter 2.2.2.2.

2.2.3. Western blot analysis

Western blot analysis was conducted to determine the expression levels of specific proteins. Total protein was extracted from cells and quantified using either the modified (Bramhall) or regular Bradford assay (Bramhall *et al*., 1969; Bradford, 1976). Proteins were then separated according to size using reducing sodium dodecyl sulphate-polyacrylamide gel electrophoresis (SDS-PAGE) and a broad range pre-stained protein standard used for reference (New England BioLabs). Target proteins contained in the gel were transferred onto a nitrocellulose membrane and probed for using specific antibodies. Protein bands were detected using chemiluminescence and signals captured using x-ray film for quantification.

2.2.3.1. Lysate preparation

Cells were seeded into 10 cm dishes and treated with 100 µM H_2O_2 for 3 h or 18 h (and later 5 µM SFN or 40 µM tBHQ for 24 h as determined from MTT assays). The concentration and treatment times of H_2O_2 were selected based on conditions used in previous studies in order

to investigate the influence of H_2O_2 treatment on various proteins over both a short and long term period (Tan *et al*., 2011; Zucker *et al*., 2014). Culture medium was aspirated and cells washed twice with cold 1X PBS. Cells were collected into 1 ml of 1X PBS using a cell scraper and pelleted by centrifugation at 11 000 rpm for 10 min at 4 °C. The 1X PBS was removed and cells lysed in either native lysis buffer (Table A1), for PXDN detection, or 1X radioimmunoprecipitation assay (RIPA) buffer (Table A1) for Nrf2, NQO1 (positive control) and β-actin (loading control) detection. Lysis was achieved by vortexing the samples every 5 min for 25 min while keeping samples cold on ice. Lysates were centrifuged at 12 500 rpm for 5 min at 4 °C in order to separate the soluble protein from cell debris. Total protein was quantified and stored at −70 °C.

2.2.3.2. Protein quantification

2.2.3.2.1. Bradford assay

Cells lysed with native lysis buffer had total cytoplasmic protein quantified using the Bradford assay (Bradford, 1976). A 50 mg/ml stock solution of bovine serum albumin (BSA) (HyClone Technologies) was used to prepare standard solutions ranging from 5–150 µg/ml. Cell lysates and the native lysis buffer (blank), were diluted by a factor of 1/50 or 1/200. Each solution was added to a separate well of a 96-well plate (160 µl), in triplicate, and 40 µl of 5X Bradford reagent (Table A1) was added to each well. The solutions were mixed and left to stand for 5 min. Absorbance readings were taken at 595 nm using a Multiskan GO microplate reader (ThermoFisher Scientific). A standard curve of protein concentration (µg/ml) vs. absorbance (arbitrary units) was plotted using Microsoft Office Excel 2007 and protein concentrations in cell lysates calculated using the equation derived from the standard curve.

2.2.3.2.2. Modified Bradford assay

The 1X RIPA buffer used to obtain whole cell lysate contained a higher concentration of SDS which is known to interfere with coomassie blue within the Bradford reagent; this results in inaccurate protein concentration determination (Bradford, 1976). Total protein obtained using 1X RIPA buffer was thus quantified using a modified version of the Bradford assay (Bramhall *et al*., 1969). A grade 1 Whatman™ filter paper was soaked, with gentle shaking, in the following solutions in the order presented: distilled water (dH_2O) for 20 min, 95% (v/v) ethanol for 5 min, 100% (v/v) ethanol for 5 min and 100% (v/v) acetone for 5 min. The filter

paper was then allowed to dry. A standard curve was set up using a 1 mg/ml BSA stock solution (1 µg= 1 µl) with 1 µl, 3 µl, 6 µl, 12 µl, 16 µl and 20 µl being pipetted separately onto the filter paper, along with 2 µl of each unknown sample. Protein samples were allowed to dry and the filter paper then soaked in 7.5% (v/v) trichloroacetic acid (TCA) for 45 min, with shaking, to precipitate and fix the proteins to the filter paper (Link and LaBaer, 2011). The filter paper was then briefly rinsed with a small volume of coomassie blue dye (Table A1) to remove TCA and 1X RIPA buffer from the samples, and then soaked in fresh coomassie blue dye for 1 h, with shaking, to stain the proteins. A destain solution (Table A1) was added to the filter paper for 1 h, with shaking. The filter paper was allowed to dry and then each standard and sample area was cut out and placed individually into 5 ml of elution buffer (Table A1) overnight, in the dark. Eluted samples were homogenised and 100 µl of each sample was pipetted into a well of a 96-well plate. Absorbance values were measured at 595 nm using a Multiskan GO microplate reader. A standard curve of protein concentration (µg/µl) vs. absorbance (arbitrary units) was plotted using Microsoft Office Excel 2007 and unknown protein concentrations calculated using the equation of the standard curve.

2.2.3.3. SDS-PAGE

The CVS10CBS omniPAGE mini dual vertical electrophoresis and electroblotting system (Sigma-Aldrich, EP1301) was used to perform reducing SDS-PAGE. Either a 10% separating gel with 5% stacking gel or an 8% separating gel with 4% stacking gel (for PXDN detection) were prepared according to Table 2.1. Protein samples were prepared in a 3:1 ratio of protein to 4X protein loading buffer (Table A1) and boiled in water for 5 min to denature the proteins. Samples were loaded and the tank filled with SDS-PAGE running buffer (Table A1). The gel was electrophoresed at a constant voltage of 180 V until the dye front had just run off of the gel.

Table 2.1: SDS-PAGE polyacrylamide gel recipes.

	Separating gel (10 ml)		Stacking gel (5 ml)	
Reagent	**8%**	**10%**	**4%**	**5%**
dH_2O	4.6 ml	4.0 ml	3.5 ml	3.4 ml
29:1 Acrylamide:Bisacrylamide	2.7 ml	3.3 ml	690 µl	830 µl
Tris-HCl	2.5 ml*	2.5 ml*	630 µl**	630 µl**
10% (v/v) SDS	100 µl	100 µl	50 µl	50 µl
10% (v/v) Ammonium persulfate (APS)	100 µl	100 µl	50 µl	50 µl
Tetramethylenediamine (TEMED)	6 µl	6 µl	4 µl	4 µl

Reagents were added in the order shown with 10% (v/v) APS and TEMED added just before casting.
* 1.5 M Tris-HCl, pH 8.8
** 1 M Tris-HCl, pH 6.8

2.2.3.4. Electrophoretic transfer and blocking

Following electrophoresis, the gel was removed and regions containing proteins of interest were excised and placed into transfer buffer (Table A1) for 5 min in order to equilibrate. Unused pieces of gel were stained in coomassie blue dye for 1 h and then destained overnight in order to assess the quality of the electrophoresis. A transfer sandwich was assembled using nitrocellulose membranes and placed into the transfer tank (Sigma-Aldrich, EP1301) filled with ice cold transfer buffer. Electrophoretic transfer was carried out at 4 °C for 2.5 h at a constant 300 mA. Once the transfer was complete, the used SDS-PAGE gel was stained with coomassie blue dye and destained, as described previously, in order to assess transfer quality. Nitrocellulose membranes were briefly rinsed in 1X Tris buffered saline/Tween-20 (TBS/T, Table A1) and then placed into blocking buffer (Table A1) for 1 h at room temperature (RT) with gentle shaking. After 1 h of blocking, the nitrocellulose membranes were rinsed three times with cold 1X TBS/T for 5 min each and placed into primary antibody solutions.

2.2.3.5. Antibody probing

All antibodies used in this thesis were purchased from Santa Cruz Biotechnology unless otherwise stated. Primary antibodies were diluted in either 5% (w/v) fat-free milk or 5% (w/v) BSA in 1X TBS/T (Table 2.2) and incubated with corresponding nitrocellulose membranes overnight at 4 °C with gentle agitation. The nitrocellulose membranes were washed three times in cold 1X TBS/T for 5 min each and incubated with a corresponding horse radish peroxidase-conjugated secondary antibody (goat anti-rabbit sc-2004 or donkey

anti-goat sc-2020), diluted in 5% (w/v) fat-free milk in 1X TBS/T (Table 2.2) for 1 h at RT, in the dark, with gentle agitation. Nitrocellulose membranes were washed another four times with cold 1X TBS/T and taken to a dark room for visualisation.

Table 2.2: Antibody information and dilutions required for western blot analysis.

Antibody target (product code)	Primary antibody species	Secondary antibody species	Primary antibody dilution	Secondary antibody dilution
Nrf2 (sc-722)	Rabbit	Goat	1/1000 in BSA	1/1000
PXDN (sc-168598)	Goat	Donkey	1/200 in milk	1/1500
NQO1 (sc-16464)	Goat	Donkey	1/1000 in milk	1/1500
β-actin (sc-130656)	Rabbit	Goat	1/800 in milk	1/1000

2.2.3.6. Protein visualisation

WesternBright^{TM} Chemiluminescent substrate (Advansta) was added to each nitrocellulose membrane and left for 2 min for the signal to develop. Excess substrate was poured off and the nitrocellulose membranes were covered in plastic wrap. Bands were detected using x-ray film which was first exposed to the nitrocellulose membranes and then placed into developer (Table A1), rinsed briefly in water and then placed into fixer (Table A1). The developed films were rinsed in water once more and allowed to dry. Band intensity was quantified by densitometric analysis using Image Studio Lite (Ver. 5.2) software.

2.2.3.7. IP for PXDN detection

For PXDN detection, cells were treated with 1 µg/ml Brefeldin-A (Sigma-Aldrich) for 24 h, prior to lysis, in order to prevent the secretion of PXDN into the ECM (Cheng *et al*., 2011). Immunoprecipitation (IP) was performed prior to western blotting to enrich for PXDN protein and improve subsequent PXDN detection. For IP, cells were lysed with native lysis buffer and protein quantified using the Bradford Assay. PXDN was enriched for by incubating 150 µg total protein extract in 1 ml IP buffer (Table A1), with 4 µl goat anti-PXDN antibody (sc-168598), overnight at 4 °C with rotation. Protein A/G agarose beads (20 µl) (Santa Cruz Biotechnologies, sc-2003) were then added to bind to the PXDN/antibody complexes and this was incubated for a further 4 h at 4 °C with rotation. The PXDN/antibody/bead complexes were collected by centrifugation at 5 000 rpm for 5 min at 4 °C, and washed three times in IP buffer with centrifugation at 5 000 rpm for 1 min at 4 °C after each wash. After the final wash, all IP buffer was removed, but 15 µl was left with the

beads to which 8 µl of 4X protein loading buffer was added. Samples were then boiled for 10 min to dissociate the proteins from the beads and to denature the proteins. The beads were pelleted by centrifugation at 5 000 rpm for 1 min and equal volumes of protein-containing supernatant were electrophoresed using SDS-PAGE, as previously described, with PXDN antibody conditions according to Table 2.2.

2.2.4. IF microscopy to observe protein expression

IF confocal microscopy was used to visualise the localisation and indicate the expression levels of Nrf2, PXDN and NQO1. Cells were seeded onto glass coverslips in 6-well plates (120 000 cells/well) and after 48 h, were treated for 3 h or 18 h with 100 µM H_2O_2 or were treated with 5 µM SFN or 40 µM tBHQ for 24 h. All subsequent steps included gentle agitation at RT unless otherwise specified. Cells were washed once with cold 1X PBS for 5 min and fixed to coverslips for 15 min using 3% (v/v) formaldehyde in 1X PBS. Cells were washed three times with cold 1X PBS for 5 min each and permeabilised for 1 h with 0.25% (v/v) Triton X-100 in 1X PBS, in order to allow antibodies to enter through the cellular membranes. The cells were washed another three times with cold 1X PBS for 5 min each and coverslips blocked with 0.5% (w/v) BSA in 1X PBS for 30 min in order to reduce non-specific antibody binding. Cells were washed once more with 1X PBS for 5 min and incubated with primary antibodies, diluted in 0.5% (w/v) BSA in 1X PBS according to Table 2.3, overnight at 4 °C with gentle agitation. Following overnight incubation, cells were washed three times with 0.5% (w/v) BSA in 1X PBS for 5 min each and incubated for 2 h in the dark with corresponding secondary antibodies that were diluted in 0.5% (w/v) BSA in 1X PBS according to Table 2.3. Secondary antibodies required were: fluorescein isothiocyanate (FITC)-conjugated (goat anti-rabbit sc-2012 or donkey anti-goat sc-2024) or allophycocyanin (APC)-conjugated (goat anti-rabbit, Abcam ab72567). All subsequent steps were conducted in the dark in order to prevent photobleaching. After the 2 h incubation, cells were washed three times with 1X PBS for 5 min each and nuclei counterstained with 0.1 µg/ml 4', 6-diamidino-2-phenylindole dihydrochloride (DAPI) (Sigma-Aldrich) in 1X PBS for 5 min. Cells were washed four more times in 1X PBS for 5 min each and coverslips then attached to slides using Fluoromount^{TM} Aqueous Mounting Medium (Sigma-Aldrich) and sealed with clear nail polish. Stained cells were visualised using a Carl Zeiss LSM 780 confocal microscope with Zen 2010 software. Fluorophores were detected at the following excitation (ex) and emission (em) wavelengths: APC $630_{ex}/660_{em}$, DAPI $405_{ex}/454_{em}$ and FITC $488_{ex}/525_{em}$. Gain settings for capturing images were kept constant for experiments where

fluorescence intensity was compared between treatments. Analysis of colocalisation of nuclear proteins with the nucleus was performed using Image-Pro (Ver. 10.0) software and is presented in Appendix B. In addition, autofluorescence controls for the different cell lines, as well as secondary antibody only controls (samples without primary antibody or DAPI staining), were also prepared and visualised (Figure B1).

Table 2.3: Antibody information and dilutions required for all IF microscopy.

Antibody target (product code)	Primary antibody species	Secondary antibody species	Secondary antibody conjugate	Primary antibody dilution	Secondary antibody dilution
Nrf2 (sc-722)	Rabbit	Goat	FITC/APC	1/200	1/200
PXDN (sc-168598)	Goat	Donkey	FITC	1/200	1/500
NQO1 (sc-16464)	Goat	Donkey	FITC	1/200	1/500
Snai1 (sc-28199)	Rabbit	Goat	FITC	1/200	1/200
E-cadherin (24E10)	Rabbit	Goat	FITC	1/200	1/200

E-cadherin antibody was purchased from Cell Signalling Technology.

2.2.5. MTT assay to determine SFN and tBHQ concentrations

Cell cytotoxicity assays were conducted to determine the non-toxic concentrations of the specific compounds SFN (0-20 µM) and tBHQ (0-160 µM). Cells were seeded into 96-well plates (8 000 cells/well) and left to settle for 48 h. Cells were treated as required and incubated at 37 °C for a further 24 h. The medium was replaced with 100 µl of 3-(4,5-dimethylthiazol-2-yl)-2,5 diphenyltetrazolium bromide (MTT) solution (0.5 mg/ml in cell culture medium) and incubated at 37 °C for 1.25 h to allow viable cells to reduce the MTT into formazan. The MTT solution was removed (80 µl) and formazan crystals dissolved in 100 µl dimethyl sulfoxide, followed by incubation at 37 °C for 5 min. The plate was shaken in the dark for 10 min at RT and absorbance measured at 570 nm using a Multiskan GO microplate reader.

2.2.6. ChIP to determine Nrf2 binding to the *PXDN* promoter

ChIP was performed to identify the interaction of Nrf2 with the *PXDN* promoter, as this method can be used to identify whether a TF is binding to a gene promoter sequence. This procedure involved cross-linking all bound proteins to DNA, then the DNA sonicated into smaller pieces that are amenable to PCR. The DNA complexes were then added to an IP solution with an antibody targeting the protein (TF) of interest. If the protein was present, it would bind to the antibody, along with the promoter region that it was cross-linked to. Protein A/G agarose beads were then added which bind the antibody complexes and provide a method for separating the beads from remaining unbound components. The isolated promoter DNA was then amplified by PCR in order to determine whether the promoter regions of interest were bound to the target protein.

2.2.6.1. Bioinformatic analysis of the PXDN promoter

Since we identified that PXDN expression is modified by H_2O_2 and the Nrf2 specific inducers, SFN and tBHQ, we conducted a bioinformatic analysis of the *PXDN* promoter using JASPAR software (Mathelier *et al*., 2016). The first 1 500 base pairs (bp) upstream of the *PXDN* translation start site were scanned for any putative Nrf2 binding sites and the consensus sequence was taken as TGAnTCnGCn (Chorley *et al*., 2012; Kuosmanen *et al*., 2016). We identified a putative Nrf2 binding site 992 bp upstream of the *PXDN* translation start site therefore primers for ChIP PCR were designed against two regions of the *PXDN* promoter: one region that contained the potential Nrf2 binding site and one that did not contain the Nrf2 binding site (used as a negative control).

2.2.6.2. Primers for ChIP PCR and sequencing

Primers (Table A2) were designed to amplify the two *PXDN* promoter regions: one pair amplified across the putative Nrf2 binding site ($PXDN^{Nrf2+}$) and the other amplified across the region without Nrf2 binding sites ($PXDN^{Nrf2-}$), as depicted in Figure 2.7A. The *NQO1* promoter was used as a positive control and two primer sets were also used: one pair amplified across the Nrf2 binding site ($NQO1^{Nrf2+}$) and the other pair covered a region without the Nrf2 binding site ($NQO1^{Nrf2-}$), also depicted in Figure 2.7A. (Chorley *et al*., 2012). The full 1 500 bp region of the *PXDN* promoter was also amplified using primers ($PXDN^{Full}$, Table A2) in order to compare the sequence of the *PXDN* promoter found in the HeLa cells to that found in the HEK293 cells.

2.2.6.3. Genomic DNA extraction

In order to first test the ChIP PCR primers and sequence the *PXDN* promoter regions for both cell lines, genomic DNA was extracted using a standard phenol:chloroform method. Cells were cultured in 10 cm dishes, washed three times with 1X PBS, then scraped into 1 ml of 1X PBS. Cells were collected by centrifugation at 5 000 rpm for 5 min at 4 °C then lysed using 1X RIPA buffer (without protease inhibitors). The lysate was incubated with 20 µg/ml RNase A (ThermoFisher Scientific) for 1 h at 37 °C to degrade RNA, followed by a 2 h incubation with 100 µg/ml Proteinase K (ThermoFisher Scientific) at 50 °C to degrade all protein. Buffered phenol was mixed at a 50:50 ratio with chloroform:isoamyl alcohol (24:1) and was mixed in with the lysate in equal volumes. The lysate was centrifuged at 13 000 rpm for 25 min at RT to separate the components into phases. The upper aqueous phase, containing DNA, was transferred into a new microcentrifuge tube and an equal volume of the phenol:chloroform:isoamyl alcohol solution was added. Centrifugation was repeated and the new upper aqueous phase transferred into a new tube, to which an equal volume of chloroform:isoamyl alcohol (24:1) was added, followed by centrifugation at 13 000 rpm for 25 min at 4 °C. This step was repeated. This final aqueous phase was transferred into a new tube and 0.1 volumes of 3 M sodium acetate was added followed by 2 volumes of 100% (v/v) ethanol, and the sample incubated at −20 °C overnight. DNA was collected by centrifugation at 13 000 rpm for 15 min at 4 °C and the DNA pellet was washed three times with 70% (v/v) ethanol, with centrifugation at 13 000 rpm for 5 min each at 4 °C. The DNA pellet was air-dried and re-suspended in 10 mM Tris-HCl pH 7.8, quantified on a NanoDrop ND-1000 Spectrophotometer at 260 nm and 280 nm, and stored at −20 °C.

2.2.6.4. *PXDN* promoter sequencing

PCR was used to amplify 1 500 bp of the *PXDN* promoter from both the HEK293 and HeLa cell lines for comparison. KAPA HiFi HotStart ReadyMix (KAPA Biosystems) was used for the PCR: 60 ng genomic DNA, 10 µl 2X HiFi HotStart ReadyMix, 0.4 µM each of forward and reverse primers ($PXDN^{Full}$, Table A2) and nuclease free water up to 20 µl. PCR was conducted using a GeneAmp® PCR System 2700. PCR products were purified with the GeneJET PCR Purification Kit (ThermoFisher Scientific), eluted in 20 µl 10 mM Tris-HCl pH 7.8 and sent to Inqaba Biotec for Sanger DNA sequencing. Sequencing was performed using $PXDN^{Full}$ primers (Table A2) and sequences analysed using FinchTV (Ver. 1.4.0) software.

2.2.6.5. ChIP

As the sequence of the *PXDN* promoter in the two cell lines was identical, ChIP was only performed on the HeLa cells. HeLa cells were seeded into 10 cm dishes until 70% confluent then treated with 5 µM SFN or 40 µM tBHQ for 24 h. Protein/DNA interactions were cross-linked using 1% (v/v) formaldehyde in 10% (v/v) FBS culture medium for 10 min with agitation, followed by quenching the cross-linking agent with 125 mM glycine for 5 min. Cells were washed three times with 1X PBS, scraped into a microcentrifuge tube and collected at 5 000 rpm for 5 min at 4 °C. Cells were then lysed in 1X RIPA and sonicated at power output wattage 3 for 15 s, with cooling on ice, fifteen times using a MISONIX Ultrasonic Liquid processor XL-2000 series sonicator. Cell debris was separated out by centrifugation at 10 000 rpm for 10 min at 4 °C. Sonicated DNA was resolved on a 1.5% (w/v) agarose gel, as described previously, in order to ensure the DNA fragments were the correct size for downstream PCR (<1000 bp). A portion of the sonicated DNA was extracted from the lysate using the aforementioned phenol:chloroform method, which was the input PCR positive control, and was quantified at 260 nm and 280 nm on a NanoDrop ND-1000 Spectrophotometer. ChIP was performed on 15 µg of the unpurified sonicated lysate, diluted 1:10 in ChIP IP buffer (Table A1), to which 4 µg of the rabbit anti-Nrf2 antibody (sc-722) was added, and incubated at 4 ^{o}C for 4 h with mixing. Protein A/G agarose beads (sc-2003) were then added (20 µl/sample) and samples mixed overnight at 4 °C. A 'beads only' control was also included with the samples to monitor that the DNA isolated was specific to the Nrf2 antibody immunocomplex and did not result as an interaction with the agarose beads. The following steps were performed at 4 ^{o}C: the DNA/protein/bead complexes were collected by centrifugation at 5000 rpm for 5 min, washed three times with ChIP wash buffer (Table A1) with centrifugation at 5 000 rpm for 1 min each and then washed once with ChIP final wash buffer (Table A1) with centrifugation at 5 000 rpm for 1 min. DNA/protein cross-links were reversed by heating the samples in ChIP elution buffer (Table A1) at 65 °C for 1 h with beads then separated from the supernatant by centrifugation at 5 000 rpm for 1 min. DNA within the supernatant was purified with the GeneJET PCR Purification Kit and eluted in 50 µl 10 mM Tris-HCl pH 7.8. Purified DNA was immediately used in ChIP PCR.

2.2.6.6. ChIP PCR

KAPA HiFi HotStart ReadyMix was used for the ChIP PCR: 8.4 µl ChIP DNA or 60 ng input DNA, 10 µl 2X HiFi HotStart ReadyMix, 0.4 µM each of forward and reverse primer pairs

($PXDN^{Nrf2+}$, $PXDN^{Nrf2-}$, $NQO1^{Nrf2+}$ and $NQO1^{Nrf2-}$, Table A2) and nuclease free water up to 20 µl. PCR was conducted using a GeneAmp® PCR System 2700 and PCR products then resolved on 1.5% (w/v) agarose gels, prepared as described previously. Agarose gels were visualised using the Bio-Rad Gel Doc XR system and Image Lab 6.0 software used to perform a densitometric analysis on PCR bands (Bio-Rad).

2.2.7. IF microscopy to observe effects of Nrf2 over-expression

The Nrf2 over-expression vector, pcDNA3-EGFP-C4-Nrf2 (Addgene plasmid #21549), was first verified using IF microscopy and the effects of Nrf2 over-expression on PXDN and NQO1 assessed (Furukawa and Xiong, 2005). Cells were seeded onto glass coverslips in a 6-well plate and after 48 h, were transfected with pcDNA3-EGFP-C4-Nrf2 for 24 h. The transfection solution was prepared by diluting 2.5 µg of pcDNA3-EGFP-C4-Nrf2 vector in serum-free medium (SFM) (up to 250 µl) in a microcentrifuge tube, followed by the addition of 7.5 µl of the *Trans*IT-X2® System transfection reagent (Mirus); a transfection reagent only control was also included. Transfection solutions were incubated at RT for 30 min and then added drop-wise to cells cultured in 2.5 ml of 10% (v/v) FBS culture medium. Cells were then prepared for IF microscopy, as previously described, and probed with the Nrf2, PXDN and NQO1 primary and fluorophore-conjugated antibodies (Table 2.3).

2.2.8. Luciferase reporter assays on the *PXDN* promoter

Luciferase assays were performed to quantify and determine the level of downstream gene expression from a particular TF binding site of a promoter. This was accomplished by inserting the putative TF binding site or promoter region into a pGL4.10 luciferase reporter vector (Promega). The promoter was inserted upstream of a firefly luciferase reporter gene (*Photinus pyralis*) and the constructed vector was used to transfect mammalian cells. Expression levels of the firefly luciferase enzyme are dependent on the ability of the inserted TF binding sites or promoter regions to drive expression. A Steady-Glo or Dual-Glo reagent was used according to manufacturer's instructions (Promega Corporation, 2013). The reagents both lyse transfected cells and also contain beetle luciferin enzyme, which is oxygenated by the firefly luciferase enzyme to form oxyluciferin and light:

$$\text{Beetle luciferin} + \text{ATP} + O_2 \xrightarrow[Mg^{2+}]{\text{Firefly luciferase}} \text{Oxyluciferin} + \text{AMP} + PP_i + CO_2 + \text{light}$$

The amount of light produced is therefore an indicator of the amount of firefly luciferase enzyme translated in the transfected cells. The level of light was thus used to determine whether the TF binding site or promoter of interest, has the ability to drive gene expression.

2.2.8.1. Preparation of luciferase vector constructs

Primers used in the ChIP experiments above, were used to clone the *PXDN* promoter into the pGL4.10 luciferase vector via the addition of NheI and EcoRV restriction sites on the forward and reverse primers, respectively (Table A2). HeLa genomic DNA was extracted using the phenol:chloroform protocol described previously, and the *PXDN* and *NQO1* promoter regions amplified using the KAPA HiFi HotStart ReadyMix PCR kit. Briefly, 60 ng HeLa DNA, 10 µl 2X HiFi HotStart ReadyMix, 0.5 µM each of forward and reverse primer pairs ($REPXDN^{Nrf2+}$, $REPXDN^{Nrf2-}$, $RENQO1^{Nrf2+}$ and $RENQO1^{Nrf2-}$, Table A2) and nuclease free dH_2O up to 20 µl, and PCR conducted using a GeneAmp® PCR System 2700. PCR products were purified using the GeneJET PCR Purification Kit and 600 ng of purified DNA and pGL4.10 luciferase vector was restricted using 1 µl each of NheI and EcoRV restriction enzymes (ThermoFisher Scientific), which was incubated at 37 °C for 16 h followed by inactivation of NheI at 65 °C for 20 min and inactivation of EcoRV at 80 °C for 20 min. Restricted products were purified using the GeneJET PCR Purification Kit and then ligated at a 3:1 ratio into 50 ng restricted pGL4.10 luciferase vector overnight at 4 °C, using KAPA 2X Rapid ligase (KAPA Biosystems). The ligation mixture was then used for transformation immediately.

2.2.8.2. Competent bacteria and transformation

To create competent bacteria for transformation, JM109 *E.coli* were cultured in 2 ml of 2% (w/v) LB broth, overnight at 37 °C, then added to 50 ml fresh 2% (w/v) LB broth and grown at 37 °C until an absorbance of 0.5–0.6 arbitrary units at 600 nm was achieved. *E.coli* were collected by centrifugation at 4 000 rpm at 4 °C for 5 min, the *E.coli* pellet gently re-suspended in 15 ml of chilled 0.1 M $MgCl_2$, chilled on ice for 30 min and again pelleted by centrifugation at 4 000 rpm for 5 min at 4 °C. The bacterial pellet was re-suspended in 2 ml of 0.1 M $CaCl_2$ (with 15% (v/v) glycerol), dispensed into 50 µl aliquots and stored at −70 °C.

To transform competent *E.coli*, an aliquot of bacteria was thawed on ice and 2 µl of ligation mixture (5-7 ng ligated vector) was added and chilled on ice for 30 min. Heat shock was then performed on the *E.coli* for 2 min at 42 °C followed by immediate chilling on ice for 5 min,

followed by the addition of 950 µl of pre-warmed SOC broth (Table A1). Transformed bacteria were then incubated at 37 °C for 1 h with vigorous shaking, in order to promote bacterial growth, after which transformed *E.coli* were spread onto ampicillin-containing (100 µg/ml) LB agar and incubated overnight at 37 °C.

2.2.8.3. Colony PCR

Colonies containing the vector with the insert DNA were identified by colony PCR. Colonies were carefully selected, each re-suspended in 50 µl of 2% (w/v) LB broth and incubated at 37 °C for 1 h, with vigorous shaking, after which cultures were placed on ice to stop growth. PCR was performed across the multiple cloning site of the pGL4.10 vector using KAPA Taq ReadyMix DNA Polymerase: 8 µl colony/LB broth mixture, 10 µl 2X ReadyMix with Mg^{2+}, 0.5 µM each of pGL4 forward and reverse primers (Table A2), and a GeneAmp® PCR System 2700. PCR products were resolved on a 1.5% (w/v) agarose gel, prepared and visualised as described previously, in order to identify vectors that contained the insert of interest.

Once it was confirmed that the insert was present in the vector, the vectors were amplified by placing the remaining 42 µl of colony/LB broth mixture into 5 ml of fresh 2% (w/v) LB broth with 100 µg/ml ampicillin, followed by incubation at 37 °C overnight with vigorous shaking. Vectors were extracted from *E.coli* using a standard alkaline lysis protocol.

2.2.8.4. Alkaline lysis

A glycerol stock of successfully transformed *E.coli* was prepared by mixing 1 ml of the above overnight broth with 250 µl glycerol, and stored at −70 °C. The remaining 4 ml of broth was centrifuged at 12 000 rpm for 1 min at 4 °C to pellet the bacteria, which was then re-suspended in 110 µl of Solution A (Table A1) and an additional 100 µl of Solution B (Table A1) to lyse the bacteria. The tube was inverted six times to mix, then 120 µl of cold 5 M potassium acetate (pH 5.5) was added. The sample was incubated at RT for 3 min then centrifuged at 12 000 rpm for 4 min to remove the precipitate. The clear supernatant was transferred into a new microcentrifuge tube and 200 µl of 2-propanol added, the tube then inverted and incubated at RT for 1 min. The sample was centrifuged at 13 000 rpm for 1 min and the 2-propanol removed. The DNA pellet was washed once with 500 µl of 70% (v/v) ethanol then centrifuged at 13 000 rpm for 1 min. Once the DNA pellet had air-dried, it was

re-suspended in 10 mM Tris-HCl pH 7.8, quantified at 260 nm and 280 nm on a NanoDrop ND-1000 Spectrophotometer, then stored at −20 °C.

The sequences of all inserts were confirmed by Sanger DNA sequencing (Inqaba Biotec) using pGL4.10 primers (Table A2) and analysed using FinchTV (Ver. 1.4.0) software, prior to use of the vectors in luciferase reporter assays.

2.2.8.5. Luciferase reporter assay

HEK293 cells were used for luciferase experiments since these cells are highly transfectable and have been shown to express all of the proteins of interest. HEK293 cells were seeded at 10 000 cells/well of a 96-well plate and after 48 h, were treated with 5 µM SFN or 40 µM tBHQ for 3 h. Cells were then either transfected with each construct individually using 0.2 µg of pGL4.10 construct DNA or were co-transfected at a 1:1 ratio of pGL4.10 construct DNA together with the Nrf2 over-expression vector, pcDNA3-EGFP-C4-Nrf2 (Addgene plasmid #21549) (Furukawa and Xiong, 2005). Transfection reactions were prepared based on 20 µl/well: DNA was diluted in SFM, 2 µl Turbofect transfection reagent (ThermoFisher Scientific) was added and samples incubated at RT for 30 min, before being added to cells. Transfected cells were incubated at 37 °C for an additional 21 h, the luciferase assay performed using Steady-Glo or Dual-Glo reagent (Promega), according to the manufacturer's instructions, and luciferase expression, in the form of light, measured on a Glomax luminometer (Promega).

2.2.8.6. Mutagenesis of the putative Nrf2 binding site

Once the luciferase data confirmed that the *PXDN* gene promoter, containing the putative Nrf2 binding site, had the ability to drive gene expression, the specific Nrf2 binding sites within the *PXDN* and *NQO1* promoters were amplified ($REPXDN^{WtNrf2+}$ and $RENQO1^{WtNrf2+}$, Table A2) and mutated ($REPXDN^{Mt1Nrf2+}$, $REPXDN^{Mt2Nrf2+}$ and $RENQO1^{MtNrf2+}$, Table A2). The sites were mutated by designing primers that annealed to each other and contained variations of prominent bp required for Nrf2 binding (Figure 2.10A). These promoter regions were prepared in the same manner described previously, and following Sanger sequencing (Inqaba Biotec), were used for luciferase reporter assays.

2.2.9. Statistical analysis

Unless otherwise stated, all quantification was attained from experiments performed a minimum of three times where n = the number of independent biological replicates ± standard deviation (SD). Comparisons were made by Student's t-tests and $P \leq 0.05$ was considered statistically significant. Significance is made relative to 'Untreated' samples, taken as 100%, unless otherwise specified. Significance is depicted on graphs as follows: *: $P \leq 0.05$, **: $P < 0.01$ and ***: $P < 0.001$.

2.3. Results

2.3.1. PXDN mRNA is expressed in HEK293 and HeLa cells

Total RNA was extracted from HEK293 and HeLa cells with two distinct 28S and 18S ribosomal RNA bands present at 1 800 and 900 bp, respectively, based on a DNA ladder (Figure 2.1A). Clear GAPDH PCR bands at 496 bp for both samples indicated that cDNA was successfully synthesised and the absence of a band in the no template control (NTC) lane indicated that the PCR was not contaminated with foreign DNA (Figure 2.1B). Subsequent PXDN PCR on cDNA confirmed that PXDN mRNA was present in both the HEK293 and HeLa cell lines due to the presence of the PCR bands at 636 bp, no contamination was seen in the NTC as expected (Figure 2.1C). Once it was confirmed that PXDN mRNA was present, these two cell lines were used for subsequent experiments.

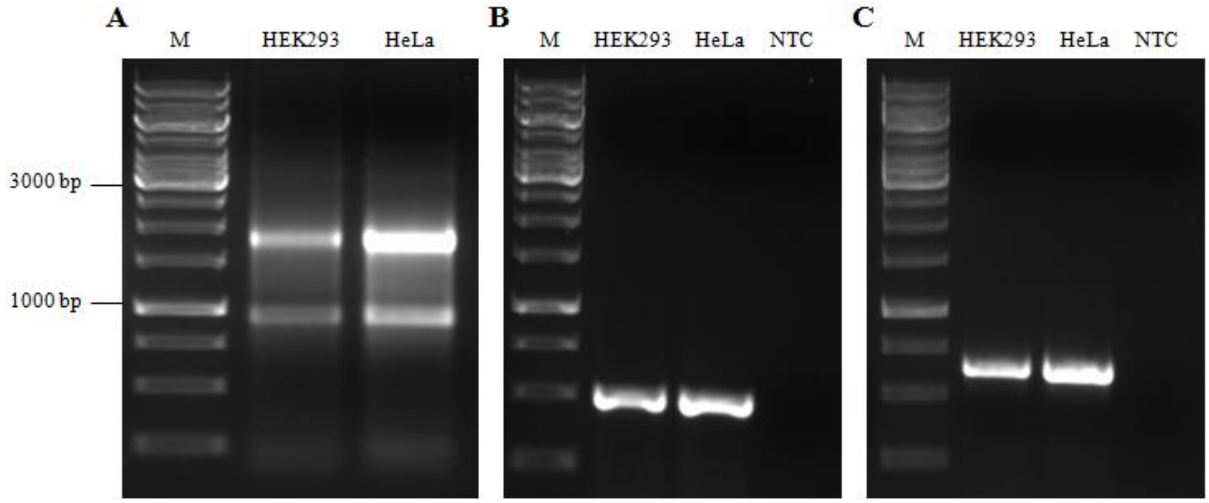

Figure 2.1: PXDN mRNA expression in HEK293 and HeLa cells. **A)** Total RNA was extracted from HEK293 and HeLa cell lines, and quality indicated by the two prominent bands for 28S and 18S ribosomal RNA at 1800 base pairs (bp) and 900 bp, respectively. **B)** GAPDH PCR bands at 496 bp confirmed the synthesis cDNA. **C)** PCR bands at 636 bp confirmed the presence of PXDN mRNA in HEK293 and HeLa cell lines. Molecular weight marker (M): GeneRuler^{TM} 1 kb DNA ladder, NTC: no template control.

2.3.2. PXDN expression increases with H_2O_2 treatment

Once the cell lines were confirmed to express PXDN mRNA, we then established PXDN protein expression and whether the expression level was influenced by H_2O_2. Nrf2 expression was first investigated since the TF is known to respond to ROS such as H_2O_2. In HEK293 cells, western blot analysis showed that Nrf2 expression increased by 28% (128 ± 17%) and

20% (120 ± 8%) after 3 h and 18 h of H_2O_2 treatment, respectively (Figure 2.2A). PXDN expression also increased in HEK293 cells upon treatment with H_2O_2, as indicated by the increase in density in the western blot bands (Figure 2.2A), with a 40% (140 ± 15%) increase after 3 h and a 48% (148 ± 11%) increase after 18 h. NQO1 expression (positive control) in HEK293 cells increased, as expected, by 29% (129 ± 23%) and 15% (115 ± 9%) after 3 h and 18 h of H_2O_2 treatment, respectively (Figure 2.2A). In HeLa cells, after 3h and 18 h of H_2O_2 treatment, Nrf2 expression increased by 21% (121 ± 5%; 121 ± 11%) while PXDN expression increased by 15% (115 ± 11%) and 20% (120 ± 15%), respectively (Figure 2.3A), and as anticipated, NQO1 expression in HeLa cells also increased by 38% (138 ± 22%) and 33% (133 ± 19%), respectively (Figure 2.3A).

IF microscopy also reflected the alterations in Nrf2, NQO1 and PXDN expression in both HEK293 and HeLa cells following H_2O_2 treatment. In HEK293 cells, Nrf2 expression increased, as shown by an increase in FITC intensity, and was translocated into the DAPI-stained nucleus, as shown by blue-green nuclei, after H_2O_2 treatment (Figure 2.2B and Table B1). FITC intensity of PXDN also increased following H_2O_2 treatment and appeared to collect around and between HEK293 cells (Figure 2.2B). Increased FITC intensity also indicated that NQO1 expression in HEK293 cells increased following treatment with H_2O_2 and was more prominent in the cytoplasm as expected, which correlated with increasing levels of Nrf2 (Figure 2.2B). In HeLa cells, Nrf2 expression and nuclear translocation increased after H_2O_2 treatment (Table B1) and FITC intensity indicated that PXDN expression also increased following H_2O_2 treatment with accumulation around the cells and around the nuclei, which may indicate increased PXDN in the endoplasmic reticulum (Figure 2.3B). In HeLa cells, NQO1 expression also increased within the cytoplasm after H_2O_2 treatment, as expected (Figure 2.3B).

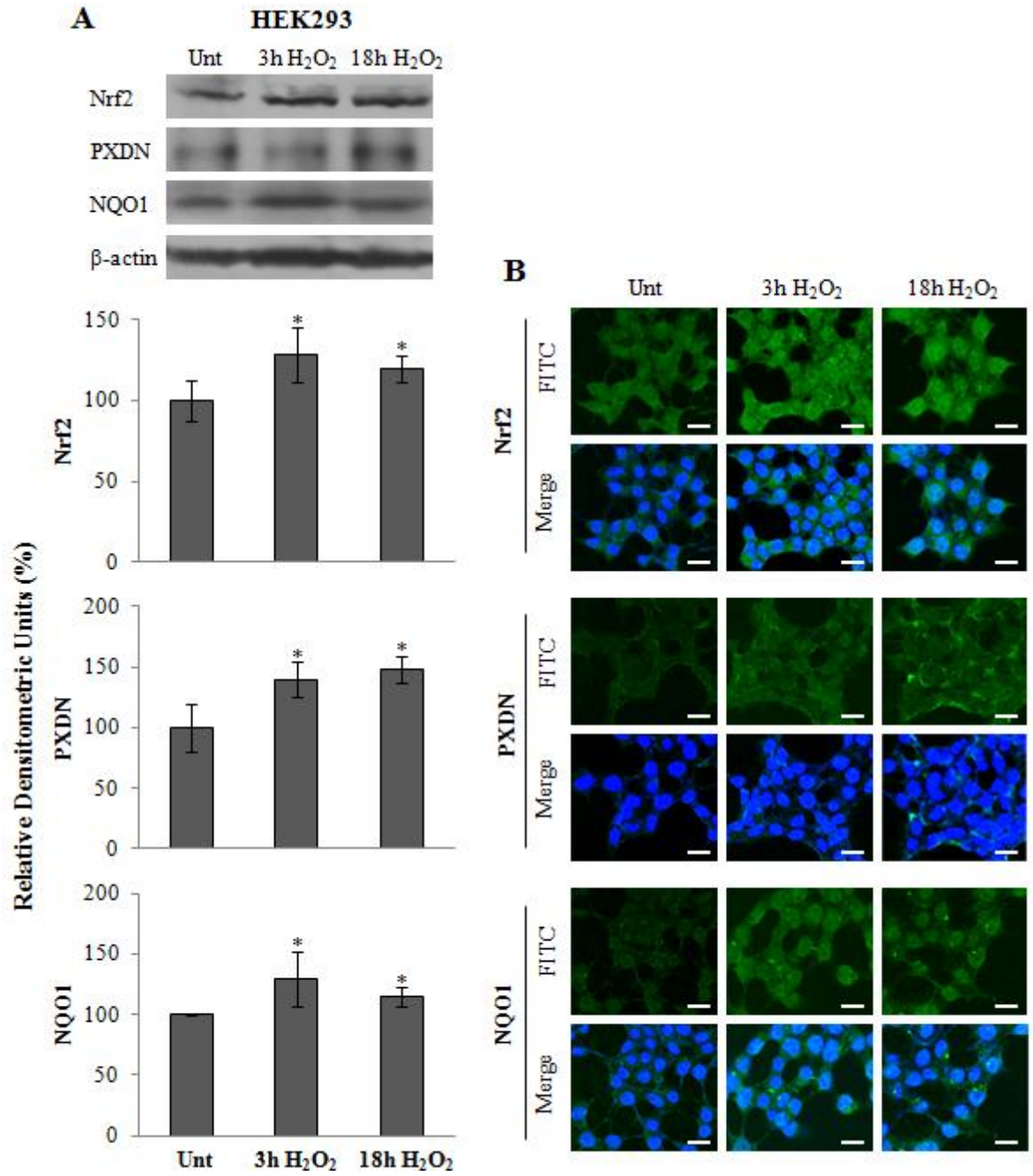

Figure 2.2: PXDN expression and localisation in HEK293 cells in response to H_2O_2. A) HEK293 cells were treated with 100 µM H_2O_2 (3 h or 18 h) and protein expression determined for PXDN (165 kDa), NQO1 (31 kDa) and total Nrf2 (61 kDa) using western blot analysis. H_2O_2 treatments increased Nrf2, NQO1 and PXDN expression. β-actin (43 kDa) was used for the loading control (*n* = 3, mean ± SD). **B)** HEK293 cells were treated and protein expression and localisation determined using FITC-labelled secondary antibodies. DAPI stained nuclei blue. Increased Nrf2 nuclear translocation (brighter green nuclei) was observed with H_2O_2. Increased NQO1 was evident in H_2O_2 treated cells. PXDN expression was more localised around the cells with 18 h H_2O_2 treatment (63X magnification; scale bar = 20 µm).

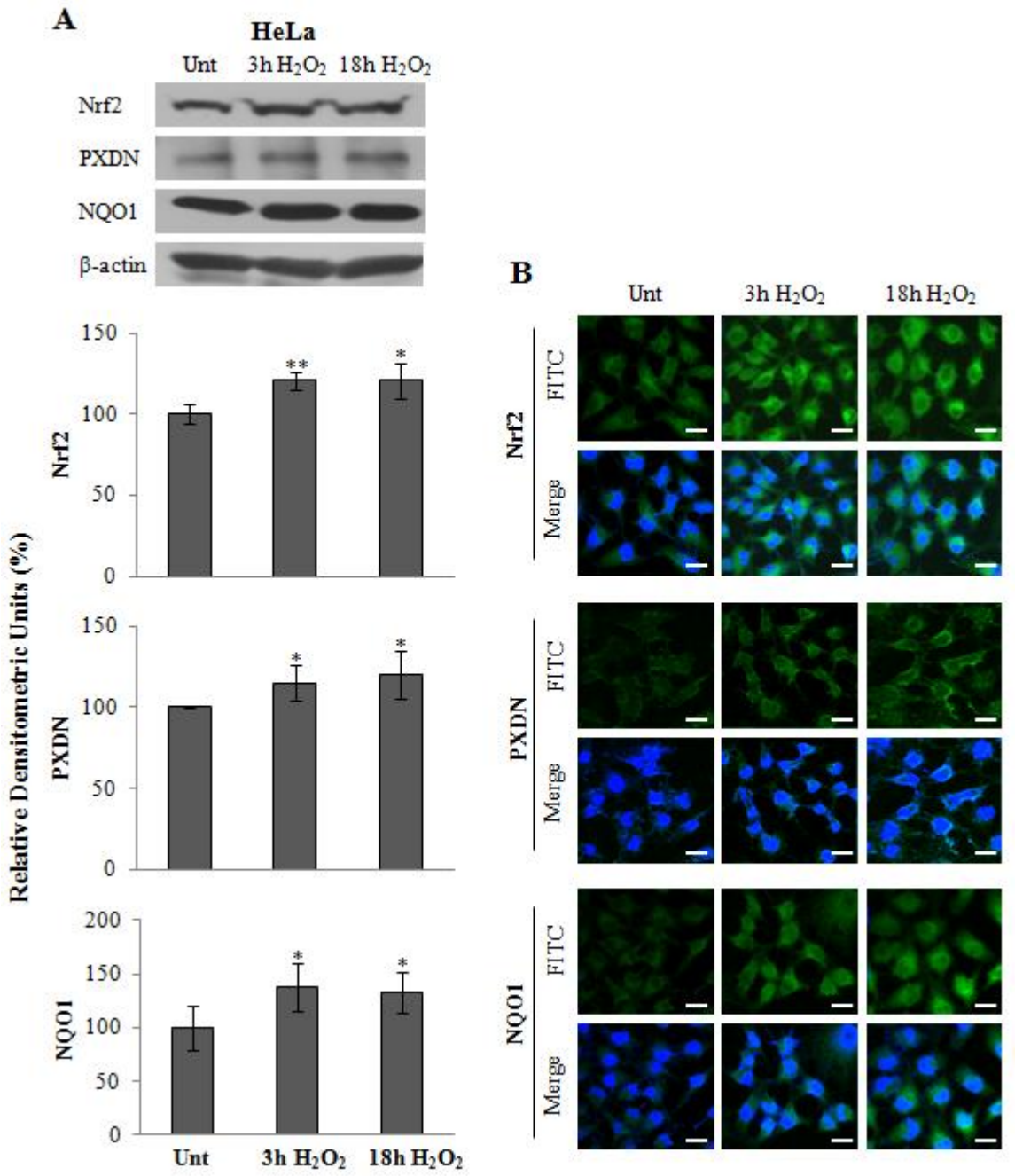

Figure 2.3: PXDN expression and localisation in HeLa cells in response to H_2O_2. A) HeLa cells were treated with 100 µM H_2O_2 (3 h or 18 h) and protein expression determined using western blot analysis. There was increased Nrf2 (61 kDa), NQO1 (31 kDa) and PXDN (165 kDa) expression after H_2O_2 treatments. β-actin (43 kDa) was used for the loading control (n = 3, mean ± SD). **B)** IF microscopy showed altered protein localisation with H_2O_2 increasing Nrf2 nuclear translocation together with greater cytoplasmic staining of NQO1 and greater cytoplasmic and extracellular localisation of PXDN. DAPI stained nuclei blue (63X magnification; scale bar = 20 µm).

2.3.3. PXDN expression increases in response to SFN and tBHQ

Since H_2O_2 appeared to enhance both Nrf2 and PXDN expression, specific Nrf2 inducers, rather than the broad activator H_2O_2, were used to investigate the potential influence of Nrf2 on PXDN. MTT assays were first conducted on HEK293 and HeLa cells in order to determine optimal SFN and tBHQ concentrations (Figure 2.4) as both of these compounds can be cytotoxic (Pappa *et al*., 2007; Eskandani *et al*., 2014). From the MTT data, which showed decreased cell viability after treatment with 10 μM SFN and 160 μM tBHQ in both cell lines, we decided to use the lower doses of 5 μM SFN and 40 μM tBHQ for 24 h for all downstream experiments.

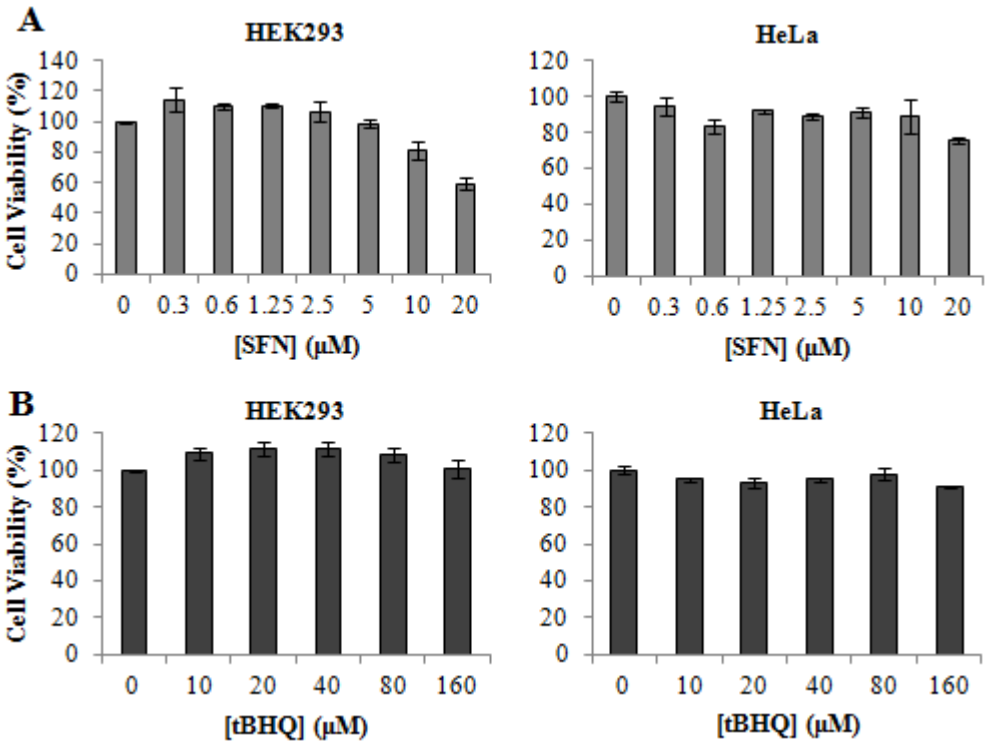

Figure 2.4: Determination of doses of SFN and tBHQ. A) Sulforaphane (SFN) and **B)** *tert*-butylhydroquinone (tBHQ) treatment concentrations for downstream experiments were chosen following MTT cytotoxicity assays performed on HEK293 and HeLa cells treated for 24 h, since both SFN and tBHQ can be toxic to cancer cells (n = 3, mean ± SD).

Cells treated with either SFN or tBHQ were analysed for protein expression by western blot analysis and IF microscopy. Western blot analysis indicated that HEK293 cells treated with Nrf2 inducers, SFN and tBHQ, had a 27% (127 ± 18%) and 20% (120 ± 10%) increase in Nrf2 expression, respectively (Figure 2.5A). Interestingly, in HEK293 cells there was a 12% (112 ± 7%) increase in PXDN expression following SFN treatment and a 12% (112 ± 4%) increase with tBHQ treatment (Figure 2.5A). Similarly, NQO1 expression in HEK293 cells increased in response to treatment with Nrf2 inducers with a 67% (167 ± 13%) and 65% (165 ± 30%) increase following SFN or tBHQ treatment, respectively, as expected (Figure 2.5A). In HeLa cells, Nrf2 expression increased by 49% (149 ± 21%) and by 35% (135 ± 22%) after treatment with SFN and tBHQ, respectively (Figure 2.6A). Similarly to HEK293, HeLa cells treated with SFN had a 20% (120 ± 10%) increase in PXDN expression, while tBHQ resulted in a 16% (116 ± 4%) increase (Figure 2.6A). In HeLa cells, NQO1 expression increased by 22% (122 ± 12%) and 27% (127 ± 9%) following treatment with SFN or tBHQ respectively (Figure 2.6A).

IF microscopy also indicated that the Nrf2 inducers increased Nrf2 expression and nuclear translocation in both cell lines, as expected (Figure 2.5B, 2.6B and Table B2). Interestingly, SFN or tBHQ treatment increased PXDN expression in both cell lines; however, HEK293 cells showed only a slight increase with much of the PXDN being localised in the extracellular space (Figure 2.5B), while PXDN in HeLa cells had a stronger response to Nrf2 inducers (Figure 2.6B). Nrf2 inducers also increased NQO1 expression in both cell lines, as expected, as seen by increased intensity of cytoplasmic FITC staining (Figure 2.5B and 2.6B).

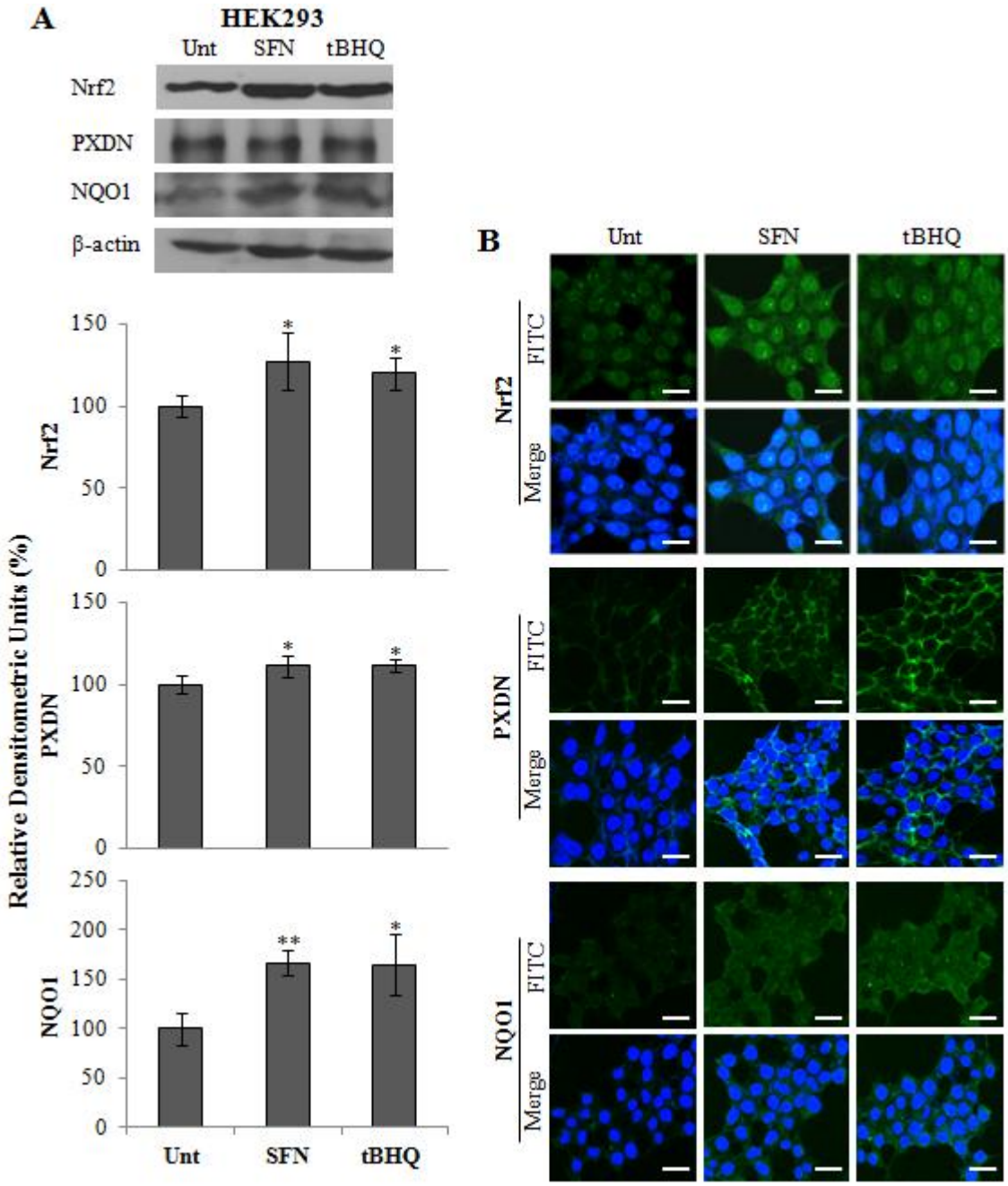

Figure 2.5: PXDN expression and localisation in HEK293 cells after SFN and tBHQ treatment. A) HEK293 cells treated with 5 µM SFN or 40 µM tBHQ for 24 h showed increased Nrf2 (61 kDa), PXDN (165 kDa) and NQO1 (31 kDa) expression following western blot analysis. β-actin (43 kDa) was used for the loading control (n = 3, mean ± SD). **B)** IF microscopy showed that both SFN and tBHQ caused Nrf2 nuclear translocation and increased cytoplasmic staining of NQO1. PXDN was highly localised within the extracellular space and this was elevated with both SFN and tBHQ. DAPI stained nuclei blue (63X magnification; scale bar = 20 µm).

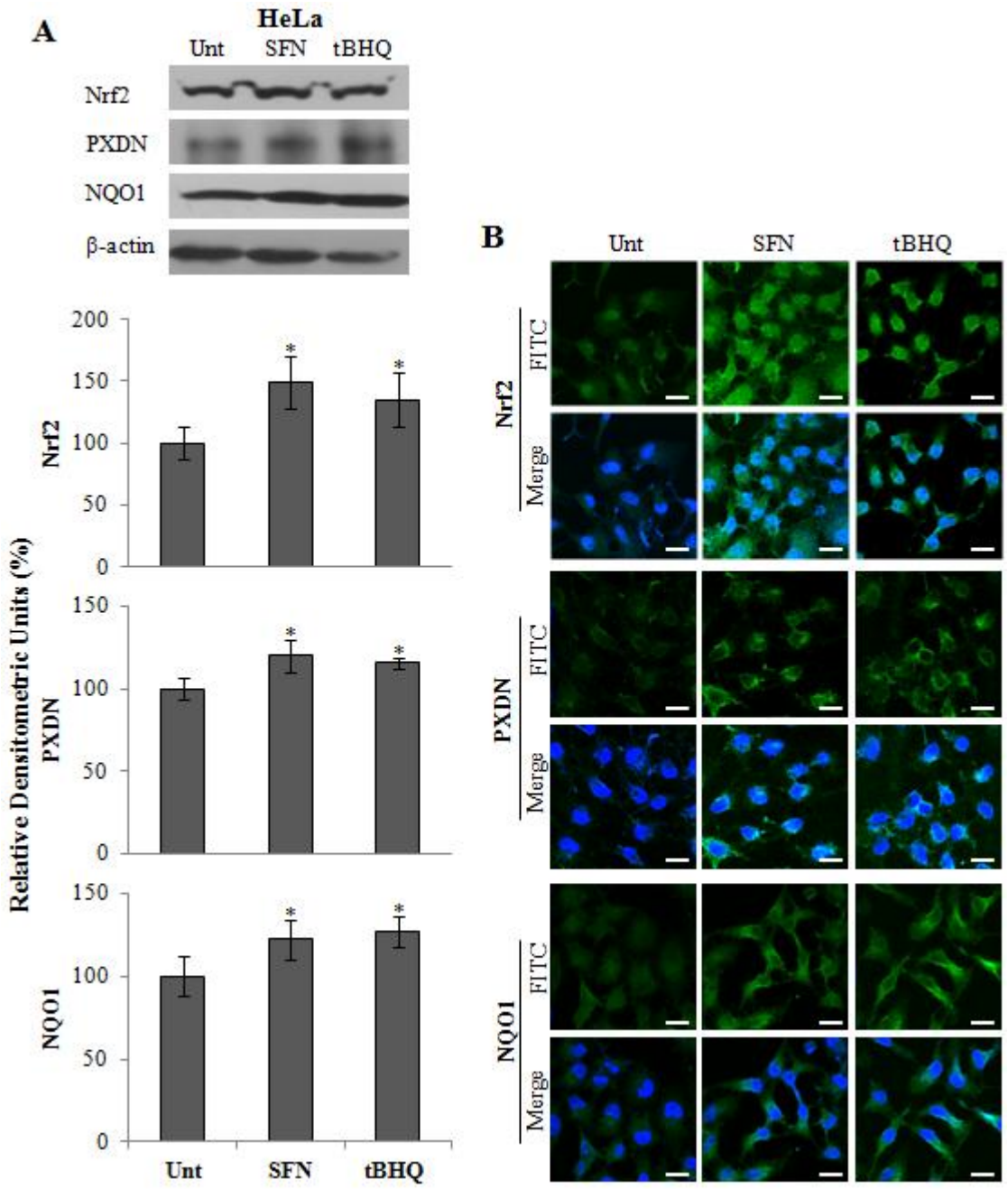

Figure 2.6: PXDN expression and localisation in HeLa cells after SFN and tBHQ treatment. A) HeLa cells treated with 5 µM SFN or 40 µM tBHQ for 24 h, showed increased expression of Nrf2 (61 kDa), PXDN (165 kDa) and NQO1 (31 kDa) following western blot analysis. β-actin (43 kDa) was used for the loading control (*n* = 3, mean ± SD). **B)** IF microscopy showed Nrf2 nuclear translocation was enhanced with SFN and tBHQ treatment and increased cytoplasmic staining of NQO1 was evident. PXDN showed more cytoplasmic and extracellular staining with SFN and tBHQ treatment. DAPI stained nuclei blue (63X magnification; scale bar = 20 µm).

2.3.4. Nrf2 binds to the *PXDN* promoter

We observed that, like NQO1, PXDN expression increased upon treatment with Nrf2 specific inducers. As such, we investigated whether PXDN may be regulated by Nrf2. Firstly, ChIP was used to determine if Nrf2 can bind to the *PXDN* promoter. A bioinformatics analysis using JASPAR revealed a potential Nrf2 binding site within the *PXDN* promoter (Figure 2.7A). Therefore for ChIP analysis, primers were designed to span two separate regions of the *PXDN* and *NQO1* promoters, one with and one without the Nrf2 binding site. An agarose gel of the cross-linked DNA, following sonication, showed that the DNA fragment sizes fall within the required range for the PCR products– around 50 bp to 600 bp (Figure 2.7B). Following ChIP (performed on three biological replicates), using an anti-Nrf2 antibody, the immunoprecipitated DNA was amplified by PCR using the aforementioned primers and PCR products were resolved on a 1.5% (w/v) agarose gel.

Clear bands, of the expected size, were present in the Nrf2-antibody lanes (lane 1) for both $PXDN^{Nrf2+}$ and $NQO1^{Nrf2+}$ but not for $PXDN^{Nrf2-}$ or $NQO1^{Nrf2-}$ as expected (Figure 2.7C). There were also no bands visible in either of the 'beads only' control lanes or NTC PCR controls (lanes 2 and 4 respectively), as anticipated. Bands present in all of the input PCR positive control lanes (lane 3) indicated that PCR was successful (Figure 2.7C). Interestingly, PCR products within the Nrf2-antibody lanes for the $PXDN^{Nrf2+}$ region of the promoter increased in intensity from cells treated with the Nrf2 inducers in comparison to the PCR products from untreated cells. Densitometric analysis (mean ± SD) of the PCR product from cells treated with SFN showed a more than two-fold increase (243 ± 144%; P=0.02) and the PCR product from cells treated with tBHQ increased in intensity by more than three-fold (316 ± 195%; P=0.02) (Figure 2.7C). A similar pattern with the PCR product intensity was observed for $NQO1^{Nrf2+}$, with an increase in Nrf2 binding observed in cells treated with SFN (163 ± 35%; P=0.04) and a significant increase in Nrf2 binding in cells treated with tBHQ (205 ± 47%; P=0.02) (Figure 2.7C). Altogether, the ChIP PCR data confirmed that Nrf2 binds within the $PXDN^{Nrf2+}$ region of the *PXDN* promoter and that this binding is enhanced in response to treatment with Nrf2 inducers.

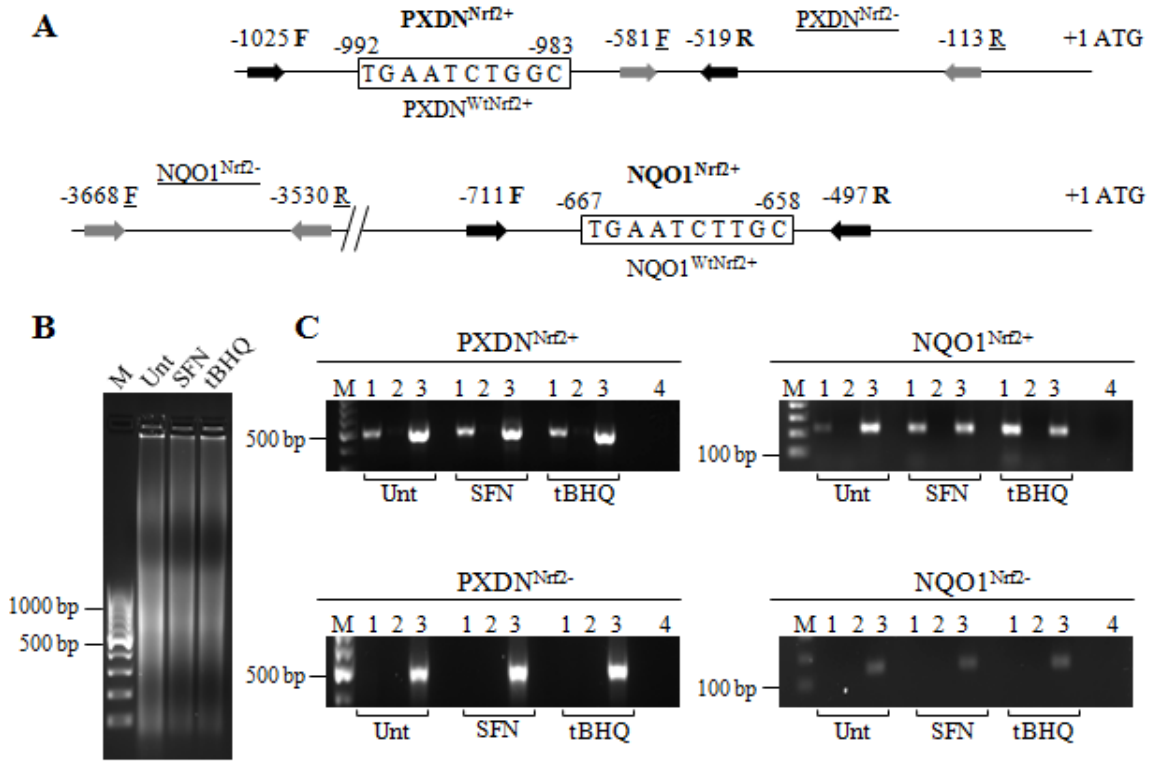

Figure 2.7: ChIP PCR of Nrf2 binding to the *PXDN* promoter. A) Primers were designed to amplify the *PXDN* promoter in two sections: one with the putative Nrf2 binding site, PXDN^{Nrf2+} (black arrows) and one without, PXDN^{Nrf2-} (grey arrows). This was repeated with the *NQO1* promoter: with the Nrf2 binding site, NQO1^{Nrf2+} (black arrows) and one without, NQO1^{Nrf2-} (grey arrows) (Chorley *et al.*, 2012). Numbering is relative to the translation start site. Boxed sequences display the putative Nrf2 binding site within PXDN^{Nrf2+} and the known site in NQO1^{Nrf2+}. **B)** Sonication performed on Unt (untreated), 5 µM SFN and 40 µM tBHQ treated HeLa cells, indicated DNA fragment sizes suitable for ChIP PCR. **C)** ChIP PCR results for either PXDN^{Nrf2+} (507 bp), NQO1^{Nrf2+} (214 bp), PXDN^{Nrf2-} (471 bp) or NQO1^{Nrf2-} (139 bp) promoter regions. Lane 1: Nrf2-antibody treated, lane 2: beads only control, lane 3: input DNA and lane 4: PCR NTC. A PCR band was observed in lane 1 for the PXDN^{Nrf2+} and NQO1^{Nrf2+} promoter regions which increased in intensity when cells were treated with SFN and tBHQ, indicating that Nrf2 binds within these regions of the promoters and treatment with Nrf2 inducers enhances binding. No PCR band was observed in lane 1 for the PXDN^{Nrf2-} or NQO1^{Nrf2-} regions. For all control lanes, results were as expected with no bands in the negative control lanes 2 and 4, and a positive PCR band for the input DNA control in lane 3. M: GeneRuler^{TM} 100 bp DNA ladder.

2.3.5. Nrf2 is responsible for increasing PXDN expression

ChIP experiments established that Nrf2 binds to the *PXDN* promoter and level of Nrf2 binding increases with increasing levels of Nrf2. It was then necessary to conduct more quantitative experiments to determine the degree to which Nrf2 induction could regulate and increase PXDN expression using luciferase assays. To conclusively determine that Nrf2 regulates PXDN expression, we introduced an Nrf2 over-expression vector for use in the luciferase reporter assays. The Nrf2 over-expression vector, pcDNA3-EGFP-C4-Nrf2, contains the complete sequence of the human Nrf2 coding region and subsequent transfection results in enhanced Nrf2 production, nuclear translocation and binding to ARE-containing promoters. We first established the effects of Nrf2 over-expression on PXDN by conducting IF microscopy (Figure 2.8). Upon transfection with the pcDNA3-EGFP-C4-Nrf2 vector, we observed significant increased Nrf2 expression and nuclear translocation in both cell lines, when compared to the untransfected control, as seen by the increase in intensity of the red APC staining and purple staining in the Nrf2/DAPI merge IF microscopy images (Figure 2.8 and Table B3). Complementary to earlier data, the IF images showed that Nrf2 over-expression clearly increased PXDN expression in both cell lines (Figure 2.8A). There was also a significant increase in the expression of the NQO1 control with increased Nrf2 translocation in both cell lines as expected (Figure 2.8B).

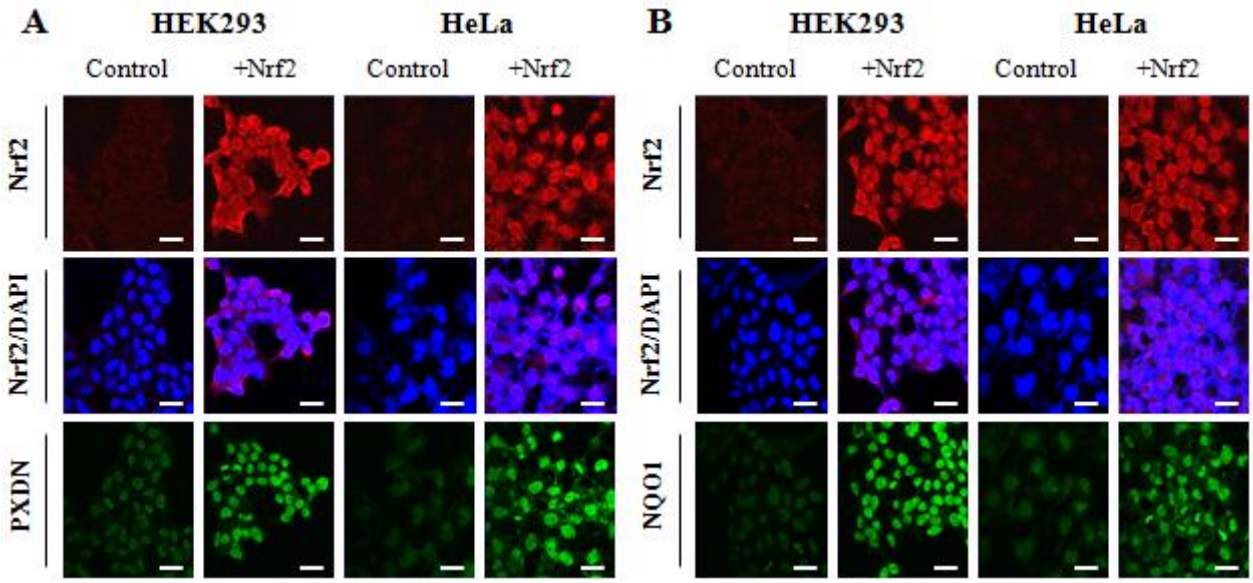

Figure 2.8: Effects of Nrf2 over-expression on PXDN and NQO1 expression. Control: cells treated with transfection reagent only for 24 h. +Nrf2: cells transfected with pcDNA3-EGFP-C4-Nrf2 over-expression vector for 24 h. **A)** IF microscopy showed that Nrf2+ HEK293 and HeLa cells had increased Nrf2 expression (red APC), Nrf2 nuclear translocation (purple stain) and PXDN expression (green FITC) as compared to control cells. **B)** Nrf2+ HEK293 and HeLa cells had increased Nrf2 nuclear translocation and amplified levels of NQO1, as expected for the positive control (63X magnification; scale bar = 20 μm).

In order to quantify the level of Nrf2 regulation, luciferase assays were performed on the *PXDN* and *NQO1* promoter regions, after the same promoter regions used in ChIP were cloned into pGL4.10 luciferase reporter vectors. Luciferase data showed that Nrf2 binds to and drives reporter gene expression from the $NQO1^{Nrf2+}$ promoter region with the luciferase signal significantly increasing upon treatment with the Nrf2 inducers, SFN (1679 ± 189%) and tBHQ (2959 ± 325%) (Figure 2.9A). In contrast, the $NQO1^{Nrf2-}$ promoter region had only a slight and statistically insignificant increase in light output following treatment with the Nrf2 inducers. Similarly, the $PXDN^{Nrf2+}$ promoter region was able to drive expression of the luciferase reporter gene with greater induction after treatment with SFN (161 ± 14%) and tBHQ (134 ± 10%) (Figure 2.9B). There was no significant luciferase reporter gene expression from the $PXDN^{Nrf2-}$ promoter region, thus supporting the ChIP data.

To identify the exact putative Nrf2 binding site within the *PXDN* promoter, a smaller promoter region was amplified ($PXDN^{WtNrf2+}$) and the same was done with the *NQO1* promoter as a positive control ($NQO1^{WtNrf2+}$). Nrf2 inducers significantly increased downstream luciferase reporter gene expression from the $NQO1^{WtNrf2+}$ region (SFN 131 ±

8%; tBHQ 166 ± 19%) (Figure 2.9C) as well as the $PXDN^{WtNrf2+}$ region (SFN 113 ± 5%; tBHQ 126 ± 8%) (Figure 2.9D), thus further confirming the presence of the Nrf2 binding site identified in the *PXDN* promoter (Figure 2.7A).

The effect of the pcDNA3-EGFP-C4-Nrf2 vector was then assessed by co-transfecting with the NQO1 and PXDN promoter pGL4.10 constructs. A significant increase in light output was observed with both the $NQO1^{Nrf2+}$ (943 ± 38%) and $PXDN^{Nrf2+}$ (150 ± 7%) regions but not with the $NQO1^{Nrf2-}$ or $PXDN^{Nrf2-}$ regions as expected (Figure 2.9E and 2.9F, respectively).

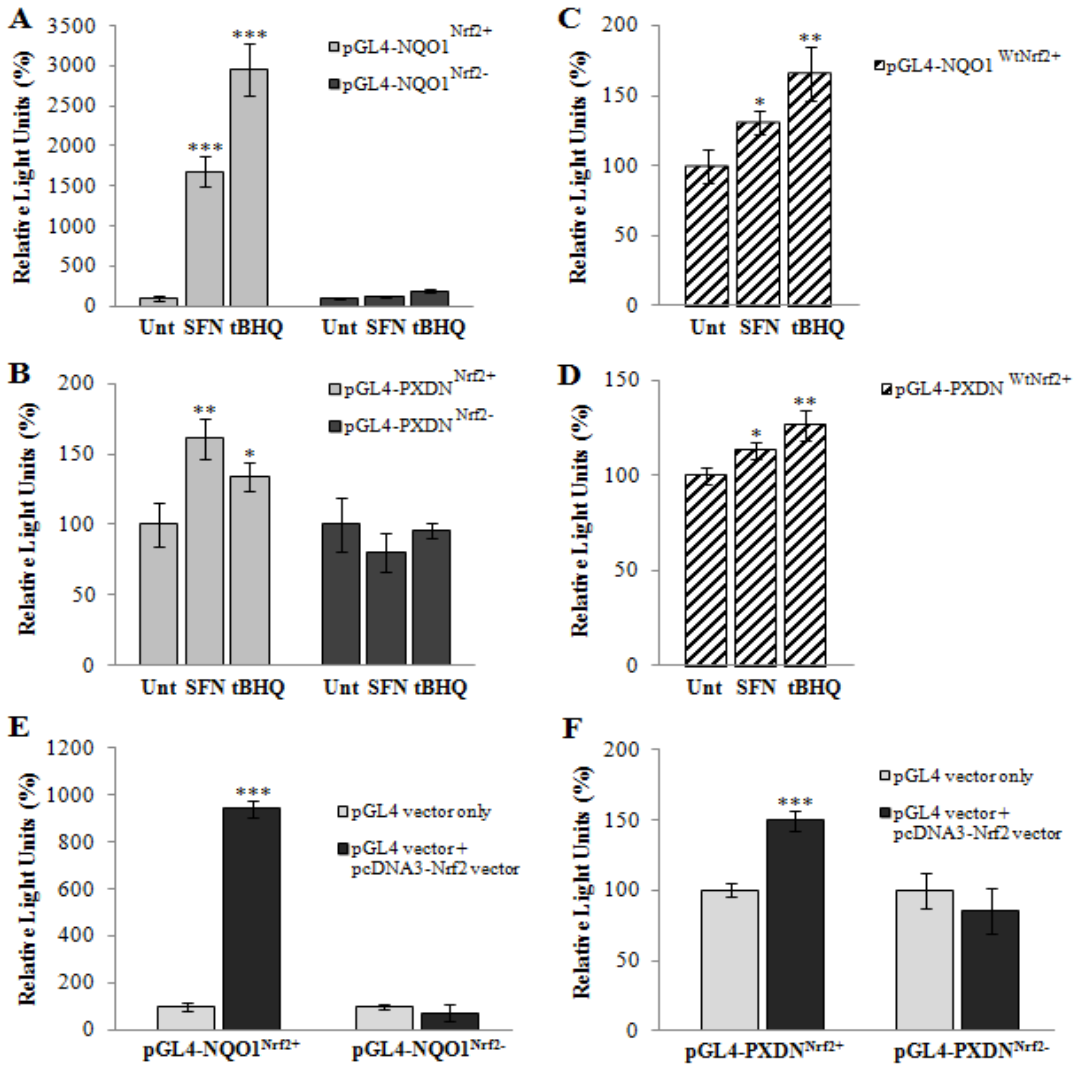

Figure 2.9: Luciferase reporter gene expression for the *PXDN* and *NQO1* promoter regions. A) HEK293 cells were transfected with luciferase reporter vector constructs and treated with 5 μM SFN or 40 μM tBHQ for 24 h. Increased luciferase reporter gene expression was detected in pGL4-NQO1^{Nrf2+} transfected and treated cells while the pGL4-NQO1^{Nrf2-} region showed a small and statistically insignificant increase. **B)** Increased luciferase reporter gene expression was detected in the pGL4-PXDN^{Nrf2+} transfected and treated cells, but not with the pGL4-PXDN^{Nrf2-} promoter region. **C)** The smaller pGL4-NQO1$^{WtNrf2+}$ construct increased luciferase reporter gene expression after treatment; **D)** transfection with pGL4-PXDN$^{WtNrf2+}$ and treatment also resulted in a significant increase. **E)** Luciferase reporter gene expression increased in cells co-transfected for 24 h with pcDNA3-EGFP-C4-Nrf2 and the positive control gene promoter pGL4-NQO1^{Nrf2+} but not with pGL4-NQO1^{Nrf2-}. **F)** Significantly increased luciferase reporter gene expression was detected for cells co-transfected with pcDNA3-EGFP-C4-Nrf2 and pGL4-PXDN^{Nrf2+}, with no increase for pGL4-PXDN^{Nrf2-}. For all experiments, n = 3, mean ± SD.

To further verify the Nrf2 binding site, the putative site within PXDN$^{WtNrf2+}$ was mutated and cloned into the pGL4.10 vector. We tested two mutants PXDN$^{Mt1Nrf2+}$ and PXDN$^{Mt2Nrf2+}$ (Figure 2.10C). We also mutated the Nrf2 site within NQO1$^{WtNrf2+}$ to serve as a control (NQO1$^{MtNrf2+}$) (Figure 2.10A). HEK293 cells were either transfected with these constructs alone or were co-transfected with the pcDNA3-EGFP-C4-Nrf2 vector for 24 h; luciferase assays were then performed. We observed that luciferase reporter gene expression significantly increased when either pGL4-NQO1$^{WtNrf2+}$ (893 ± 173%) or pGL4-PXDN$^{WtNrf2+}$ (218 ± 37%) were co-transfected with the pcDNA3-EGFP-C4-Nrf2 vector (Figure 2.10B and 2.10D, respectively). Interestingly, transfection with the mutated pGL4-NQO1$^{MtNrf2+}$ vector alone gave higher luciferase reporter gene expression (300 ± 22%) than transfection with pGL4-NQO1$^{WtNrf2+}$ alone. However, co-transfection with the pGL4-NQO1$^{MtNrf2+}$ construct and pcDNA3-EGFP-C4-Nrf2 did not result in as great an increase (802 ± 253%) as compared to the Nrf2 co-transfection involving pGL4-NQO1$^{WtNrf2+}$ (Figure 2.10B). Co-transfection with the pcDNA3-EGFP-C4-Nrf2 vector and the pGL4-PXDN$^{Mt1Nrf2+}$ mutant vector resulted in a slight increase in downstream luciferase reporter gene expression compared to transfection with pGL4-PXDN$^{Mt1Nrf2+}$ alone; however, both single and pcDNA3-EGFP-C4-Nrf2 co-transfections involving pGL4-PXDN$^{Mt1Nrf2+}$ exhibited significantly decreased luciferase expression levels as compared to transfection with pGL4-PXDN$^{WtNrf2+}$ alone (38 ± 8% and 51 ± 3%, respectively) (Figure 2.10D). Conversely, transfection with pGL4-PXDN$^{Mt2Nrf2+}$ alone and co-transfection with the pcDNA3-EGFP-C4-Nrf2 vector resulted in significantly increased luciferase reporter gene expression as compared to transfection with pGL4-PXDN$^{WtNrf2+}$ alone (301 ± 40% and 830 ± 214%, respectively) (Figure 2.10D).

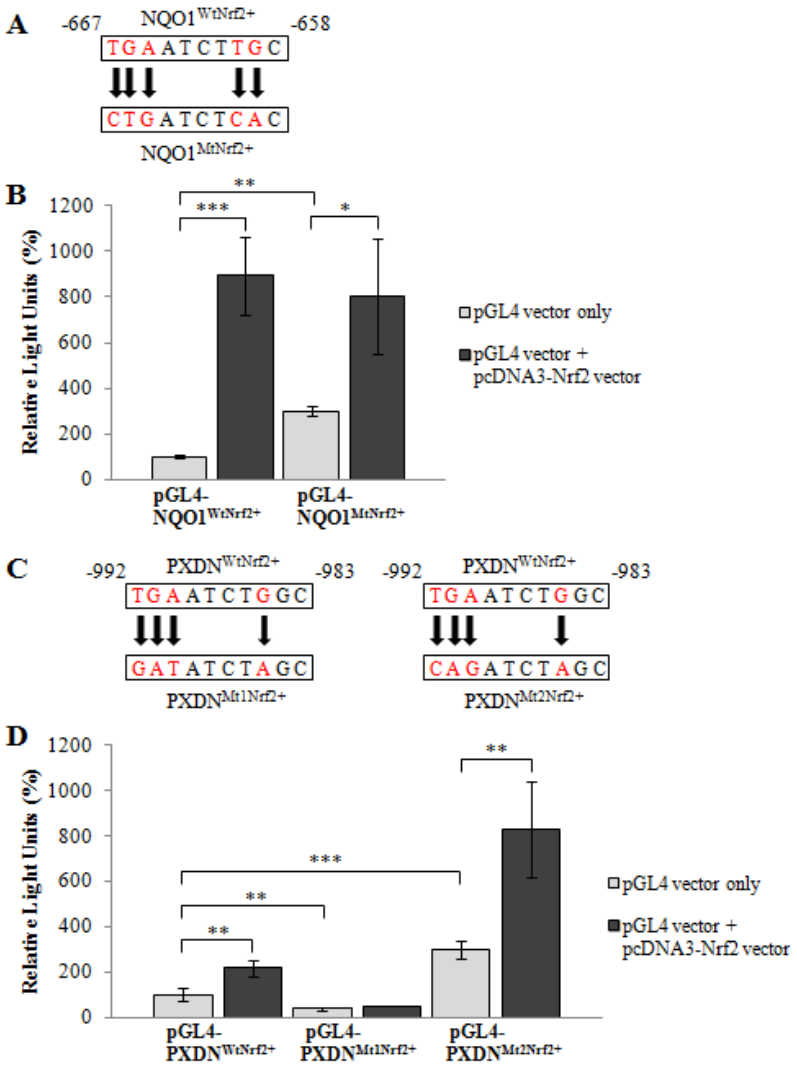

Figure 2.10: Luciferase reporter gene expression assays on mutant *PXDN* and *NQO1* promoter regions. A) and **C)** Sequences display normal and mutated Nrf2 binding sites within NQO1^{Nrf2+} and PXDN^{Nrf2+} respectively. Numbering is relative to the translation start site. **B)** HEK293 cells were transfected with the shorter *NQO1* promoter regions alone or co-transfected with pcDNA3-EGFP-C4-Nrf2 for 24 h. Luciferase reporter gene expression increased with co-transfection involving pGL4-NQO1$^{WtNrf2+}$. Transfection with pGL4-NQO1$^{MtNrf2+}$ alone had higher light output than pGL4-NQO1$^{WtNrf2+}$ alone. Co-transfection with pGL4-NQO1$^{MtNrf2+}$ did not result in as great an increase in light output as compared to pGL4-NQO1$^{WtNrf2+}$ co-transfection. **D)** HEK293 cells were transfected with shorter *PXDN* promoter regions alone or co-transfected with pcDNA3-EGFP-C4-Nrf2 for 24 h. Light output doubled with co-transfection involving pGL4-PXDN$^{WtNrf2+}$. Transfections involving pGL4-PXDN$^{Mt1Nrf2+}$ exhibited lower light output compared to pGL4-PXDN$^{WtNrf2+}$, while transfections involving pGL4-PXDN$^{Mt2Nrf2+}$ had greater light output. For all experiments, n = 3, mean ± SD.

2.4. Discussion

PXDN is potentially involved in the pathogenesis and progression of a variety of diseases such as fibrosis and cancer and although the exact functions of PXDN are still being elucidated, PXDN has been shown to respond H_2O_2 and facilitate the consolidation of the ECM (Péterfi *et al*., 2009; Tauber *et al*., 2010; Bhave *et al*., 2012; Paumann-Page *et al*., 2017). Due to the known functions of PXDN and involvement with ROS, we investigated whether the master redox response regulator, Nrf2, is involved in the regulation of *PXDN* as very little research into the regulation of *PXDN* has been conducted even though it is a potential therapeutic target for several conditions.

Firstly, our data indicates that PXDN expression increased in the presence of H_2O_2 which correlates to previous studies where PXDN was shown to increase with H_2O_2 treatment in a time and concentration dependent manner (Cheng *et al*., 2008; Shi *et al*., 2011; Zhang *et al*., 2012). We observed that PXDN expression of both HEK293 and HeLa cell lines increases upon treatment with the Nrf2 specific inducers, SFN and tBHQ, suggesting that there may be a link between Nrf2 activation and PXDN expression. This interaction between Nrf2 and PXDN was identified and confirmed using ChIP, where we showed that Nrf2 binds to a specific region within the *PXDN* promoter in which we identified a putative Nrf2 binding site. Furthermore, Nrf2 binding increased with the activation of Nrf2 by the inducers SFN and tBHQ. Subsequently, we performed luciferase reporter assays to show that Nrf2 drives expression from the *PXDN* promoter region containing the putative Nrf2 binding site. Data showed that similarly to *NQO1*, the *PXDN* promoter region containing the putative Nrf2 site drives the activation of luciferase reporter gene expression upon treatment with Nrf2 inducers. Although SFN and tBHQ are known inducers of Nrf2, we also employed a more direct means of increasing Nrf2 levels through the use of an Nrf2 over-expression vector. Transient transfections with the pcDNA3-EGFP-C4-Nrf2 vector showed that PXDN expression is increased with increased levels of Nrf2– further highlighting a somewhat more direct interaction between the two proteins. Subsequently, additional luciferase assays involving co-transfections with the pcDNA3-EGFP-C4-Nrf2 vector and pGL4-PXDN promoter constructs, confirmed that Nrf2 regulates PXDN expression.

Additionally, we performed mutagenesis experiments involving the putative Nrf2 binding site within the *PXDN* promoter; these revealed that modifications of this specific sequence resulted in altered responses to Nrf2 over-expression, although the data from the mutagenesis

studies were unexpected. Mutagenesis of the Nrf2 site within the positive control *NQO1* promoter resulted in increased downstream expression of the luciferase reporter gene, as did co-transfection with the pcDNA3-EGFP-C4-Nrf2 vector, although this was not as great an increase as observed for the normal/wild type sequence. The PXDN$^{Mt1Nrf2+}$ construct resulted in significantly lower luciferase reporter gene expression, even with co-transfection of the pcDNA3-EGFP-C4-Nrf2 vector, which is usually expected from mutagenesis studies. However, similarly to *NQO1* mutagenesis, transfections with PXDN$^{Mt2Nrf2+}$ resulted in substantially increased gene expression as compared to the normal/wild type sequence.

Albeit unusual, upon further investigation, we speculated that the binding affinity of Nrf2 was increased by the PXDN$^{Mt2Nrf2+}$ mutant sequence. Nrf2 is an exceptionally versatile TF and although there is a common consensus binding sequence, TGAnTCnGCn, Nrf2 has the ability to associate with a multitude of sequence variants where 'n' may represent either of the four DNA nucleotides: T, G, A or C (Chorley *et al*., 2012; Kuosmanen *et al*., 2016). Kuosmanen *et al*. (2016) designed a mathematical model to calculate the likely binding affinity of Nrf2 to variations within a promoter sequence. The model uses an Nrf2 consensus sequence located within the *NQO1* promoter as a reference; a variance table was then designed from comparing experimentally determined Nrf2 binding sequences within multiple gene promoters to the reference sequence. Each DNA nucleotide was then appointed a specific score for binding strength for each position of the Nrf2 binding sequence. The score for the specific nucleotides at each position are then multiplied together and the higher the score, with a score of 1 perfectly matching the reference sequence, the stronger the binding affinity of Nrf2 (Kuosmanen *et al*., 2016). Indeed, when we applied the mathematical model to the *NQO1* and *PXDN* wild type and mutant sequences, we observed that NQO1$^{WtNrf2+}$ has a score of 0.09 and NQO1$^{MtNrf2+}$ a score of 0.0835; PXDN$^{WtNrf2+}$ has a score of 0.202, PXDN$^{Mt1Nrf2+}$ a score of 0 and PXDN$^{Mt2Nrf2+}$ a score of 0.216, which all seem to correlate with the luciferase results (Kuosmanen *et al*., 2016). The score for the NQO1$^{MtNrf2+}$ sequence is very close to, but not as high as, the score of the NQO1$^{WtNrf2+}$ sequence suggesting that the binding affinity for Nrf2 to the mutant sequence is very similar to that of the wild type, which correlates with our observed luciferase results. The score for the PXDN$^{Mt1Nrf2+}$ sequence is 0, which suggests that the binding affinity of Nrf2 will be significantly less than that of PXDN$^{WtNrf2+}$, as demonstrated by our luciferase results. On the other hand, the score for PXDN$^{Mt2Nrf2+}$ is greater than that of the PXDN$^{WtNrf2+}$ sequence meaning that Nrf2 is more

likely to bind to the mutated Nrf2 binding sequence than wild type which also explains our observations from the luciferase assay.

Although the results from the mutagenesis studies were not entirely as expected, the fact that the luciferase reporter gene expression driven by Nrf2 activation was altered by the sequence variation, confirms the probable Nrf2 binding sequence within the *PXDN* promoter which is TGAATCTGGC. Since this is the first time that this TF has been identified in the involvement of PXDN regulation, the reasons for this interaction can only be hypothesised.

As previously mentioned, PXDN is predominantly expressed in the cardiovascular system and so the connection to Nrf2 relate to the functions in this tissue type (Cheng *et al*., 2008). It is known that PXDN utilises H_2O_2 to produce hypohalous acids, which is also a well-established function of the PXDN family relative, MPO. MPO is greatly involved in immune defence by neutrophils and mononuclear phagocytes as MPO is able to generate HOCl that is involved in an oxidative burst against foreign micro-organisms (Gaut *et al*., 2001; Klebanoff, 2005; Davies *et al*., 2008; Cheng *et al*., 2011; Li *et al*., 2012; Paumann-Page *et al*., 2017). It is therefore plausible that PXDN may also be involved in similar antibacterial innate immune defence mechanisms within the cardiovascular system (Cheng *et al*., 2011; Shi *et al*., 2011; Li *et al*., 2012; Zhang *et al*., 2012). A previous study has already shown that HOCl produced by PXDN kills bacteria, such as *E.coli*, and most likely has an antimicrobial function within circulating plasma where it is secreted (Cheng *et al*., 2011; Li *et al*., 2012). Nrf2 may thus bind to PXDN in these instances in order to promote an immune response (Thimmulappa *et al*., 2006; Reddy *et al*., 2009). Indeed, Nrf2 has been shown to activate HO-1 during the innate immune response due to the ability of HO-1 to direct cytotoxic free haem into haem-containing metabolites thus reducing inflammation (Wagener *et al*., 2003). As mentioned earlier, HO-1 and PXDN expression has been linked, albeit in a cancer context, and this supports the notion that Nrf2 may therefore activate PXDN in similar immune processes (Tauber *et al*., 2010).

Another reason that Nrf2 may activate PXDN could be during wound healing. PXDN has a conserved peroxidase domain as well as additional ECM-interacting domains that allow it to catalyse dityrosine cross-links (Cheng *et al*., 2011). MPO has also been shown to catalyse dityrosine cross-links during the inflammatory response caused by neutrophils so it is probable that PXDN may be capable of forming these cross-links during injury (Heinecke *et al*., 1993). Recent evidence shows that Nox4 deficiency results in impaired cross-linking

during wound healing and since PXDN utilises H_2O_2 produced by Nox, it is possible that PXDN may be the protein responsible for the formation of these cross-links (Cheng *et al*., 2008; Ma *et al*., 2013; Liu *et al*., 2014; Lévigne *et al*., 2016). Furthermore, Nrf2 is able to cause changes in cellular movement and architecture through ECM modifications and has recently been shown to be important during the wound healing process in diabetes (Rachakonda *et al*., 2010; Kim *et al*., 2012). Diabetic patients are known to have higher levels of oxidative stress and as a result, develop skin ulcers that do not heal efficiently (Long *et al*., 2016). A study found that *Nrf2*$^{-/-}$ diabetic mice have delayed wound closure which was alleviated by treatment with SFN (Long *et al*., 2016). Since our data indicates that PXDN expression increases in response to SFN, it is possible that Nrf2 may activate PXDN in order to prevent infection, through the use of its peroxidase domain, as well as to enhance dityrosine and collagen IV cross-links required for wound closure. It may be worth investigating whether there is an alteration in PXDN expression in the wounded areas of diabetic patients as it may be an effective therapeutic target.

PXDN is able to consolidate and alter the ECM by using hypohalous acid intermediates to form sulfilimine bonds (Bhave *et al*., 2012; McCall *et al*., 2014; Lázár *et al*., 2015; Paumann-Page *et al*., 2017). It should be noted that these sulfilimine bonds have been shown to be reversible in reducing environments and could therefore be a feature in vascular tissues that require a degree of plasticity or whose tissue architecture is required to respond to the redox status of the cell (Vanacore *et al*., 2009; Dyksterhuis *et al*., 2011). Atherosclerosis is an inflammatory condition where blood flow becomes restricted due to the narrowing and hardening of arteries (Stoneman and Bennett, 2004). PXDN has already been implicated in the mediation of ox-LDL-induced endothelial cell apoptosis– a process which is thought to increase inflammation and injury in cardiovascular tissue and accelerate atherosclerosis initiation and progression (Stoneman and Bennett, 2004; Bai *et al*., 2011; Ma *et al*., 2013). PXDN has also been implicated in atherosclerosis development through the oxidation and subsequent dysfunction of the lipid transportation glycoprotein apolipoprotein E and through the promotion of vascular tissue calcification/hardening (Yang *et al*., 2013; Tang *et al*., 2015). An interesting link between Nrf2, PXDN and atherosclerosis is that Nrf2 may activate PXDN in order to regulate NO produced by endothelial nitric oxide synthase (eNOS) (Liu Z. *et al*., 2017). NO is an important signalling molecule within the vascular system that is able to protect against atherosclerosis by modulating endothelial vascular tone, inflammation and blood pressure; however, excess levels of NO can actually induce apoptosis resulting in

inflammation and disease (Rochette *et al*., 2013; Liu Z. *et al*., 2017). The levels of NO therefore need to be regulated. NO has been shown to activate Nrf2 resulting in downstream ARE gene activation such as HO-1, it is therefore possible that Nrf2 may also activate PXDN (Liu *et al*., 2007; Howden, 2013). Nrf2 may activate PXDN in order to regulate NO levels since PXDN has been shown to decrease NO production through the inhibition of eNOS using HOCl (Liu Z. *et al*., 2017). PXDN reduces NO levels potentially resulting in a decrease in muscle relaxation that is usually induced by NO and PXDN itself may stiffen muscle through modifying sulfilimine bonds within the ECM. Mutations in Nrf2 in vascular structures were shown to cause alterations in endothelial cell function and cells became unresponsive to oxidative stress resulting in compromised cell movement and decreased smooth muscle contractibility– requirements for the development of atherosclerosis and asthma (Rangasamy *et al*., 2005; Kim *et al*., 2010; Rachakonda *et al*., 2010). Over-expression of Nrf2 and subsequent over-expression of PXDN may also result in excess ROS production, since the uncoupling of eNOS increases superoxide production, causing apoptosis, inflammation, enhanced BM stiffening by PXDN and ultimately, accelerated atherosclerosis progression (Howden, 2013; Rochette *et al*., 2013; Liu Z. *et al*., 2017). Asthma is a chronic lung disease characterised by difficult breathing due to the narrowing of the airways created by chronic inflammation; due to the similarities between atherosclerosis and asthma initiation, it could be worth investigating whether PXDN has a role to play in the disease especially since Nrf2 mutations are common within these diseases (Rangasamy *et al*., 2005). A recent study also found PXDN to be over-expressed in the lung tissues of patients suffering from lung conditions, such as asthma and pulmonary fibrosis, resulting from sulphur mustard exposure and the accompanied increased ROS production (Tahmasbpour *et al*., 2016). The researchers only hypothesised that PXDN was facilitating the thickening of the BM that was observed in mustard lung patients and did not investigate Nrf2 expression, but based on the similarities between atherosclerosis and asthma, PXDN may have been involved in altering the level of NO which was also found to be decreased in the lung biopsies samples (Tahmasbpour *et al*., 2016). It would be beneficial to further monitor the regulation of PXDN in atherosclerosis, and potentially in asthma, as it may be a therapeutic target in order to prevent initiation and progression of these diseases.

PXDN has a major role within eye development as several studies have found a strong association between PXDN mutations and individuals who suffer from corneal opacification, congenital cataracts and congenital glaucoma (Khan *et al*., 2011; Choi *et al*., 2015; Micheal

et al., 2016). Indeed, PXDN KO mouse models display phenotypes such as microphthalmia (abnormally small eyes) and other phenotypes that are associated with anterior segment dysgenesis such as corneal opacity; this suggests that PXDN is essential for eye development (Yan, X. *et al*., 2014). The exact role of PXDN within the eye is still unknown, but it is hypothesised that PXDN may protect the eye from oxidative damage through its use of H_2O_2 (Khan *et al*., 2011). Interestingly, Nrf2 has been shown to be expressed within the eye and plays a role in preventing oxidative damage to the eye caused by environmental factors such as UV radiation and cigarette smoke (Nakagami, 2016). Nrf2 protects the eye by activating ARE genes that remove excess ROS, such as HO-1, and are able to repair wounds within the eye created from oxidative stress (Liu X.F. *et al*., 2017). Since Nrf2 has been shown to bind to and upregulate PXDN, perhaps Nrf2 activates PXDN within the eye in order to carry out antioxidant reactions and repair wounds. Therefore, the cause of the above eye diseases may be due to the inability of mutated PXDN to prevent oxidative damage, especially in patients with corneal clouding which is a consequence of aggregate formation resulting from proteins and lipids in the eye being oxidised by excessive ROS (Khan *et al*., 2011; Yan, X. *et al*., 2014). It would be of interest to determine the expression levels of Nrf2 within these patients in order to investigate the link between Nrf2 and PXDN further.

Due to the broad nature of both established and putative functions of PXDN, the interaction between Nrf2 and PXDN was investigated in two different cell types: HEK293 and HeLa. HEK293 cells treated with either H_2O_2 or the Nrf2 inducers resulted in a great deposition of PXDN into the ECM surrounding the cells which corroborates previous findings. Fibrosis is a potentially life-threatening condition that occurs when tissue repair goes awry resulting in elevated ECM deposition and tissue hardening causing organ dysfunction (Shin *et al*., 2010). Interestingly, studies found that elevated PXDN expression is involved in kidney damage and fibrosis; TGF-β1-induced myofibroblast differentiation causes greater deposition of PXDN into the ECM thereby forming a fibril-like network (Péterfi *et al*., 2009). In kidney fibrosis, TGF-β1 was found to increase ROS formation through the upregulation of Nox4 and since Nox4 is a supplier of H_2O_2 to PXDN, it would be interesting to determine if the elevated deposition of PXDN is regulated by Nrf2 (Hecker *et al*., 2009; Okamura and Pennathur, 2015). Furthermore, the production of hypohalous acids and ox-LDL have also been implicated in renal fibrosis and diabetes-related nephropathy; features that are clearly linked to PXDN expression (Chade *et al*., 2005; Brown *et al*., 2015; Okamura and Pennathur, 2015).

In this instance, the role of Nrf2 and its link to PXDN in fibrosis progression should be investigated further in order to determine possible therapeutic targets for the condition.

Regarding the increase in PXDN expression upon Nrf2 activation in HeLa cells specifically, aberrant PXDN expression has previously been observed in cancer, with both up and down-regulation seen in different cancer types such as breast, melanomas, glioblastomas and ovarian and prostate tumours (Liu *et al*., 2010; Tauber *et al*., 2010; Barnett *et al*., 2011). The roles for PXDN in cancer have yet to be determined; perhaps without PXDN stabilisation of the ECM, cancer cells are able to detach from their surroundings to become more motile and therefore metastatic. Indeed, PXDN has been shown to influence HO-1 mediated cellular attachment whereby silencing of PXDN resulted in decreased cellular attachment of choriocarcinoma cells and PXDN has also been shown to promote invasion of melanoma cells (Tauber *et al*., 2010; Jayachandran *et al*., 2016). Interestingly, inactivating mutations in Nrf2 have been correlated to increased cancer cell metastasis and whilst this is not well understood, the evidence of Nrf2 regulating PXDN suggests an involvement of PXDN in this process (Vanacore *et al*., 2009; Satoh *et al*., 2010; Moriguchi, 2016). Perhaps with less PXDN activation by Nrf2, cancerous cells may detach from the ECM due to diminished sulfilimine bond formation and become metastatic. On the contrary, other studies have found that cancer patients that exhibit Nrf2 over-expression have higher metastatic incidence and have a poorer prognosis than patients with lower Nrf2 expression (Guo and Shen, 2017). In this instance, over-activation of Nrf2, and subsequent over-expression of PXDN, may result in increased cancer metastasis through PXDN stiffening collagen IV in the ECM and formation fibrous networks (Péterfi *et al*., 2009; Bhave *et al*., 2012). This hypothesis may be confirmed by examining instances of breast cancer metastasis and hepatocellular carcinoma, where thickened collagen IV networks have been observed and cancer cells have been shown to travel along these hardened networks thus migrating and spreading to other organs; as such the role of PXDN expression within these stiffened networks should be investigated (Wyckoff *et al*., 2007; Fang *et al*., 2014). It is clear that the balance between Nrf2 and PXDN expression is crucial at different stages of cancer initiation and progression and identifying this balance in processes such as epithelial-mesenchymal transition (EMT), could identify novel therapeutic targets as well as new prognostic markers (Radisky, 2005; Giannoni *et al*., 2012; Guo and Shen, 2017).

In conclusion, this is the first study to show that PXDN is regulated by the redox responsive master regulator Nrf2. Nrf2 binds to the putative ARE site, TGAATCTGGC, within the *PXDN* promoter and enhances PXDN protein expression during oxidative stress. The discovery of this regulatory mechanism identifies PXDN as a novel ECM protein candidate that may participate in multiple redox-related processes and modifications in both normal and disease states. Since PXDN expression has to date been implicated in multiple diseases such as atherosclerosis, fibrosis and cancer, it would be beneficial to further investigate the functional aspects of the link between Nrf2 and PXDN within these pathological states as PXDN may serve as a novel therapeutic target for many different conditions.

Chapter 3: PXDN influences migration and invasion in cervical cancer during oxidative stress

3.1. Introduction

3.1.1. EMT and oxidative stress

EMT is a cellular process that occurs when epithelial cells alter gene and protein expression patterns, which change cell-cell and cell-ECM interactions that allow cells to dissociate from neighbouring cells and tissues. Such cells transition from cells with epithelial properties to cells with characteristics of the mesenchymal phenotype (Giannoni *et al*., 2012). Cells undergo EMT during various physiological processes, such as when cells need to move from their current location, and then, once cells have moved to their new location, they often undergo a reverse transition process known as MET (Yang and Weinberg, 2008). EMT occurs both in regular and irregular processes and has been categorised into three types: Type I, II and III (Kalluri and Weinberg, 2009; Giannoni *et al*., 2012).

An interesting aspect of all three types of EMT, is that ROS, and in some cases oxidative stress, greatly influence initiation and progression of all types of EMT. More recently, the effects of ROS, including H_2O_2, on cellular processes are being elucidated, with one major recent focus being the influence of ROS on EMT (Holmström and Finkel, 2014; Gill *et al*., 2016). Whilst the exact roles of ROS in the aforementioned three types of EMT are still being investigated, several studies have determined that oxidative stress has a major influence on Type II and Type III EMT, which are responsible for the pathogenesis of fibrosis and cancer metastasis, respectively (Mori *et al*., 2004; Kalluri and Weinberg, 2009; Gill *et al*., 2016).

Type I EMT takes place during early embryonic development, when undifferentiated cells are required to move into different positions before becoming specialised cells through MET, as well as during embryo implantation (Yang and Weinberg, 2008; Nieto *et al*., 2016). Whilst there is little information regarding the effects of ROS on Type I EMT, ROS are known to have an important role in activating cell signalling pathways in the developing embryo and can influence proliferation, apoptosis and cellular respiration (Guérin *et al*., 2001; Harvey *et al*., 2002). Embryonic cells have also been shown to activate antioxidant proteins and control levels of ROS in the early stages of development and studies on embryos used for *in vitro* fertilisation have demonstrated oxidative stress has a negative effect on embryo development

(Harvey *et al*., 2002; Bedaiwy *et al*., 2004). Since ROS play an important role as signalling molecules, further examination of the effect of ROS on Type I EMT in relation to developmental disorders would be worthwhile.

Type II EMT occurs during the process of wound healing and tissue regeneration when cells need to migrate towards a site of injury in order to repair the damage (Kalluri and Weinberg, 2009). When an injury occurs, four events take place: coagulation/blood clotting, inflammation, cellular proliferation and ECM remodelling (Ambrozova *et al*., 2017). Recent research has established that ROS are involved, and are often essential, in all four wound healing events, as observed in Figure 3.1 (André-Lévigne *et al*., 2017; Dunnill *et al*., 2017). Physical trauma results in an increase in ROS, which occurs primarily as part of the immune response. Macrophages and neutrophils arrive at the injury site and undergo respiratory bursts of ROS in order to destroy foreign microorganisms and protect against infection (Li *et al*., 2012). Once the inflammation starts to subside, ROS trigger cell proliferation in the area of the injury which assists in wound closure (André-Lévigne *et al*., 2017). In addition to this, Type II EMT occurs, where cells near the wound assume mesenchymal characteristics in order to move along the edges and seal the injury. Cells undergoing Type II EMT have been found to be essential during wound healing as openings are closed faster by moving cells rather than by enhanced proliferation (Lévigne *et al*., 2016; André-Lévigne *et al*., 2017). Although ROS have been shown to promote keratinocyte migration and are most likely involved in triggering pathways that alter cell-ECM interactions, it is still not entirely clear how ROS are fully involved during Type II EMT (Dunnill *et al*., 2017). Once Type II EMT cells have closed the wound, cells will undergo MET in order to remodel the ECM and complete the repair process. Collagen is especially important in the wound healing process and organises into thick fibril networks during these final healing stages (Ehrlich and Hunt, 2012; Lévigne *et al*., 2016). One recent study found that ROS produced by Nox4 are able to modify the ECM deposition pathways especially during MET, as Nox4-deficient mice had impaired wound repair compared to wild type due to insufficient collagen IV cross-linking (Lévigne *et al*., 2016). From a pathology perspective, a dysregulated response during wound healing can lead to an inflammatory response that produces excessive oxidative stress that can have detrimental effects, commonly in the form of fibrosis (Kalluri and Weinberg, 2009). During chronic oxidative stress, cells continuously undergo Type II EMT and excessively deposit ECM components thus resulting in hardened tissue as observed in cases of kidney fibrosis (Péterfi *et al*., 2009; Shin *et al*., 2010). Studying the involvement of ROS during

Type II EMT may also open new avenues for therapeutic options for treatment of chronic inflammation and fibrosis. ROS are therefore important during both Type II EMT and MET.

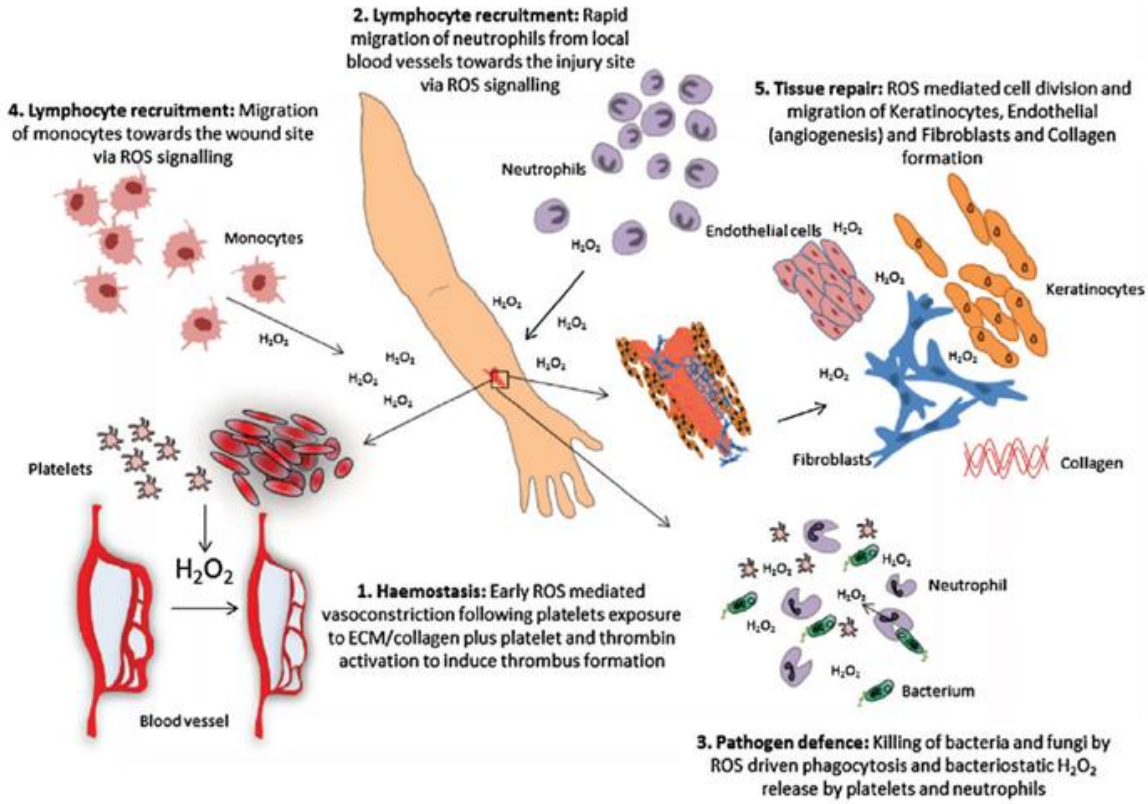

Figure 3.1: Role of ROS during wound healing. ROS are involved at all four stages of wound healing including blood clotting, inflammation, cell proliferation and ECM remodelling (Dunnill *et al*., 2017).

Type III EMT is observed during cancer development and progression whereby cancer cells separate from tumours, become motile and metastasise to other areas of the body (Porporato *et al*., 2014). More recently, the extent of the role of ROS and oxidative stress on this form of EMT is being appreciated as both vast and greatly complex (Jordan *et al*., 2011; Nieto *et al*., 2016; Jian *et al*., 2017). Studies have found that different cancer cell types respond differently to varied levels of ROS, and that ROS at different stages of EMT have varying consequences (Poillet-Perez *et al*., 2015; Gill *et al*., 2016; Jayachandran *et al*., 2016). Adding to the complication of understanding Type III EMT, is the emerging evidence that not all cancerous cells undergo the full transition and may stably exist at intermediate stages (Figure 3.2) (Nieto *et al*., 2016).

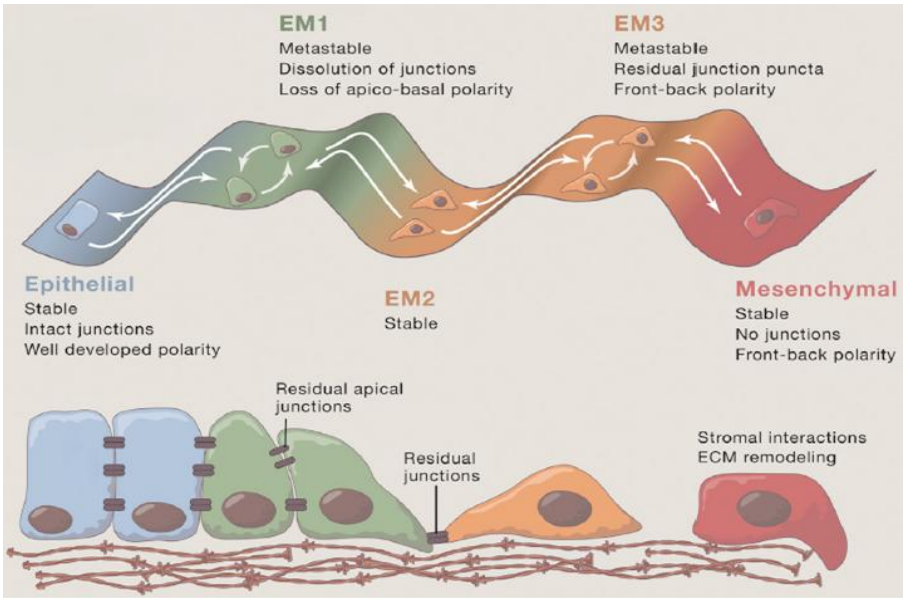

Figure 3.2: Intermediary stages of Type III EMT. Certain cancer cells have the ability to exist at intermediate (EM) stages of EMT and do not need to transition fully into mesenchymal cells (Adapted from Nieto *et al*., 2016).

The ECM is comprised of a network of proteins such as collagen IV, laminin and fibronectin and receptor proteins known as integrins help connect cells to this protein substrate (McCall *et al*., 2014). In addition to cell-ECM contacts, there are connections that hold neighbouring cells together, such as tight and adherens junctions (Zavadil and Böttinger, 2005). Regular cells are therefore anchored to both the ECM and to other cells and these interactions are modified when cancer cells undergo Type III EMT (Mitra *et al*., 2015). The process of Type III EMT is often triggered when DNA is damaged leading to altered expression patterns of many different proteins especially TFs (Gill *et al*., 2016). For instance, DNA damage can result in increased Nrf2 activation which enhances the expression of antioxidant proteins that promote cell survival and can remodel the ECM (Jung *et al*., 2018). Snai1 activation is also often enhanced in Type III EMT which leads to reduced E-cadherin expression, and therefore fewer adherens junctions, thus allowing cells to separate from each other (Zavadil and Böttinger, 2005). During Type III EMT, the expression patterns of integrins are also altered to allow cells to move along or through the ECM (Giannoni *et al*., 2012). A family of proteins known as matrix metalloproteinases (MMPs) are known to degrade various components of the ECM (Kessenbrock *et al*., 2010). Alterations in MMP expression may enhance degradation of the BM, release cells from surrounding tissue and promote cancer cell invasion (Cannito *et al*., 2010).

Since cancer cells undergoing Type III EMT modify cell-cell and cell-ECM interactions, cells undergoing this process have altered characteristics such as: an alteration in cell morphology, decreased proliferation, decreased cell attachment, increased migration and increased invasive ability (Giannoni *et al*., 2012). However, as illustrated in Figure 3.2, cells may not adopt the full mesenchymal phenotype and may exist in stable intermediate stages (Nieto *et al*., 2016). This would mean that cancer cells may undergo EMT but will not exhibit changes in all of the above mentioned features. For example, several breast cancers and ovarian carcinomas have been shown to metastasise by gaining enhanced migratory abilities without becoming invasive or reducing E-cadherin expression (Huang *et al*., 2012; Gao *et al*., 2014).

The process of Type III EMT has been found to be greatly influenced by ROS at various stages with the Nox enzymes being the most common source of ROS (Morry *et al*., 2017). Prolonged oxidative stress often results in the previously mentioned DNA mutations leading to altered protein function (Gill *et al*., 2016). ROS can alter the activation of several TFs, such as Nrf2, leading to altered downstream protein expression (Osburn and Kensler, 2008). ROS are also able to directly affect protein conformation by oxidising cysteine residues that may result in the activation, inactivation or degradation of important proteins necessary for cell anchorage (Giannoni *et al*., 2012). Cell proliferation pathways, such as ERK 1/2, are also altered by ROS which can promote tumour growth. The expression and activation of MMPs has also been shown to be influenced by oxidative stress with enhanced ROS, especially HOCl, increasing MMP expression and activation causing enhanced ECM degradation and cell invasion (Alfakry *et al*., 2016). MMPs not only degrade proteins such as collagen IV within the ECM, but are also able to interact with and degrade integrins, thus allowing cells to detach from the BM and migrate away from the primary tumour (Friedl and Gilmour, 2009). However, cancer cells respond differently to ROS depending on the cell type and factors such as the level of ROS and exposure time.

Although more research into the influence of ROS on Type III EMT is being conducted, there are still many unanswered questions as regards to what proteins and pathways are being activated by ROS and how these influence EMT. Currently, there are a few proteins that have been found to be constantly altered during Type III EMT such as the TF Snai1 and cell-cell adherens junction protein, E-cadherin, so there are definitely proteins that exist as markers for EMT although many proteins influenced by ROS still need to be determined (Nieto, 2002; Zavadil and Böttinger, 2005). The complexity of the role of ROS on cancer metastasis is

making it exceptionally difficult to develop therapeutic options for cancer patients especially since multiple cancer cells undergoing metastasis develop the ability to survive with and become immune to current cancer treatments, especially treatments that would kill the cancer cells by inducing oxidative stress such as those used in chemotherapy (Mitra *et al*., 2015).

Recently, PXDN was found to be involved in Type III EMT as PXDN was shown to be downregulated by the EMT TF Snail1 (Sitole and Mavri-Damelin, 2018). Since PXDN expression can be affected by ROS levels and influences the strength of the ECM, identifying whether a link exists within a ROS-PXDN-EMT pathway, could provide insight into potentially utilizing PXDN expression as a therapeutic target for treating EMT pathologies including cancer and cancer metastases.

3.1.2. Role of PXDN in EMT

PXDN expression has been shown to be upregulated by ROS, such as H_2O_2, and is an important protein that is involved with strengthening and forming the ECM; it can thus be hypothesised that PXDN expression would be altered during EMT (Cheng *et al*., 2008; Shi *et al*., 2011; Bhave *et al*., 2012; Zhang *et al*., 2012).

Biological processes that occur due to Type I EMT include embryo implantation and placenta formation (Kalluri and Weinberg, 2009). A recent study in mice found fluctuations in PXDN expression during the early stages of pregnancy (Jones-Paris *et al*., 2017). Jones-Paris *et al*. (2017) found that PXDN expression decreases during the later stages of pre-implantation and increases again during embryo implantation, suggesting that a decrease in PXDN is necessary before implantation can occur. Collagen IV was also shown to be colocalised with PXDN during embryo implantation where it is hypothesised that PXDN would be responsible for creating new collagen IV cross-links between the uterus and the embryo thus allowing for secure implantation (Jones-Paris *et al*., 2017). Alterations in PXDN expression may thus be important in allowing Type I EMT to occur by adjusting cell-ECM interactions and allowing cells to migrate. It can also be hypothesised that PXDN is an important protein required during MET as cells may be reattached to the BM due to the collagen IV cross-linking capabilities of PXDN. PXDN has also been identified as having an important role during eye development with PXDN mutations resulting in severe corneal opacification, congenital cataracts and congenital glaucoma, which are most likely caused by disruptions to the structural integrity of the ocular BM due to missing PXDN (Khan *et al*., 2011; Yan, X. *et al*., 2014; Micheal *et al*., 2016).

As already mentioned, it is realistic to hypothesise that PXDN is involved in the process of wound healing due to the ability of PXDN to strengthen collagen IV of the BM and potential to act as an antimicrobial agent (Li *et al*., 2012; Paumann-Page *et al*., 2017). Type II EMT that is involved during the healing process requires that cells move to sites of injury; PXDN expression may need to be altered in order to assist with detaching cells from the ECM so cells may become more motile (Dunnill *et al*., 2017). After the migration of cells, cells will need to securely reattach to the ECM of the new location which is a likely role for PXDN to perform. Other studies also propose the involvement of PXDN in wound healing MET since Nox4 deficiency results in decreased ECM cross-links and impaired wound healing; because ROS produced by Nox4 are utilised by PXDN, PXDN is most likely involved during this stage of wound healing (Cheng *et al*., 2008; Lévigne *et al*., 2016). PXDN over-expression has also been identified in patients with kidney fibrosis with PXDN likely contributing to the development of the disease due to the cross-linking capabilities of PXDN (Péterfi *et al*., 2009). Since Type II EMT is involved in wound healing and can lead to fibrosis caused by chronic inflammation, PXDN is likely to be involved in this form of EMT.

Lastly, Type III EMT invokes the alteration of gene expression and enhanced migration of cancer cells and oxidative stress has already been proven to influence the initiation and progression of Type III EMT (Kalluri and Weinberg, 2009; Gill *et al*., 2016). PXDN expression has already been shown to have altered expression in multiple cancer types such as breast cancer, melanomas, glioblastomas and ovarian and prostate tumours (Liu *et al*., 2010; Tauber *et al*., 2010; Barnett *et al*., 2011). However, the exact role of PXDN in cancer in general and in Type III EMT is still relatively unknown. PXDN potentially has a role in Type III EMT due to the ability of PXDN to alter the ECM to allow cells to detach in order to migrate; since PXDN has already been shown to affect Type I and II EMT in this sense, it is highly plausible that a similar role is performed during Type III EMT. PXDN has been shown to influence HO-1 mediated cellular attachment and silencing of PXDN resulted in decreased cellular attachment of choriocarcinoma cells (Tauber *et al*., 2010). A very recent study, from our laboratory, found that the Type III EMT promoting TF, Snai1, binds to the *PXDN* promoter and represses PXDN expression; thus creating a strong possibility that like E-cadherin, silencing of PXDN is necessary for some stages of EMT in cancer cells (Sitole and Mavri-Damelin, 2018).

The role of PXDN in Type III EMT is still mostly unclear and should be a main focus of attention since this form of cellular transition is responsible for cancer metastasis. Having

previously shown that Nrf2 is able to bind to the *PXDN* promoter and upregulate PXDN expression, and having established that ROS and Nrf2 expression have roles to play in Type III EMT, the potential functions of PXDN in Type III EMT were investigated. This was achieved by examining the different and well known features of EMT, such as cell attachment, migration and invasion, and determining what affect silencing of PXDN expression in the presence of oxidative stress had on each of these processes. In addition, a 3D colony formation assay was carried out using soft agar in order to see how PXDN may influence this process in a model that has a more realistic environment to that found *in vivo*. Since the role of PXDN in Type III EMT was to be investigated, two cervical carcinoma cell lines, HeLa and SiHa, were used in the experiments. Both HeLa and SiHa cells have been used in previous studies and have been shown to express PXDN (Sitole and Mavri-Damelin, 2018). HeLa cells also have less metastatic potential as compared to SiHa cells which provided further insight into the role of PXDN in Type III EMT in different cancer types.

3.2. Methods

3.2.1. PXDN knockdown

PXDN expression was silenced in both HeLa and SiHa cell lines using 1 μg of MISSION® esiRNA Human PXDN (Sigma Aldrich, EHU004721) combined with 2.5 μl of TransIT-X2® System transfection reagent (Mirus) in SFM and incubated at RT for 30 min prior to transfection. Cells were transfected for a total 24 h prior to use in downstream assays. A negative control (esi) was included in all experiments whereby the esiRNA for PXDN was replaced with MISSION® esiRNA FLUC which targets firefly luciferase (Sigma Aldrich, EHUFLUC). For all assays, cells were either untreated (siUnt) or treated with 100 μM H_2O_2 (siH_2O_2) which was added to cells 3 h post-transfection and left for the remaining 21 h. Cells treated with 5 ng/ml TGF-β1 (Sigma-Aldrich) for 24 h to serve as controls, were deprived of serum for 24 h prior to treatment.

3.2.2. PXDN quantification using ELISA

In order to quantify changes in PXDN protein expression following transfection performed on small numbers of cells (siRNA treatments), the more sensitive enzyme linked immunosorbent assay (ELISA) was conducted. This was necessary since silencing of PXDN was conducted in wells that would not yield high enough amounts of protein required for PXDN IP. Briefly, HeLa and SiHa cells were seeded into the wells of a 24-well plate (15 000–40 000 cells/well) and after 48 h, were transfected and/or treated as required. Cells were washed twice with 1X PBS and lysed in 300 μl native lysis buffer. Lysates were centrifuged at 4 000 rpm for 10 min at 4 °C to remove cell debris. The level of PXDN expression was determined using the Human PXDN/MG50 ELISA kit (LS-F12454, LifeSpan BioSciences, Inc.) by following the manufacturer's instructions. Absorbance was measured at 450 nm using a Multiskan GO microplate reader. A Bradford assay was also conducted on the lysates, as described previously, to determine the amount of total protein and ELISA values were corrected accordingly.

3.2.3. Observing PXDN knockdown using IF microscopy

Cells were seeded onto glass coverslips and after 48 h were transfected and/or treated as described. IF microscopy was carried out as described in Chapter 2.2.4, to observe PXDN expression in response to PXDN silencing and treatment.

3.2.4. Cell morphology using DIC microscopy

In order to visualise changes to cell morphology that occur during EMT and upon PXDN silencing, DIC microscopy was performed. Briefly, cells were seeded onto glass coverslips and left for 48 h. Cells were then transfected and/or treated as described previously. Live cells were rinsed twice and overlaid with 1X PBS and visualised on an Olympus BX63 microscope under 10X magnification.

3.2.5. Protein expression and localisation during EMT using IF microscopy

Cells were seeded onto glass coverslips and after 48 h, were transfected and/or treated as described. IF microscopy was carried out as described in Chapter 2.2.4, to observe Snai1 (sc-28199), E-cadherin (Cell Signalling Technology, 24E10) and PXDN expression and localisation in response to PXDN silencing and treatment.

3.2.6. MTT assay to determine influence of PXDN on proliferation

The effects of PXDN on cellular proliferation were investigated using the MTT assay. HeLa and SiHa cells were seeded and transfected and/or treated as described. MTT assays were then conducted and the data analysed as described in Chapter 2.2.5.

3.2.7. Cell adhesion assays to determine effect of PXDN on attachment

To determine the effect of PXDN on cellular attachment, HeLa and SiHa cells were first seeded into 24-well plates and after 48 h, were transfected and/or treated. Cells were then trypsinised, counted and 10 000 cells/well seeded into 96-well plates. After 15 min incubation at 37 °C, which is an adequate amount of time to analyse cell attachment, unattached cells were removed by discarding the seeding medium and washing the cells with 1X PBS (Humphries, 2009). Fresh medium was added, cells briefly visualised using an inverted light microscope and cells then returned to the 37 °C incubator. After 1 h, an MTT assay according to Chapter 2.2.5 was performed on all wells in order to determine how many cells had attached.

3.2.8. Scratch assays to determine effect of PXDN on migration

Scratch assays were performed on HeLa and SiHa cells in order to determine the potential role of PXDN during cell migration. Cells were seeded into 24-well plates and following 48 h, were transfected and/or treated. Following 24 h of transfection, culture medium was

removed, cells washed once with 1X PBS and fresh 1X PBS added to cells. A p200 pipette tip was used to create a scratch in each well. The 1X PBS was removed, cells washed once more with 1X PBS to remove detached cells and fresh culture medium added to each well. Scratches were photographed at time 0 h then returned to the 37 °C incubator and cells were photographed again after 12 h and 24 h (and at 48 h for HeLa cells only). Sizes of scratches were measured using ImageJ (Ver. 1.50i) software. Due to the varied sizes of the scratches at 0 h, the size of each scratch following 48 h (for HeLa cells) and 24 h (for SiHa cells) was made relative to the size of the corresponding 0 h scratch for each condition. The relative size of each scratch was plotted on a graph as scratch closure (%) and comparisons of the degree of scratch closure were made between each condition and untreated.

3.2.9. Invasion assays to determine contribution of PXDN to cell invasion

Permeable supports of a 96-well Corning HTS Transwell® plate (Sigma-Aldrich, CLS3374) were each coated with 200 µg/ml ECM gel from Engelbreth-Holm-Swarm murine sarcoma (Sigma-Aldrich, E1270) in SFM and incubated overnight at 37 °C. Residual SFM was removed and supports rehydrated with fresh SFM for 1 h prior to seeding cells. HeLa and SiHa cells were harvested by trypsinisation, and centrifuged for 5 min at 1 500 rpm at 4 °C to collect cells and remove trypsin-EDTA. After being re-suspended in 10% (v/v) FBS culture medium, cells were counted and seeded on top of the ECM-coated supports at 10 000 cells/well. After 3 h in the 37 °C incubator, 10% (v/v) FBS medium was removed and replaced with 1% (v/v) FBS containing medium (SFM for cells to be treated with TGF-β1) and cells returned to the incubator. Following 24 h incubation, cells were transfected and/or treated, and SFM in the chambers below the supports was replaced with 10% (v/v) FBS culture medium to act as a chemoattractant. After 24 h incubation at 37 °C, invaded cells on the permeable supports were fixed for 15 min using 100% (v/v) ice-cold methanol then stained with crystal violet (Table A1) for 20 min. The supports were thoroughly washed with dH_2O and left to dry overnight. Supports were transferred into a new 96-well plate and crystal violet dissolved in 230 µl 10% (v/v) acetic acid for 20 min. Absorbance was measured at 590 nm using a Multiskan GO microplate reader.

3.2.10. Determine function of PXDN in a 3D environment

In order to determine whether PXDN has a role in 3D spheroid formation, a soft agar colony formation assay was performed (Borowicz *et al.*, 2014). The assay involved elevating cells off of the bottom of the culture plate using agar so cells may be able to survive and divide

while suspended. This procedure intended to simulate cell behaviour that may occur in an *in vivo* environment, unlike cells forming a monolayer on a plastic culture dish. Depending on the abilities of the cell types, cancer cells could form 3D structures more similar to *in vivo* growth, thus allowing the role of specific proteins in this process to be investigated.

HeLa and SiHa cells were seeded into 24-well plates and after 48 h, were transfected and/or treated for 24 h. Noble agar (Sigma-Aldrich) solutions (0.6% (w/v)) and (1% (w/v)) were prepared and autoclaved. Once slightly cooled (42 °C), 1% (w/v) Noble agar was diluted 1:1 with 2X cell culture medium (Table A1), 1.5 ml added to each well of a 6-well plate and allowed to solidify at RT for 30 min. A 1X cell culture medium was prepared using the 2X cell culture medium and filter sterilised. Cells were washed twice with 1X PBS, detached using 100 µl 1X PBS and 100 µl Trypsin-EDTA, mixed with 500 µl of 1X cell culture medium and centrifuged at 1 500 rpm for 3 min at 4 °C to remove all traces of trypsin-EDTA. Cells were re-suspended in 300 µl fresh 1X cell culture medium, counted and mixed with 1X cell culture medium to attain 10 000 cells/1.5 ml. An equal volume of cell suspension was mixed with an equal volume of 42 °C 0.6% (w/v) Noble agar and 1.5 ml of this new mixture (5 000 cells/well) was layered onto the solidified 1% (w/v) Noble agar. The cell-containing agar was allowed to set at RT for 30 min followed by incubation at 37 °C for three weeks to allow spheroid formation. To prevent agar desiccation, 200 µl of untreated or treated (100 µM H_2O_2 or 5 ng/ml TGF-β1) 1X cell culture medium was routinely added to the top layer of agar. After three weeks, a 5X5 grid was placed under each well, colonies were visualised using an inverted light microscope at 4X magnification and counted.

3.2.11 Statistical analysis

Unless otherwise stated, all quantification was attained from experiments performed a minimum of three times where n = the number of independent biological replicates ± standard deviation (SD). Comparisons were made by Student's t-tests and $P \leq 0.05$ was considered statistically significant. Significance is made relative to 'Untreated' samples, taken as 100%, unless otherwise specified. Significance is depicted on graphs as follows: *: $P \leq 0.05$, **: $P < 0.01$ and ***: $P < 0.001$.

3.3. Results

3.3.1. PXDN expression is reduced following siRNA transfection

An ELISA assay was first conducted on both HeLa and SiHa cell lines in order to ensure that transfections using PXDN siRNA reduced PXDN expression. Our results showed PXDN siRNA transfections (siUnt) for 24 h successfully decreased PXDN expression by 31% (69 ± 8%) in HeLa cells while treatment with H_2O_2 increased PXDN expression by 28% (128 ± 0%). PXDN expression decreased by 51% (49 ± 14%) when PXDN siRNA transfection was combined with H_2O_2 treatment (siH_2O_2). HeLa cells treated with TGF-β1 also exhibited a 19% (81 ± 15%) decrease in PXDN expression. HeLa cells transfected with the negative control (esi) resulted in a statistically insignificant 20% (80 ± 21%) decrease in PXDN expression and had a large SD (Figure 3.3). The ELISA assay also showed that PXDN expression decreased by 18% (82 ± 6%) following PXDN siRNA transfection (siUnt) in SiHa cells while treatment with H_2O_2 caused a 28% (128 ± 7%) increase in PXDN expression. Knockdown of PXDN combined with H_2O_2 treatment (siH_2O_2) resulted in a 12% (88 ± 5%) decrease in PXDN expression and SiHa cells treated with TGF-β1 showed a 45% (55 ± 11%) decrease. Transfection of SiHa cells with the negative control (esi) did not alter average PXDN expression in SiHa cells although the SD was large (107 ± 32%) (Figure 3.3).

IF microscopy performed on both cell lines corroborates the ELISA data, illustrating decreased PXDN expression (FITC intensity) post-transfection with PXDN siRNA and PXDN expression remained reduced regardless of combination with H_2O_2 treatment (siH_2O_2), which normally increases PXDN expression (Figure 3.4).

To determine whether PXDN may have an effect on EMT, cellular morphology was observed, using DIC, following PXDN siRNA transfection. DIC images showed HeLa cells were elongated and moved towards other clusters of cells regardless of whether cells were treated with H_2O_2 or TGF-β1 (Figure 3.5). Silencing of PXDN (siUnt) did appear to slightly alter cell morphology of HeLa cells especially when transfection was combined with H_2O_2 treatment (siH_2O_2); in this case, HeLa cells appeared more rounded and did not stretch across to fill spaces between other cell clusters (Arrows in Figure 3.5). DIC images of SiHa cells revealed similar results to those observed for HeLa cells as SiHa cells were both elongated and appeared to stretch towards other cells when left untreated or treated with either H_2O_2 or TGF-β1 (Figure 3.5). However, silencing of PXDN (siUnt) in SiHa cells resulted in a rounder

cell morphology and cells preferred to clump together as opposed to stretching out regardless, of whether there was additional treatment with H_2O_2 (siH_2O_2) (Arrows in Figure 3.5).

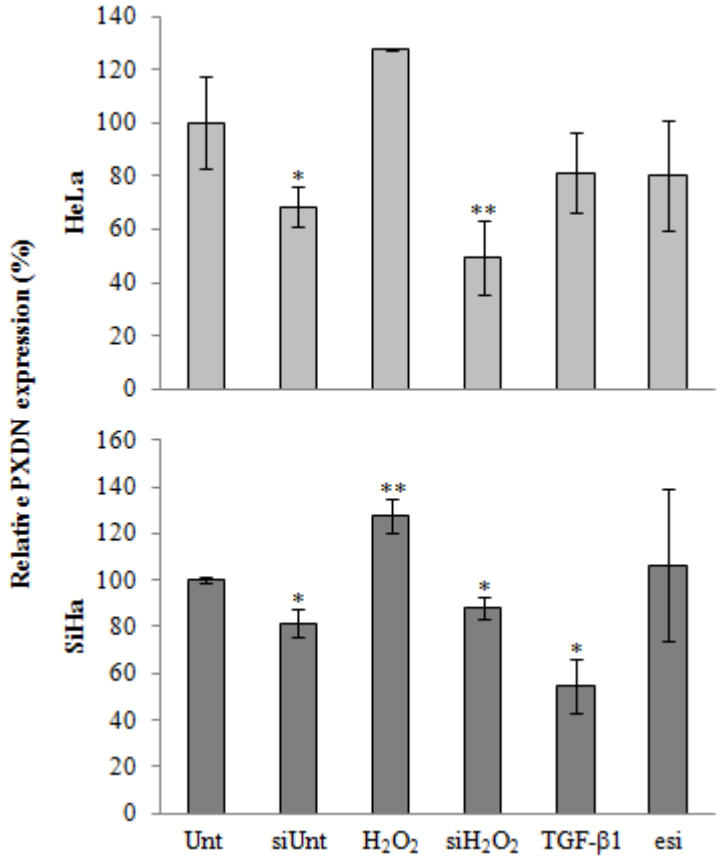

Figure 3.3: Silencing of PXDN in HeLa and SiHa cells. ELISA was performed on HeLa and SiHa cells to measure the degree of PXDN knockdown following transfection with PXDN siRNA for 24 h. Cells were treated with 100 μM H_2O_2 to observe the effects of oxidative stress on PXDN expression. Cells were transfected with PXDN siRNA only (siUnt) or additionally treated with 100 μM H_2O_2 (siH_2O_2). Transfections involving a negative control siRNA (esi) were also performed. Cells were also treated with 5 ng/ml TGF-β1 (n = 3, mean ± SD).

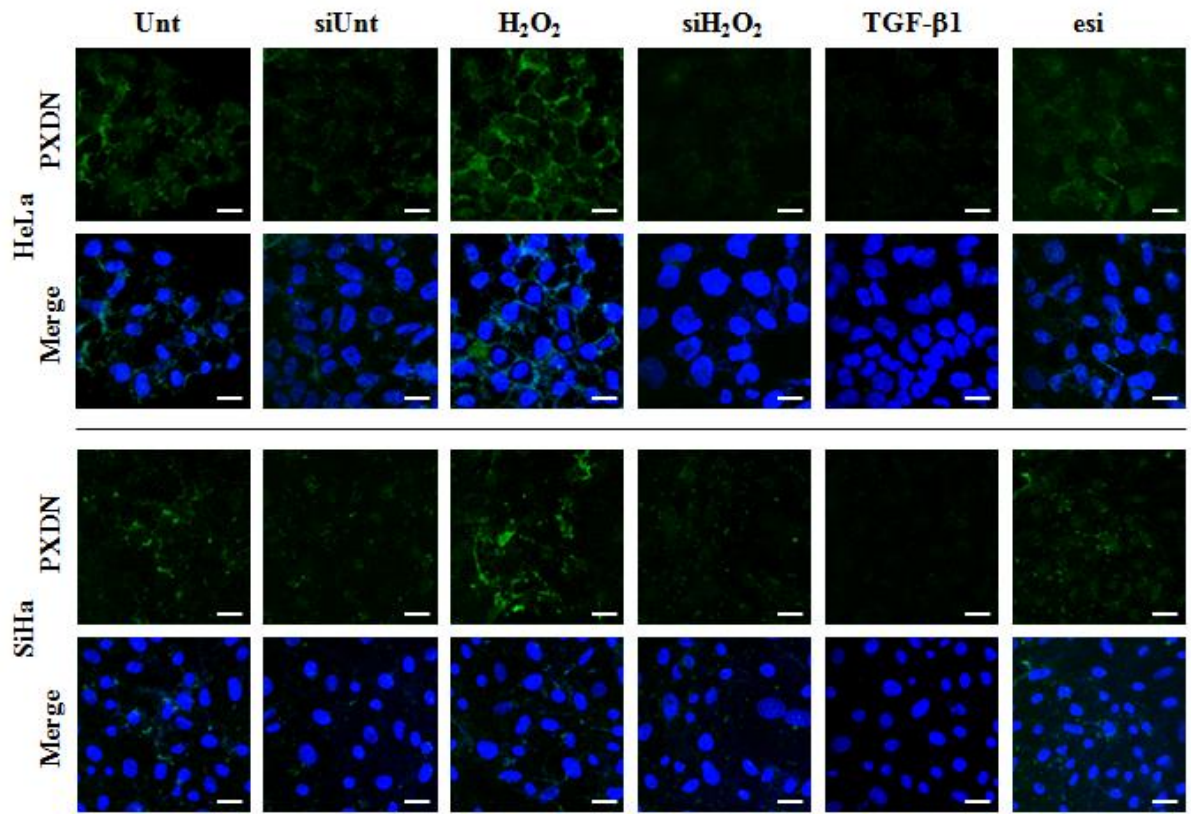

Figure 3.4: IF microscopy to observe PXDN knockdown in HeLa and SiHa cells. IF microscopy was used to corroborate the PXDN knockdown ELISA data for both HeLa and SiHa cell lines. Cells were transfected with PXDN siRNA (siUnt) or additionally treated with 100 μM H_2O_2 (siH_2O_2) for 24 h. HeLa and SiHa cells were treated with 100 μM H_2O_2 to visualise the effects of oxidative stress on PXDN. Cells were transfected with a negative control siRNA (esi) or treated with 5 ng/ml TGF-β1. PXDN expression was observed using a FITC-labelled secondary antibody. DAPI stained nuclei blue (63X magnification; scale bar = 20 μm).

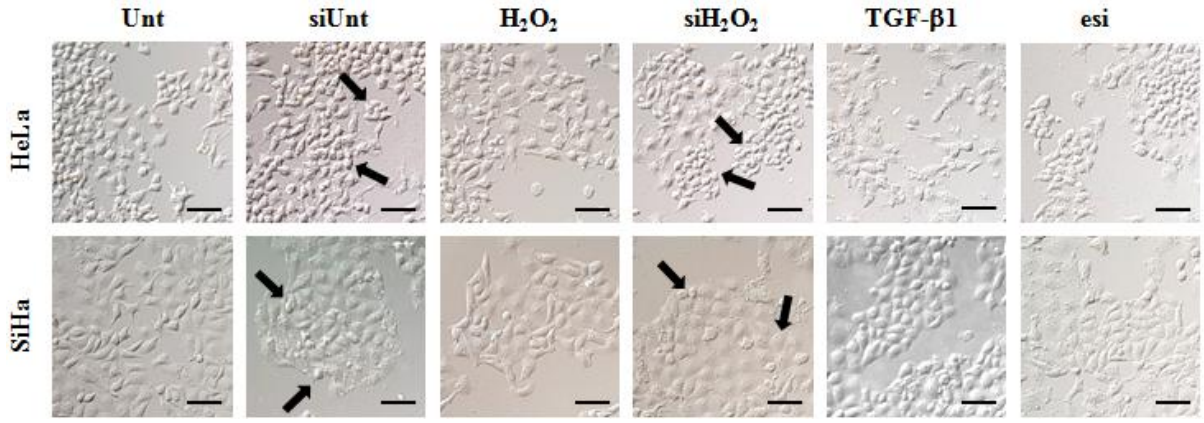

Figure 3.5: Effects of PXDN knockdown on HeLa and SiHa cell morphology. DIC microscopy was used to visualise the cell morphology of HeLa and SiHa cells following transfections and/or treatment, since morphology changes occur during EMT as cells become elongated and spread out. Cells were transfected with PXDN siRNA (siUnt) for 24 h to knockdown PXDN expression. To determine the effects of oxidative stress on morphology, cells were either treated with 100 μM H_2O_2 or were additionally transfected with PXDN siRNA (siH_2O_2). HeLa and SiHa cells were also transfected with a negative control siRNA (esi). As a positive inducer of EMT, cells were treated with 5 ng/ml TGF-β1. Arrows indicate rounded and clumped cells that were observed following PXDN knockdown (10X magnification; scale bar = 100 μm).

3.3.2. Oxidative stress alters the expression of EMT markers

As mentioned, the TF Snai1 is known to be expressed during Type III EMT, is activated by TGF-β1 treatment and decreases E-cadherin expression (Cano *et al*., 2000; Jordan *et al*., 2011). In order to further determine whether oxidative stress may be involved in Type III EMT in HeLa and SiHa cells, Snai1 activation as well as PXDN and E-cadherin expression patterns were investigated following treatment with 100 μM H_2O_2. IF microscopy revealed that Snai1 expression and nuclear translocation (blue-green nuclei) decreased during oxidative stress in both cell lines while PXDN expression and E-cadherin expression appeared to increase (FITC intensity, Table B4). Snai1 nuclear translocation increased following TGF-β1 treatment as expected, in both cell lines, while PXDN and E-cadherin expression decreased (Figure 3.6 and Table B4).

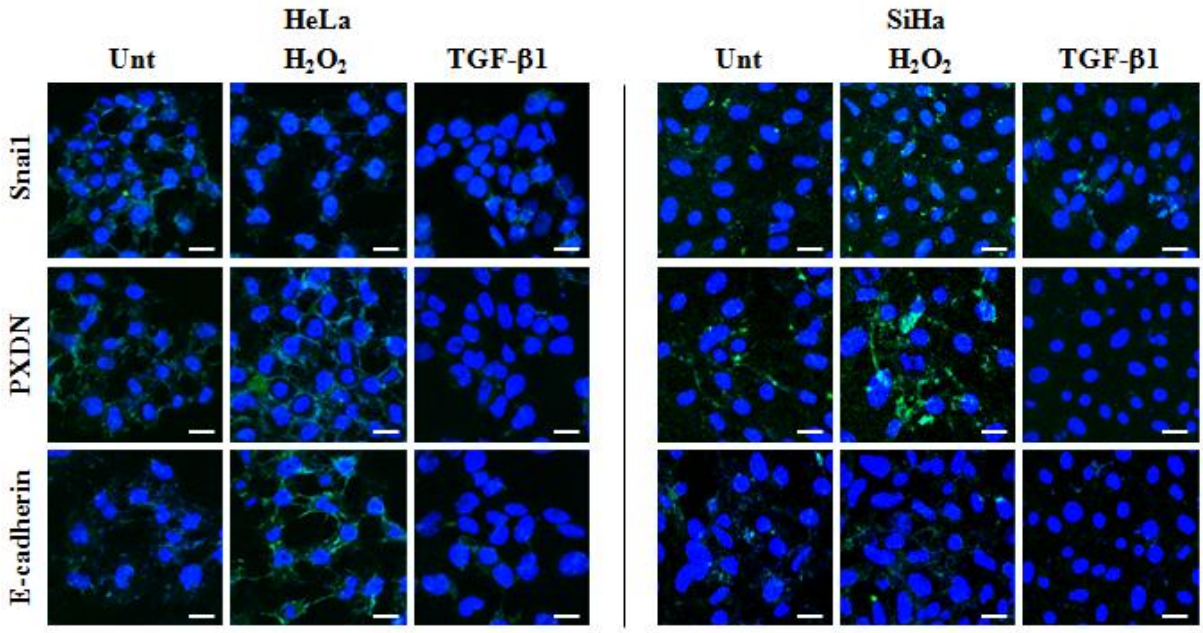

Figure 3.6: Determination of the effects of oxidative stress on EMT markers. IF microscopy images of PXDN and the EMT markers, Snai1 and E-cadherin, detected with FITC-labelled secondary antibodies. DAPI stained nuclei blue. Oxidative stress was induced by treating cells with 100 μM H_2O_2 for 24 h. Cells were also treated with 5 ng/ml TGF-β1 for 24 h as a positive control of EMT induction (63X magnification; scale bar = 20 μm).

3.3.3. PXDN contributes to cell proliferation

MTT assays were conducted to determine the effect of PXDN expression on cell proliferation. In HeLa cells, PXDN knockdown (siUnt) resulted in a 15% (85 ± 3%) decrease in proliferation while HeLa cells treated with H_2O_2 did not experience any change in proliferation relative to untreated. When PXDN was silenced and HeLa cells also treated with H_2O_2 (siH_2O_2), there was a 17% (83 ± 1%) decrease in proliferation, similar to PXDN knockdown in a regular environment (Figure 3.7). HeLa cells treated with TGF-β1 also experienced a 12% (88 ± 1%) decrease in cellular proliferation while the negative control (esi) caused an unexpected 17% (83 ± 1%) decrease in proliferation. Similarly, SiHa cells showed no change in cellular proliferation following treatment with H_2O_2 while PXDN knockdown (siUnt) resulted in a 10% (90 ± 1%) decrease in proliferation and a 12% (88 ± 4%) decrease when combined with additional H_2O_2 treatment (siH_2O_2). Unlike HeLa cells, when SiHa cells were treated with TGF-β1 there was no difference in proliferation but the negative control (esi) also resulted in an unexpected 14% (86 ± 1%) decrease in proliferation (Figure 3.7).

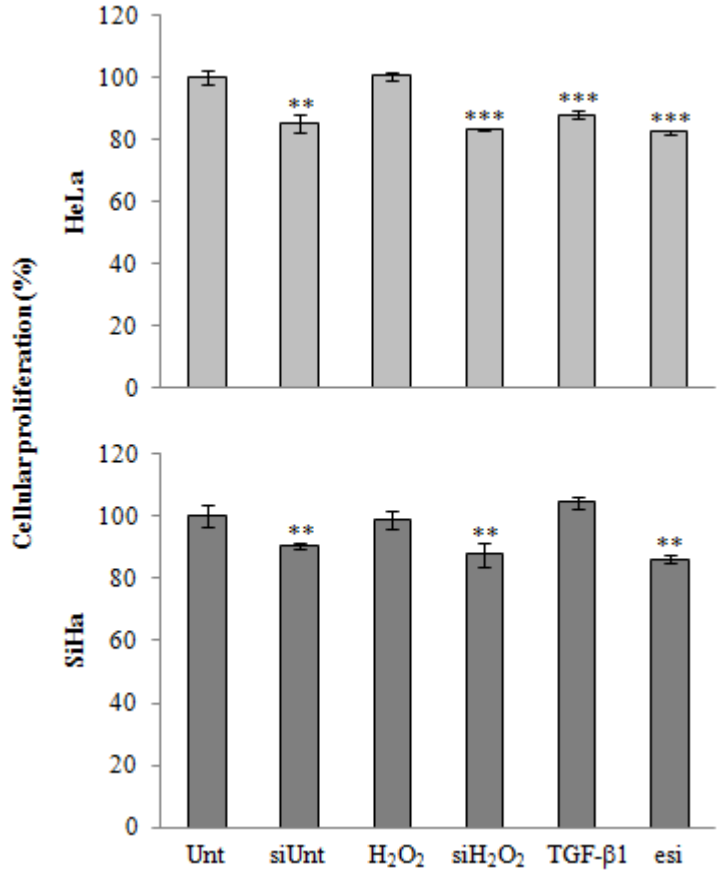

Figure 3.7: MTT assays to determine effects of PXDN expression on cell proliferation. HeLa and SiHa cells were transfected with PXDN siRNA (siUnt) for 24 h to investigate the effects of PXDN knockdown on cell proliferation. Cells were treated with 100 μM H_2O_2 to determine the effect of oxidative stress on cell proliferation. In addition, the effect of PXDN knockdown during oxidative stress (siH_2O_2) on cell proliferation was also investigated. Cells were also transfected with a negative control siRNA (esi). Treatment with 5 ng/ml TGF-β1 for 24 h was included as an EMT control (n = 3, mean ± SD).

3.3.4. Cell attachment is reduced following PXDN knockdown

Cell adhesion assays were conducted to determine the influence of oxidative stress and PXDN expression on cell attachment of HeLa and SiHa cells. HeLa cells exhibited a significant 32% (68 ± 2%) decrease in cell attachment following transfection with PXDN siRNA (siUnt) whereas treatment with H_2O_2 or TGF-β1 alone did not alter attachment. PXDN knockdown followed by H_2O_2 treatment (siH_2O_2) also resulted in a 31% (69 ± 4%) decrease in attachment, very similar to siUnt (Figure 3.8). The negative control (esi) decreased cell attachment by an insignificant 8% (92 ± 7%). In SiHa cells, PXDN knockdown (siUnt) resulted in a statistically insignificant 11% (89 ± 13%) decrease in

attachment while H_2O_2 alone reduced SiHa attachment by a significant 22% (78 ± 1%). H_2O_2 treatment combined with PXDN knockdown (siH_2O_2), also resulted in a 21% (79 ± 4%) decrease in SiHa attachment which was a more significant decrease than observed with siUnt (Figure 3.8). Similarly to HeLa cells, SiHa cells treated with TGF-β1 did not show an alteration in cell attachment and the negative control (esi) slightly reduced SiHa attachment by a statistically insignificant 9% (91 ± 11%).

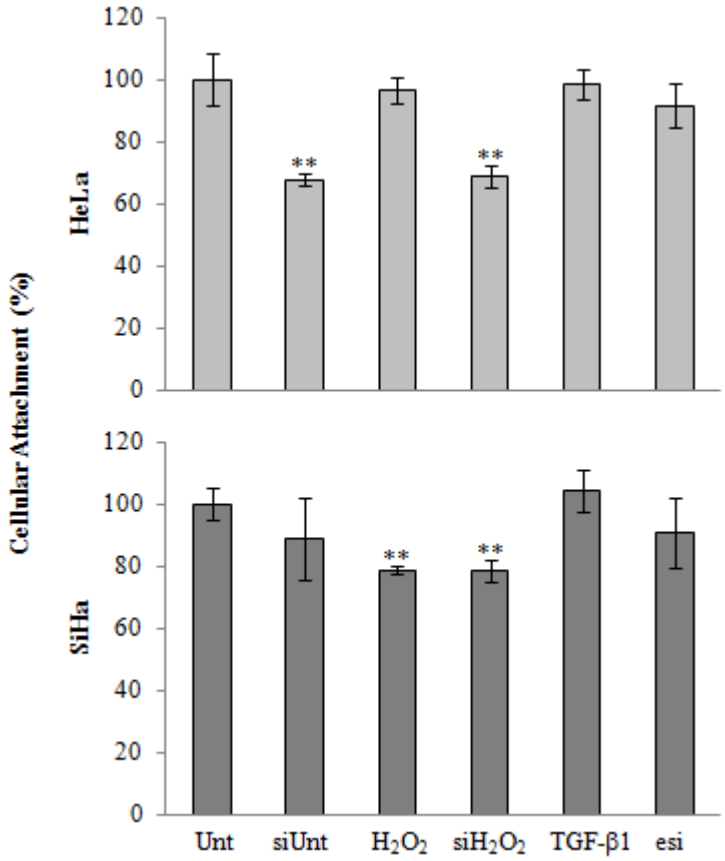

Figure 3.8: Determination of the effects of PXDN knockdown on cell attachment. Cell adhesion assays were performed to investigate the effects of PXDN knockdown on cell attachment. HeLa and SiHa cells were transfected for 24 h with PXDN siRNA (siUnt) to decrease PXDN expression. Oxidative stress was induced by treating cells with 100 μM H_2O_2 with some cells additionally transfected with PXDN siRNA (siH_2O_2). Cells were also transfected with a negative control siRNA (esi). HeLa and SiHa cells were treated with 5 ng/ml TGF-β1 to induce EMT (n = 3, mean ± SD).

3.3.5. PXDN expression influences cell migration

Scratch assays were performed in order to investigate whether PXDN expression influences cell migration. PXDN knockdown (siUnt) in HeLa cells or treatment with TGF-β1 both resulted in a slight but statistically insignificant increase in cell migration whereas treatment with H_2O_2 alone resulted in a statistically significant 10% (59 ± 3%) increase in scratch closure (Figure 3.9). Interestingly, PXDN knockdown in HeLa cells followed by H_2O_2 treatment (siH_2O_2) resulted in a statistically significant 18% (31 ± 5%) decrease in cell migration compared to untreated cells and a 28% decrease in migration when compared to HeLa cells treated with H_2O_2 only (Figure 3.9). HeLa cells transfected with the negative control (esi) had a statistically insignificant decrease in cell migration. SiHa cells migrated much faster than HeLa cells which required up to 48 h of observation. SiHa cells closed scratches after 24 h when left untreated or treated with H_2O_2 only. Treatment of SiHa cells with TGF-β1 resulted in accelerated migration, as expected, with scratches closing fully after only 12 h (data not shown). Unlike HeLa cells, PXDN knockdown (siUnt) in SiHa cells did result in a significant decrease in cell migration of 26% (68 ± 9%) (Figure 3.10). PXDN knockdown in the presence of H_2O_2 (siH_2O_2) in SiHa cells also resulted in a significant decrease in cell migration with a 39% (55 ± 14%) decrease compared to untreated cells and 42% decrease when compared to H_2O_2 treated cells (Figure 3.10). SiHa cells transfected with the negative control (esi) had an unexpected 42% (52 ± 6%) decrease in cell migration. PXDN knockdown significantly decreased cell migration in both HeLa and SiHa cell lines in an oxidative environment.

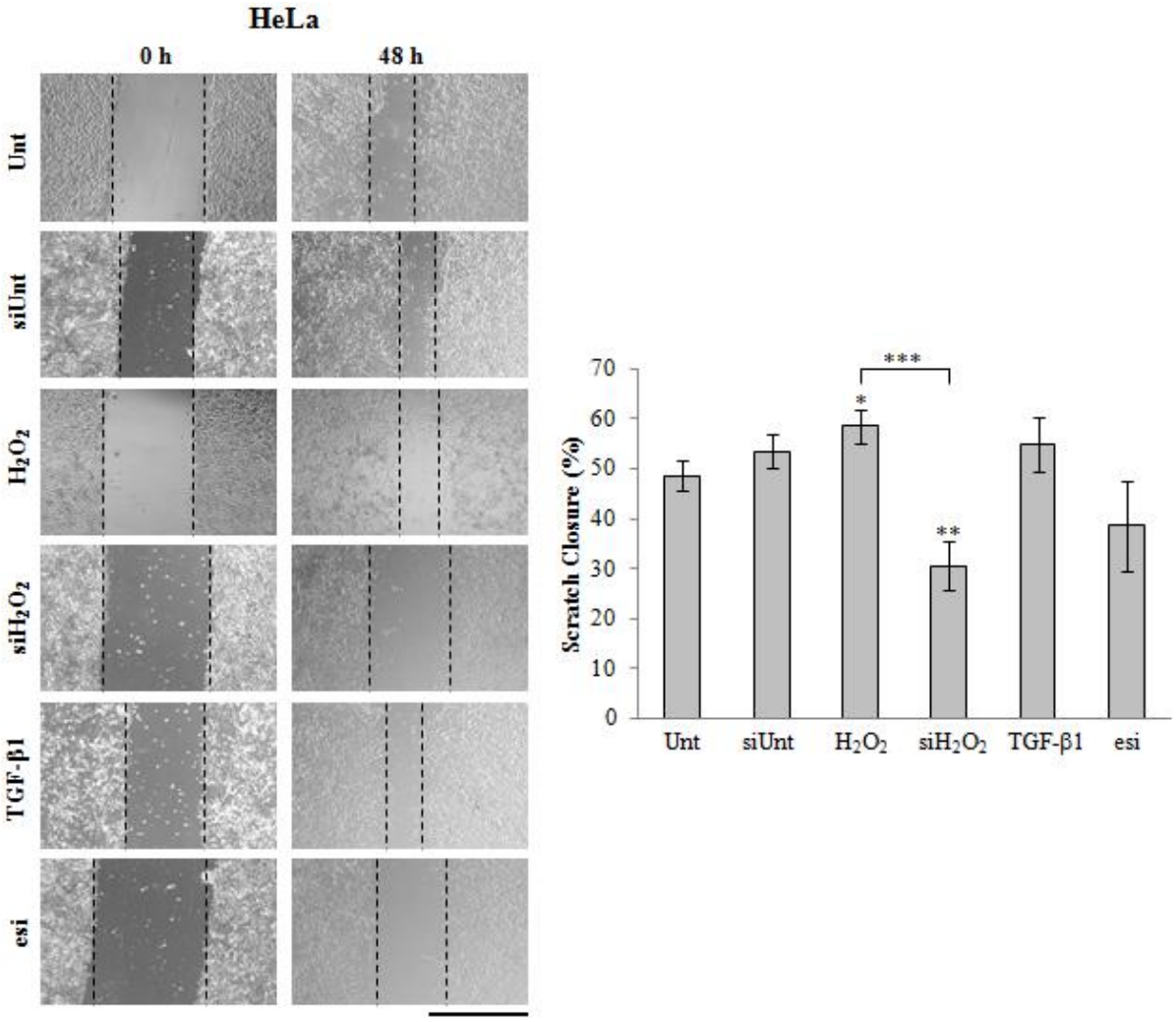

Figure 3.9: Identifying the effects of PXDN knockdown on HeLa cell migration. Scratch assays were performed on HeLa cells over a 48 h period in order to determine the effects of PXDN knockdown on cell migration. HeLa cells were transfected with PXDN siRNA (siUnt) for 24 h to decrease PXDN expression. To determine the effects of oxidative stress on HeLa cell migration, cells were treated with 100 μM H_2O_2 and some additionally transfected with PXDN siRNA (siH_2O_2). HeLa cells were also transfected with a negative control siRNA (esi) or treated with 5 ng/ml TGF-β1, which is a known inducer of EMT. Dotted lines highlight scratch borders (4X magnification; scale bar = 1 000 μm). Sizes of scratches over time were made relative to the size of the 0 h scratch of each condition (n = 3, mean ± SD).

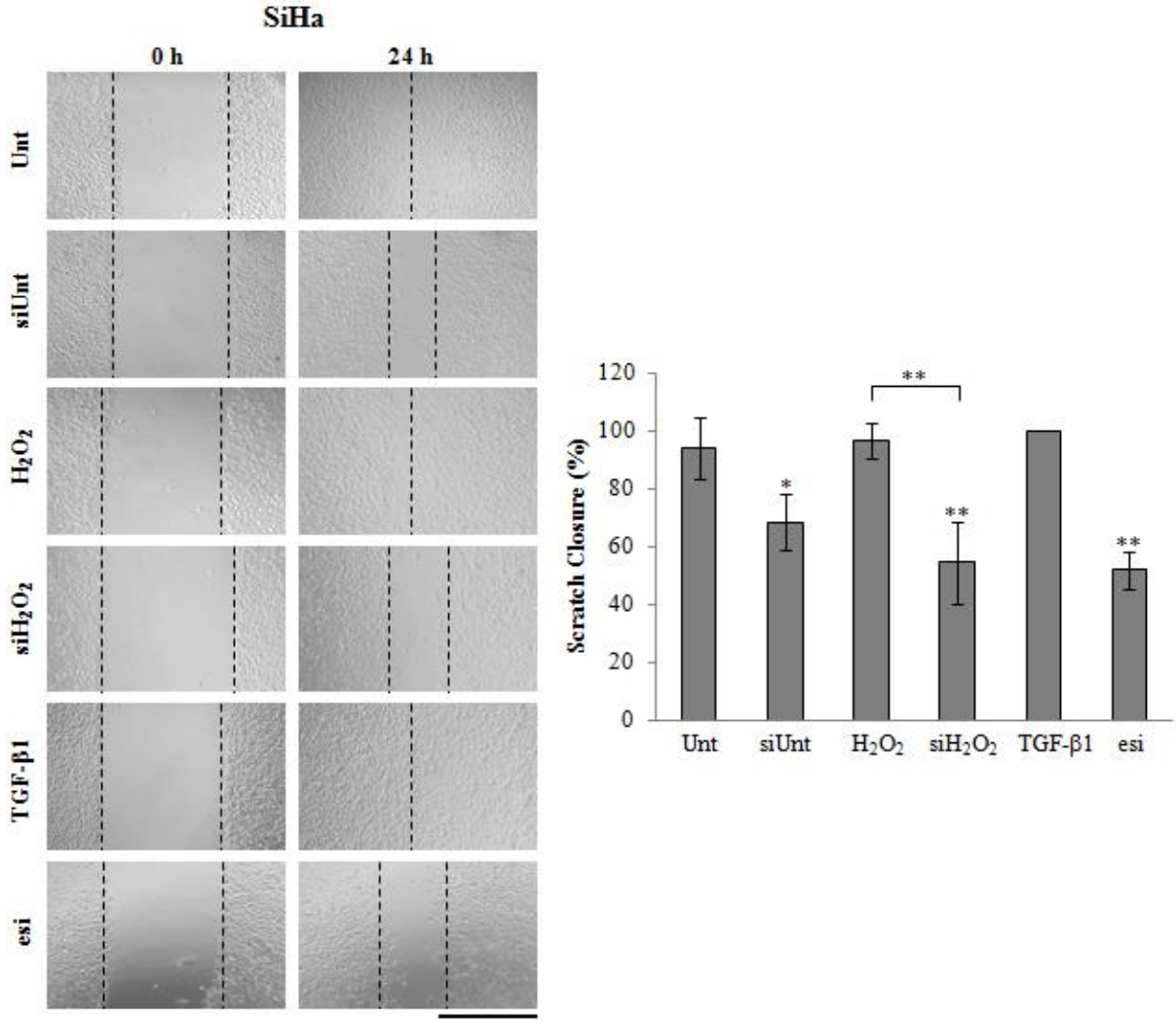

Figure 3.10: Investigating the role of PXDN in SiHa cell migration. Scratch assays were performed on SiHa cells over a 24 h period in order to determine the effects of PXDN knockdown on cell migration. SiHa cells were transfected with PXDN siRNA (siUnt) for 24 h to decrease PXDN expression. Oxidative stress was induced by treating cells with 100 μM H_2O_2 with some SiHa cells additionally transfected with PXDN siRNA (siH_2O_2). SiHa cells were treated with 5 ng/ml TGF-β1, which is a known inducer of EMT, and other cells transfected with a negative control siRNA (esi). SiHa cells treated with TGF-β1 had accelerated migration where scratches closed completely after 12 h (data not shown) (4X magnification; scale bar = 1 000 μm). Sizes of scratches over time were made relative to the size of the 0 h scratch of each condition (n = 3, mean ± SD).

3.3.6. Cell invasion is altered by PXDN expression

Since increased invasion is a feature of Type III EMT, invasion assays were performed on HeLa and SiHa cells to determine the effects of PXDN expression and oxidative stress on invasion. HeLa cells experienced a significant 20% (80 ± 5%) decrease in invasive capacity in an oxidative environment while treatment with TGF-β1 resulted in a slight but statistically insignificant increase (Figure 3.11). PXDN knockdown (siUnt) in HeLa cells resulted in a 18% (82 ± 4%) decrease in invasion and with additional treatment of H_2O_2 (siH_2O_2), there was an even greater decrease of 27% (73 ± 9%) compared to untreated cells (Figure 3.11). PXDN possibly has a role in invasion in HeLa cells experiencing oxidative stress since there was a slight 10% difference between PXDN siRNA transfected (siUnt) cells and cells that were transfected with PXDN siRNA during oxidative stress (siH_2O_2). HeLa cells experienced an unexpected 47% (53 ± 2%) decrease in invasion when transfected with the negative control (esi). Contrary to HeLa cells, SiHa cells exhibited a 14% (114 ± 7%) increase in invasion when treated with H_2O_2. Treatment with TGF-β1 resulted in a significant 19% (119 ± 4%) increase in invasion of SiHa cells which is expected (Figure 3.11). PXDN knockdown (siUnt) in SiHa cells resulted in a very slight and statistically insignificant decrease in cellular invasion. SiHa cells that were transfected with PXDN siRNA and additionally treated with H_2O_2 (siH_2O_2) had a small insignificant 9% (91 ± 7%) decrease in invasion when compared to untreated cells; however, when compared to cells treated with H_2O_2 only, there was a much greater difference in invasion with a 22% decrease observed (Figure 3.11). The difference in invasion observed between H_2O_2 and siH_2O_2 suggests that PXDN expression has a role in the invasion of SiHa cells during oxidative stress. Similarly to HeLa cells, SiHa cells transfected with the negative control (esi) had an unexpected 25% (75 ± 2%) decrease in invasion.

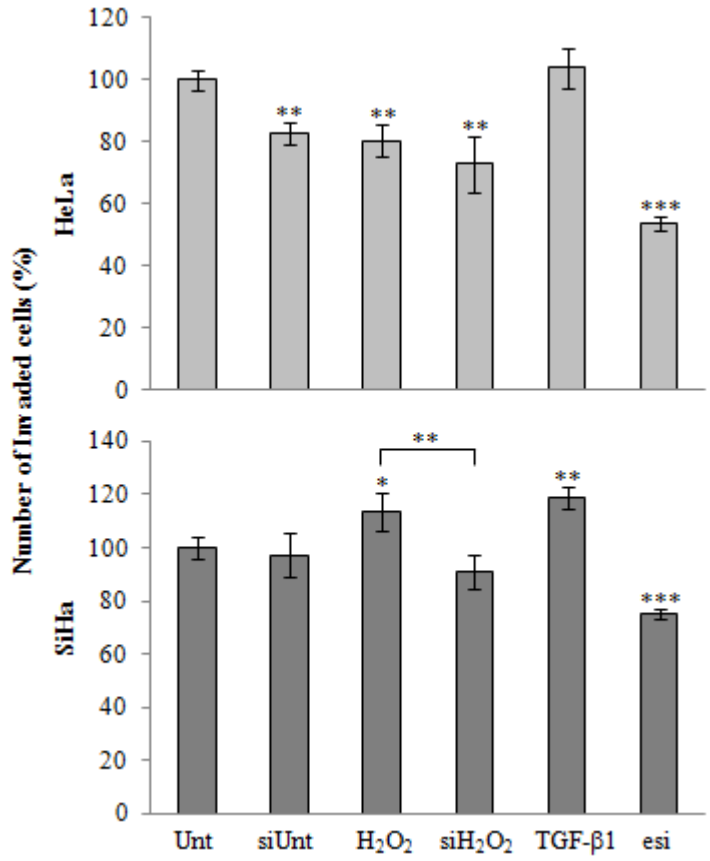

Figure 3.11: Determination of the role of PXDN in HeLa and SiHa cell invasion. Invasion assays were performed to investigate the effects of PXDN knockdown on HeLa and SiHa cell invasion. PXDN expression was decreased by transfecting cells with PXDN siRNA for 24 h (siUnt). Cells were treated with 100 μM H_2O_2 to induce oxidative stress and other cells additionally transfected with PXDN siRNA (siH_2O_2). HeLa and SiHa cells were also treated with 5 ng/ml TGF-β1 to induce EMT. Cells were also transfected with a negative control siRNA (esi) (n = 3, mean ± SD).

3.3.7. 3D colony formation is reduced following PXDN knockdown

Soft agar 3D colony formation assays were conducted in order to observe how PXDN may affect spheroid formation in an environment simulating *in vivo*. There were significantly fewer spheroids formed across all HeLa cell treatments as compared to the more metastatic SiHa cells (data not shown). HeLa cells had a 47% (53 ± 22%) decrease in spheroid formation upon PXDN knockdown (siUnt) (Figure 3.12). There was also a 67% (33 ± 13%) decrease in the number of HeLa spheroids formed following H_2O_2 treatment and a 60% (40 ± 15%) decrease when PXDN knockdown was combined with H_2O_2 (siH_2O_2), as compared to untreated cells. TGF-β1 treatment caused a 53% (47 ± 13%) reduction in spheroids formed

by HeLa cells and the negative control (esi) caused a statistically insignificant 33% (67 ± 27%) reduction in spheroid formation (Figure 3.12). HeLa cells transfected with PXDN siRNA also had smaller spheroids formed as well as reduced numbers. SiHa cells had a significant 81% (19 ± 4%) decrease in spheroid formation following PXDN knockdown (siUnt) (Figure 3.12). H_2O_2 treatment also decreased the number of SiHa spheroids formed by 60% (40 ± 4%) which changed to a 65% (35 ± 5%) decrease, as compared to untreated cells, when H_2O_2 treatment was combined with PXDN knockdown (siH_2O_2) (Figure 3.12). TGF-β1 treatment caused a 72% (28 ± 2%) decrease in SiHa spheroid number as did transfection with the negative control (esi) with an unexpected 76% (24 ± 2%) decrease.

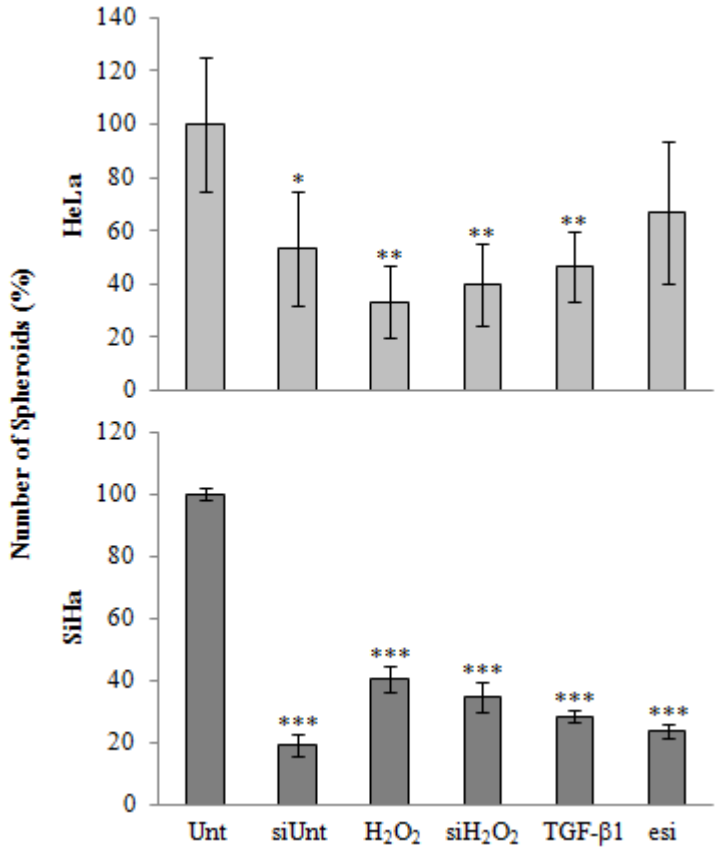

Figure 3.12: Investigating the role of PXDN in HeLa and SiHa spheroid formation. HeLa and SiHa spheroid formation was analysed after three weeks after cells had originally been either: transfected with PXDN siRNA (siUnt) to knockdown PXDN, treated with 100 μM H_2O_2 to induce oxidative stress, transfected with PXDN siRNA and treated with 100 μM H_2O_2 (siH_2O_2), transfected with a negative control siRNA (esi) or treated with 5 ng/ml TGF-β1 to induce EMT (n = 3, mean ± SD).

3.4. Discussion

The PXDN protein has the ability to form dityrosine cross-links and strengthen the collagen IV network through sulfilimine bond formation within the BM (Bhave *et al*., 2012). Since we showed that PXDN expression is regulated by the redox response TF, Nrf2, and levels increase with elevated ROS such as H_2O_2, we considered whether PXDN may be involved in oxidative stress induced EMT. The functions of PXDN in Type III EMT were investigated in two cervical carcinoma cell lines, HeLa and SiHa, by reducing PXDN expression and conducting experiments that affect the features associated with Type III EMT namely proliferation, migration and invasion. In addition to identifying the role of PXDN in Type III EMT, the cellular environment was also altered by the addition of H_2O_2 in order to determine how excess ROS affect features of Type III EMT and to determine whether there is a role for PXDN within this context.

PXDN expression was decreased in HeLa and SiHa cells using PXDN siRNA transfections and an ELISA assay was performed in order to validate whether the transfection procedure was effective or not by quantifying the degree of PXDN knockdown. When compared to untreated cells, PXDN expression was decreased by 31% in HeLa and 18% in SiHa cells. The ELISA was also used to determine the effect of H_2O_2 on PXDN expression in HeLa and SiHa cells as we, and others, have previously observed that PXDN expression increases in an oxidative environment in a dose and time dependent manner (Cheng *et al*., 2008; Shi *et al*., 2011; Zhang *et al*., 2012). ELISA data was in line with our previous western blot results where PXDN expression was shown to increase by 28% in HeLa and SiHa cells when exposed to H_2O_2. Upon silencing of PXDN in an oxidative environment, there was still a significant decrease in PXDN expression which was observed in both cell lines, and indicated that PXDN expression remained repressed post-transfection even when treated with the H_2O_2 inducer. TGF-β1 has been shown to induce EMT characteristics and so TGF-β1 treatment was used as a positive indicator for Type III EMT in our functional experiments (Peinado *et al*., 2003; Zavadil and Böttinger, 2005). TGF-β1 treatment has been shown to decrease PXDN expression, as observed in our ELISA assay, through the Snai1 TF which binds to the *PXDN* promoter (Sitole and Mavri-Damelin, 2018). However, in our studies, the influence of TGF-β1 on PXDN expression was not taken into consideration. The effects of TGF-β1 treatment were used as a comparator and to observe whether similar EMT characteristics may be observed during oxidative stress. ELISA data also showed that the negative transfection

control (esi) did not cause a statistically significant alteration to PXDN expression as compared to untreated expression levels in both cell lines; however, the SD of the esi results were relatively large and should ideally be repeated. Our ELISA data did still show that the PXDN siRNA caused a greater decrease in PXDN expression than the esi control, indicating that a decrease in PXDN expression in the PXDN siRNA transfected samples was due to the PXDN siRNA and not due to other reagents within the transfection reaction. We thus decided to perform the functional assays using the current transfection protocol.

Although the esi transfection did not cause a statistically significant alteration to PXDN expression, the esi transfections did appear to have varying effects on HeLa and SiHa cells in all downstream functional experiments. For example, the esi control greatly reduced cell proliferation and invasion of both cell lines. Although the esi control sequence targeted firefly luciferase, it is possible that the sequence had off-target effects by decreasing the expression of other proteins thus affecting cell function (Tschuch *et al*., 2008). Indeed, a BLAST analysis of the esi negative control cDNA target sequence revealed that a section of the siRNA may potentially bind to the transforming growth factor-β-induced (TGF-βI) protein precursor. TGF-βI is a protein located within the ECM and is involved in mediating cell attachment and migration through involvement with integrin receptors (Zhang *et al*., 2009). The possibility of the esi negative control affecting the expression of another ECM protein may explain the unusual results obtained from the functional assays. Since the esi control had such an unexpected effect on cells but did not alter PXDN expression, all comparisons for the functional results were made to untreated cells. However, all of the functional experiments will need to be repeated with an alternative negative control, potentially a scrambled version of the PXDN siRNA, since silencing experiments should ideally be made relative to a control siRNA. Therefore, the data obtained from the following functional assays should be viewed as preliminary and will need to be validated once a reliable negative control is available.

In addition to ELISA, IF microscopy was performed on both HeLa and SiHa cells to visualise the effects of transfections and/or treatments on PXDN protein expression. IF microscopy images revealed that PXDN expression patterns mimic those observed from ELISA and confirm that PXDN siRNA transfections were sufficient for PXDN knockdown for downstream experiments.

DIC was performed on live cells to observe any visible changes to cell morphology following PXDN knockdown and/or treatment, as well as the effects of H_2O_2 on these cell lines, as

alterations in cell appearance are observed during EMT (Yang and Weinberg, 2008). Cell morphology can be a good indicator of cells undergoing EMT since cells have connections with both each other and the ECM and when proteins involved with these connections are altered, it can cause cells to change shape and appearance (Suarez-Carmona *et al*., 2017). Factors such as ROS and TGF-β1 are expected to alter the appearance of cells due to the induction of EMT; however, this was not observed in either the HeLa or SiHa cell lines as cells appeared elongated regardless of additional treatments (Cannito *et al*., 2010; Lamouille *et al*., 2014). Even though HeLa and SiHa cells did not exhibit noticeable morphological changes upon treatment, it does not necessarily mean that the treatments are not inducing Type III EMT. Indeed, multiple human breast carcinomas have been found to be metastatic even without an alteration of the breast epithelial morphology (Tarin *et al*., 2005). In both HeLa and SiHa cell lines, PXDN knockdown resulted in cells taking on a slightly rounder appearance especially during oxidative stress. Since PXDN is able to strengthen the BM by cross-linking collagen IV, reduced PXDN expression could decrease cell attachment to the ECM making cells appear more rounded as the cells lift away from the substrate. This altered cell morphology upon PXDN knockdown is supported by observations made in a study involving glioma tumour cells where cells had a rounder morphology as the rigidity of the ECM decreased (Ulrich *et al*., 2009). Both HeLa and SiHa cells have been shown to have spindle-shaped morphology during EMT so rounder cell morphology upon PXDN knockdown potentially implicates PXDN in the EMT process (Cheng and Hao, 2017).

To determine whether oxidative stress may induce EMT, we performed IF microscopy to observe whether the EMT markers, Snai1 and E-cadherin, and PXDN expression are altered following treatment with H_2O_2. TGF-β1 treatment is known to induce EMT and cause Snai1 activation, Snai1 then downregulates E-cadherin expression (Jordan *et al*., 2011). HeLa or SiHa cells treated with TGF-β1 exhibited the expected increase in Snai1 activation and subsequent decrease of E-cadherin expression, thus indicating that Type III EMT was likely to be induced. TGF-β1 treatment also caused a decrease in PXDN expression which is expected since Snai1 has been shown to bind to and decrease PXDN expression (Sitole and Mavri-Damelin, 2018). HeLa and SiHa cells treated with H_2O_2 exhibited a decrease in Snai1 activation and an accompanying increase in PXDN and E-cadherin expression, suggesting that H_2O_2 treatment would not induce EMT since Snai1 was not activated. Although TGF-β1 treatment in our experiment was used to induce and indicate the occurrence of EMT, the pathways involved during ROS and TGF-β1 activation of Type III EMT will most likely

differ. ROS has been shown to activate EMT so although Snai1 and E-cadherin expression patterns in our images do not match those observed in the classic TGF-β1 EMT induction cases, the expression patterns are not entirely unusual (Gill *et al*., 2016). Several metastatic breast, ovarian, colon and some cervical carcinoma cell lines have all been shown to have unaltered E-cadherin expression even during metastasis; the effects of oxidative stress on other features of EMT were therefore investigated (Fadare *et al*., 2005; Tarin *et al*., 2005; Friedl and Gilmour, 2009; Gao *et al*., 2014).

Usually, cancer cells undergoing Type III EMT experience an alteration, usually in the form of a reduction, in cell proliferation (Thiery *et al*., 2009). Due to these potential changes in proliferation, MTT cell proliferation assays were performed in order to determine whether PXDN has a role in this process and determine whether an oxidative environment affects proliferation. MTT assays conducted on both HeLa and SiHa cells revealed that PXDN knockdown resulted in equally decreased proliferation in both a normal and oxidative environment. This observation suggests that PXDN is potentially involved in cell proliferation pathways; however, this result will need to be verified with repeated experiments using a new negative control. Our initial findings that PXDN may influence proliferation, corresponds with other studies: PXDN has very recently been shown to be involved in promoting pulmonary artery smooth muscle cell proliferation by utilising H_2O_2 produced by Nox4 (You *et al*., 2018). You *et al*. (2018) determined through PXDN knockdown experiments that PXDN utilises H_2O_2 and chloride ions to form HOCl, HOCl then activates NF-κB (a TF involved in activating pathways such as proliferation and migration) nuclear translocation, resulting in promoted proliferation. Another study also determined that PXDN promotes proliferation in vascular smooth muscle cells via the Nox4-H_2O_2-PXDN-HOCl-ERK 1/2 pathway (Shi *et al*., 2011). Our observations thus support previous findings and suggest a role for PXDN in the proliferation of HeLa and SiHa cells although the exact mechanism still needs to be determined. Low ROS levels have been shown to increase proliferation; however, we did not observe an alteration in proliferation in HeLa or SiHa cells following treatment with H_2O_2 (Giannoni *et al*., 2012; Gill *et al*., 2016). Perhaps HeLa and SiHa cells have elevated antioxidant response proteins like Nrf2, as is observed in multiple cancer types, that are allowing cells to clear excess H_2O_2 thus preventing the influence of ROS on proliferation (Gill *et al*., 2016; Milkovic *et al*., 2017). In fact, studies of human cervical squamous cell carcinomas found elevated Nrf2 activation which correlated with enhanced cancer cell survival and metastasis (Ma *et al*., 2015). TGF-β1

treatment induces Type III EMT and so a decrease in proliferation is expected (Thiery *et al*., 2009). Our MTT data showed TGF-β1 treatment decreased proliferation in HeLa cells but not in SiHa cells. However, studies have found that a decrease in proliferation may not be a good indicator of Type III EMT as several metastatic cancers, including melanoma and ovarian carcinoma, have been found to proliferate even during invasion (Gao *et al*., 2014; Haass *et al*., 2014; Jayachandran *et al*., 2016). Although H_2O_2 and TGF-β1 treatment did not decrease proliferation, Type III EMT may still be occurring in both HeLa and SiHa cell lines.

Another well known feature that may be affected in cells undergoing Type III EMT is cell attachment since cancer cells need to alter cell-ECM interactions to become more motile (Giannoni *et al*., 2012). Our attachment experiments focused on the ability of transfected and/or treated HeLa and SiHa cells to reattach to a surface within 15 min following trypsinisation. Our primary results showed that PXDN knockdown in both a normal and oxidative environment caused an equal and statistically significant decrease in the ability of HeLa cells to reattach. These preliminary findings indicate that in HeLa cells, PXDN expression may be important in cell adhesion and most likely has an important role during MET, when cancer cells will need to reattach to new tissue following invasion. PXDN is involved in cross-linking collagen IV and strengthening the ECM and has been found to be important during the attachment of embryos to the uterine lining in mice which occurs during Type I EMT (Bhave *et al*., 2012; Jones-Paris *et al*., 2017). Although PXDN is involved during reattachment in Type I EMT, it is highly probable that the same may be necessary during Type III EMT/MET. In a separate experiment to investigate the functional role of PXDN, HeLa and SiHa cells were transfected with a PXDN CRISPR/Cas9 KO plasmid (Santa Cruz Biotechnologies, sc-404707) in an attempt to create and establish HeLa and SiHa PXDN KO cell lines. Following successful establishment of PXDN KO HeLa and SiHa cell lines, we noticed that cells from both cell lines would not attach to substrate efficiently making it difficult to continue with downstream experimentation (data not shown). Due to the inability of PXDN KO cells to attach to substrate, we then resorted to the use of PXDN siRNA to only knockdown PXDN expression as opposed to removing it completely. In addition to the observations made from our PXDN KO studies, Tauber *et al*. (2010) found HO-1 mediated cell adhesion to be decreased in choriocarcinoma cells upon silencing of PXDN, indicating that PXDN has an important role in cell attachment. H_2O_2 treatment of HeLa cells did not alter cell attachment which could be due to H_2O_2 promoting PXDN expression thus allowing cells to reattach easily after 15 min.

SiHa cells responded differently to HeLa cells as PXDN knockdown caused only a slight and statistically insignificant decrease in cell attachment which would suggest that PXDN does not have such a major role in the process in this cell line. Contrary to observations with HeLa cells, H_2O_2 treatment resulted in a significant decrease in SiHa cell attachment; additionally, PXDN knockdown in an oxidative environment resulted in the same decrease in SiHa cell attachment as observed with H_2O_2 treatment only. These initial observations imply that the decrease in attachment of SiHa cells with PXDN knockdown in an oxidative environment is due to the effects of H_2O_2 and not because of PXDN silencing. Differences among our observations can be explained by the fact that the HeLa and SiHa cell lines each have individual characteristics and will have independent responses to treatments. SiHa cells are known to be more metastatic and invasive than HeLa cells and treatments such as H_2O_2 may elicit a different response in both cell lines (Filippova *et al*., 2014). ROS have been shown to induce Type III EMT; with the more metastatic SiHa cells, treatment with H_2O_2 activates different pathways than those in HeLa cells such that SiHa cells experiencing prolonged oxidative stress are less likely to reattach to substrate and would remain motile for longer (Giannoni *et al*., 2012). If H_2O_2 treatment alters the expression of other proteins responsible for cell-ECM contact, then reduced PXDN expression may have no effect on attachment as cells would be less likely to reattach in any case. It is also highly unlikely that metastatic SiHa cells would rely on the expression levels of one protein, such as PXDN, for providing cell-ECM adhesion which could explain why PXDN knockdown did not have such a significant effect on SiHa attachment in a non-oxidative environment.

TGF-β1 treatment did not alter cell attachment of either HeLa or SiHa cell lines. Although TGF-β1 treatment induces Type III EMT, cellular attachment may not be altered; indeed metastatic ovarian carcinoma metastasise without detaching from substrate when treated with TGF-β1 and cells also migrate to close wounds during Type II EMT without detaching completely from the ECM (Giannoni *et al*., 2012; Gao *et al*., 2014). It is also important to remember that although ROS and TGF-β1 treatment should both induce EMT, the mechanisms and proteins involved will be different and so cellular responses to the two treatments cannot be directly compared to each other.

The next major feature of Type III EMT to be investigated was cell migration which was studied by creating scratches on a confluent layer of cells then monitoring how much time was required to close the scratch. Interestingly, SiHa cells fully closed scratches only 24 h

after the scratch was created whereas HeLa cells never fully closed scratches even after 48 h, highlighting the difference in migration between these two cell lines. Our preliminary data showed that HeLa cell migration was significantly increased during oxidative stress and PXDN knockdown seemingly attenuated this effect; although all of these findings will need to be validated when a new negative control is available. Recently, Jayachandran *et al*. (2016) found decreased migration of metastatic melanoma cells following PXDN knockdown and You *et al*. (2018) found PXDN to facilitate the migration of pulmonary artery smooth muscle cells through activation of NF-κB pathways. Our initial observation that PXDN potentially influences cell migration is supported by literature; however, the exact involvement of PXDN in the migratory process still needs to be explored. As mentioned, PXDN utilises H_2O_2 to strengthen and construct the ECM by forming dityrosine cross-links and linking collagen IV fibres through sulfilimine bond formation (Cheng *et al*., 2011; Bhave *et al*., 2012; McCall *et al*., 2014; Paumann-Page *et al*., 2017). Interestingly, studies have revealed that certain cancer cells such as metastatic breast and human hepatocellular carcinoma cells migrate along collagen fibres within the ECM (Giannelli *et al*., 2001; Wyckoff *et al*., 2007; Fang *et al*., 2014). PXDN could be responsible for forming these collagen fibres that are required for migration. Since HeLa cells are not very motile, these collagen fibres may only occur during ROS-induced migration which could explain why PXDN knockdown only seemingly influenced migration in an oxidative environment.

SiHa cells migrated much faster than HeLa cells but H_2O_2 treatment did not increase migration in SiHa cells as was observed with HeLa cells. However, our preliminary observations showed PXDN knockdown in SiHa cells significantly decreased migration, more so in an oxidative environment, highlighting again that PXDN is potentially important in cell migratory mechanisms possibly due to PXDN interactions with collagen IV in the ECM. TGF-β1 treatment resulted in a very slight increase in HeLa cell migration but caused a significant increase in SiHa cell migration where scratches were completely closed only 12 h after the scratch was made. Our initial scratch assays thus illustrate that PXDN expression may greatly influence ROS-induced migration of HeLa cells and PXDN expression may also alter SiHa cell migration, slightly more so during oxidative stress.

Besides migration, the ability of cancerous cells to invade the blood stream is another notable trait of Type III EMT (Nieto *et al*., 2016). In order to determine both the influence of ROS and function of PXDN on invasion, invasion assays were performed. However, these data are mostly precursory since the esi negative control had an obvious and unexpected affect on this

assay and these experiments will need to be repeated with a replacement control before solid conclusions can be drawn. Initial results showed that HeLa cells with decreased PXDN expression were found to have a reduced number of invaded cells. Treatment with H_2O_2 also reduced the number of invaded HeLa cells, slightly more so when PXDN expression was reduced during oxidative stress. A decrease in cell invasion upon knockdown of PXDN has previously been observed with choriocarcinoma and melanoma cancer cells; PXDN thus has a potential role in promoting cell invasion (Tauber *et al*., 2010; Jayachandran *et al*., 2016). An important role for PXDN is strengthening the collagen IV network within the BM so it seems counter-intuitive to expect PXDN expression to facilitate cancer cell invasion when invasion involves the degradation of underlying substrate in order to allow cells to enter the blood stream (Thiery *et al*., 2009; Cheng *et al*., 2011; Bhave *et al*., 2012). Keeping in mind that PXDN has a peroxidase domain, PXDN may be necessary for invasion because of its ability to produce hypohalous acids that can activate various cell signalling pathways and not because of the ability of PXDN to alter the ECM (Soudi *et al*., 2012). Although studies have shown PXDN to influence invasion, to date the exact role of PXDN in this process has not been established.

The MMPs are a group of proteins that have the ability to degrade components of the ECM (Giannelli *et al*., 2001). The involvement of MMPs in cancer cell invasion is complex; however, specific MMPs, such as MMP14, have been identified as markers for aggressive and invasive cancer (Cannito *et al*., 2010). Interestingly, MMP14 and PXDN have both been found to be over-expressed in metastatic gliomas and both MMP14 and PXDN expression are known to increase during oxidative stress (Cheng *et al*., 2008; Liu *et al*., 2010; Reuter *et al*., 2010). MMPs exist as inactive pro-proteins that need to be cleaved, either by other enzymes or by autolytic cleavage, in order to become activated (Kessenbrock *et al*., 2010). MPO has been shown to activate MMPs by producing HOCl that oxidises cysteine residues of pro-MMPs resulting in autolytic cleavage (Friedrichs *et al*., 2012; Alfakry *et al*., 2016). HOCl produced by MPO also activates the ERK 1/2 pathway that promotes the expression of *MMP* genes (Kessenbrock *et al*., 2010; Wang *et al*., 2018). Perhaps PXDN expression is necessary to promote invasion as ROS produced by PXDN may trigger pathways needed to activate the expression of proteins such as MMP14; PXDN knockdown would mean insufficient activation of these pathways resulting in decreased cancer invasion. Like MPO, PXDN produces HOCl and activates the ERK 1/2 pathway, therefore the influence of PXDN on MMP activation and expression should be investigated.

Our results showed that oxidative stress, with or without PXDN knockdown, decreased HeLa cell invasion. Since HeLa cells are not especially invasive, treatment with H_2O_2 or PXDN knockdown might not have any effect on invasion and would instead influence pathways that promoted HeLa cell migration, as was observed in our earlier results. In the more invasive and metastatic SiHa cells, PXDN knockdown did not appear to alter invasion; however, H_2O_2 treatment increased SiHa invasion which was then seemingly attenuated by additional PXDN knockdown. An increase in the invasion of SiHa cells is expected in an oxidative environment since H_2O_2 treatment has previously been shown to promote EMT-driven cell invasion in SiHa, breast and prostate cancer cell lines (Mori *et al*., 2004; Kumar *et al*., 2008; Giannoni *et al*., 2012; Porporato *et al*., 2014). Since SiHa cell invasion was potentially reduced significantly upon PXDN knockdown in an oxidative environment, PXDN possibly performs an important role in promoting invasion during oxidative stress through similar activation of pathways involving MMP expression (Jayachandran *et al*., 2016). TGF-β1 treatment in HeLa cells did not significantly alter invasion, which may be due to the low metastatic potential of HeLa cells. However, TGF-β1 treatment increased the number of invaded SiHa cells which is expected to occur since TGF-β1 is an inducer of Type III EMT as observed in both lung cancer and hepatocellular carcinoma (Suarez-Carmona *et al*., 2017). Our preliminary results thus potentially assign a role for PXDN in the process of cell invasion although the exact function of PXDN in this phenomenon will need to be investigated further.

We also performed 3D colony formation assays on both cell lines using soft agar to investigate effects of PXDN on anchorage-independent growth. HeLa and SiHa cells were first transfected and/or treated, detached, re-suspended as singular cells in soft agar then monitored for three weeks. The first noticeable result was the difference in number of colonies formed between the two cell lines. Within three weeks, SiHa cells had grown and formed multiple spheroids whereas HeLa cells produced relatively few spheroids even without any additional treatment. However, as observed with the previous assays, the esi negative control had a great affect on the experiment and so the following data can only be taken as preliminary.

PXDN knockdown in both HeLa and SiHa cells seemed to result in significantly fewer colonies and the spheroids present were much smaller in size than those grown from untreated cells. These findings indicate that PXDN expression is potentially essential in 3D spheroid formation of both cell lines. The influence of PXDN in the case of tumour formation

has not been addressed before and the mechanisms involving PXDN in this process can only be hypothesised. We have demonstrated that PXDN knockdown may decrease both HeLa and SiHa cell proliferation which could explain why colony formation was restricted. We have also found that PXDN knockdown possibly affects cell attachment, therefore PXDN could also be responsible for holding the colonies together in a 3D environment which would be attenuated by PXDN knockdown, but further investigation would be required to prove this theory.

In both HeLa and SiHa cells, the number of colonies formed during oxidative stress was low and appeared mostly unaffected by additional PXDN knockdown, which suggests that it was the oxidative environment that had the negative effect on tumorigenesis. Oxidative stress had a stronger influence on HeLa cell colony formation than with SiHa cells with HeLa cells forming very few spheroids. H_2O_2 has been shown to hinder tumour progression until cancer cells alter their metabolism thus allowing cells to survive with excess ROS (Giannoni *et al*., 2012; Poillet-Perez *et al*., 2015). It is therefore expected that oxidative stress will restrict HeLa and SiHa tumorigenesis and colonies that did form most likely originated from cells that had managed to control excess ROS by enhancing antioxidant protein expression (Gill *et al*., 2016). It is also plausible that the oxidative stress induced apoptosis in both HeLa and SiHa cells which could also explain reduced colony formation (Gill *et al*., 2016). TGF-β1 treatment also diminished colony formation for both cell lines which could also be due to cells undergoing apoptosis as TGF-β1 treatment has been known to induce apoptosis instead of EMT (Yang *et al*., 2006 ; Poillet-Perez *et al*., 2015). Overall, the initial colony formation assays indicated an important potential role for PXDN during tumorigenesis of HeLa and SiHa cells during normal conditions although the reasons for the influence of PXDN in this process still needs to be determined.

Taken all together, our preliminary data has found that PXDN expression is possibly important during: cell proliferation, attachment, migration, invasion and tumorigenesis in both HeLa and SiHa cells, although the assays will need to be repeated to validate these findings. The contribution of PXDN to each of these processes seems to vary and is different between the two cell types. Our data also showed that an oxidative environment can induce Type III EMT to varying degrees depending on cell type with the non-invasive HeLa cells experiencing increased migration and metastatic SiHa cells having enhanced invasion during oxidative stress. In addition, the potential role of PXDN during ROS-induced EMT was more

apparent during HeLa cell migration and SiHa cell invasion although the exact pathways and mechanisms influenced by PXDN still need to be determined. The effects of oxidative stress on EMT are exceptionally complex and are still relatively unknown especially since most studies *in vitro* do not adequately replicate conditions that are found *in vivo* (Friedl and Gilmour, 2009). Investigations into EMT are made even more difficult by new discoveries that reveal some cancer types to stably exist in intermediate transition stages meaning that not all features of EMT will be altered (Nieto *et al*., 2016). We have shown PXDN to be potentially involved in several processes that are altered during EMT and it would be worth taking a closer look at these mechanisms in detail as reducing PXDN expression may be a promising option for the prevention or treatment of cancer.

Chapter 4: Overall conclusions and future experiments

There were two main aims of this thesis:

1) To investigate Nrf2 as a candidate TF in the regulation of *PXDN* gene expression

2) To investigate the role of PXDN in EMT during oxidative stress in HeLa and SiHa cervical carcinoma cells

Firstly, PXDN expression was shown to increase in the presence of oxidative stress, after treatment with the Nrf2 specific inducers, SFN and tBHQ, and after transfection with an Nrf2 over-expression vector. ChIP experiments revealed that Nrf2 binds to a specific region within the *PXDN* promoter and Nrf2 binding is enhanced following treatment with Nrf2 inducers. Finally, mutagenesis of the *PXDN* promoter together with luciferase assays confirmed that Nrf2 binds to the TGAATCTGGC sequence within the *PXDN* promoter and upregulated PXDN protein expression. In summary, we identified Nrf2 as a novel TF that regulates PXDN expression.

Secondly, we performed functional assays on HeLa and SiHa cells to look at whether PXDN plays a role in EMT in particular in the presence of oxidative stress. Our preliminary data using PXDN knockdown in both cell lines, with or without H_2O_2 treatment, showed that PXDN is potentially involved in multiple Type III EMT processes including: cell proliferation, attachment, migration, invasion and tumorigenesis. Our initial findings suggest that oxidative stress induced Type III EMT to varying degrees within the two cervical carcinoma cell lines. In HeLa cells, oxidative stress did not appear to alter proliferation or attachment but increased migration and reduced invasion and spheroid formation. In SiHa cells, oxidative stress did not seem to alter proliferation or migration but reduced attachment and spheroid formation and increased invasion. PXDN knockdown in HeLa cells potentially reduces proliferation, attachment, invasion and spheroid formation but has little effect on HeLa cell migration. In SiHa cells, PXDN knockdown also potentially reduces proliferation, migration and spheroid formation but has little effect on attachment and invasion. Lastly, PXDN knockdown combined with H_2O_2 treatment showed that PXDN has a potentially major influence on HeLa cell migration during oxidative stress while PXDN may be important in SiHa cell invasion in an oxidative environment.

The regulation of PXDN by the master redox regulator Nrf2 has implications for a variety of biological processes. Interestingly, Nrf2 has a major involvement in both the initiation and progression of Type III EMT in various cancer types through the prevention of anoikis, and promoting cancer metastasis (Paoli *et al*., 2013; Poillet-Perez *et al*., 2015; Gill *et al*., 2016; Wang *et al*., 2016). Further studies should aim to establish signalling pathways during Type III EMT that may involve Nrf2 and PXDN and if these relate to oxidative stress within the tumour microenvironment. This could involve silencing Nrf2 expression and performing similar Type III EMT functional assays to determine whether Nrf2 knockdown has similar effects on EMT features as PXDN knockdown. It would then be necessary to see whether the addition of PXDN, through transfection with a PXDN over-expression vector, would be able to restore the previously observed experimental results and therefore determine if Nrf2 is responsible for the regulation of PXDN in these processes. Further, consideration could be given to identifying whether an Nrf2-PXDN pathway occurs for a specific EMT process, such as migration or invasion, and therefore establish a possible unique mechanism. By determining the involvement of an Nrf2-PXDN-EMT pathway in cancer, many therapeutic options may be presented as either Nrf2, PXDN or other pathway participants, may be targeted to possibly prevent or treat cancer.

Although the exact manner in which PXDN influences EMT features was not identified, our experiments revealed that PXDN has a potential function in several processes altered during Type III EMT. Our preliminary data showed that PXDN knockdown in ROS-induced EMT significantly reduces HeLa cell migration and SiHa cell invasion. The 3D colony formation assays also revealed a possible important role for PXDN in tumorigenesis and cell adherence. These latter results are especially intriguing since they were performed with conditions that are closer to those observed *in vivo*. Future work could investigate the influence of PXDN *in vivo* by working with animal models as opposed to 2D cell culture models. However, before conducting animal studies, our functional assays will need to be repeated with an alternative negative control, perhaps a scrambled version of the PXDN siRNA, to confirm the influence of PXDN expression on EMT observed in our studies since our esi negative control was mostly unreliable. In addition, the level of PXDN knockdown could also be optimised to determine whether greater levels of knockdown can be achieved and the implications of this on EMT features studied. However, it is interesting to note that CRISPR KO of PXDN led to complete cell detachment and it was difficult to maintain these cells in culture. Future *in vivo* experiments could involve reducing PXDN expression with PXDN siRNA in various cancer

cell lines followed by xenografting these cancerous cells into mouse models. By transferring these altered cancer cells into mouse models, we would be able to observe how a reduction in PXDN expression may influence the growth and metastatic potential of cancer cells *in vivo*. These studies could provide us with an exciting new therapeutic target.

References

Alfakry, H., Malle, E., Koyani, C.N., Pussinen, P.J. and Sorsa, T. (2016) Neutrophil proteolytic activation cascades: a possible mechanistic link between chronic periodontitis and coronary heart disease. *Innate Immun*. **22**, 85–99

Alleva, R., Di Donato, F., Strafella, E., Staffolani, S., Nocchi, L., Borghi, B., Pignotti, E., Santarelli, L., Tomasetti, M. (2012) Effect of ascorbic acid-rich diet on *in vivo*-induced oxidative stress. *Br. J. Nutr*. **107**, 1645–1654

Ambrozova, N., Ulrichova, J. and Galandakova, A. (2017) Models for the study of skin wound healing. The role of Nrf2 and NF-κB. *Biomed. Pap. Med. Fac. Univ. Palacky Olomouc Czech. Repub*. **161**, 1–13

André-Lévigne, D., Modarressi, A., Pepper, M.S. and Pittet-Cuénod, B. (2017) Reactive Oxygen Species and NOX Enzymes Are Emerging as Key Players in Cutaneous Wound Repair. *Int. J. Mol. Sci*. **18**, 1–28

Bai, Y.P., Hu, C.P., Yuan, Q., Peng, J., Shi, R.Z., Yang, T.L., Cao, Z.H., Li, Y.J., Cheng, G. and Zhang, G.G. (2011) Role of VPO1, a newly identified heme-containing peroxidase, in ox-LDL induced endothelial cell apoptosis. *Free Radic. Biol. Med*. **51**, 1492–1500

Barnett, P., Arnold, R.S., Mezencev, R., Chung, L.W.K., Zayzafoon, M. and Odero-Marah, V. (2011) Snail-Mediated Regulation of Reactive Oxygen Species in ARCaP Human Prostate Cancer Cells. *Biochem. Biophys. Res. Commun*. **404**, 34–39

Bedaiwy, M.A., Falcone, T., Mohamed, M.S., Aleem, A.A., Sharma, R.K., Worley, S.E., Thornton, J. and Agarwal, A. (2004) Differential growth of human embryos in vitro: role of reactive oxygen species. *Fertil. Steril*. **82**, 593–600

Bhave, G., Colon, S. and Ferrell, N. (2017) The sulfilimine cross-link of collagen IV contributes to kidney tubular basement membrane stiffness. *Am. J. Physiol. Renal Physiol*. **313**, F596–F602

Bhave, G., Cummings, C.F., Vanacore, R.M., Kumagai-Cresse, C., Ero-Tolliver, I.A., Rafi, M., Kang, J-S., Pedchenko, V., Fessler, L.I., Fessler, J.H. and Hudson, B.G. (2012)

Peroxidasin forms sulfilimine chemical bonds using hypohalous acids in tissue genesis. *Nat. Chem. Biol.* **8**, 784–790

Blanc, A., Pandey, N.R. and Srivastava, A.K. (2003) Synchronous activation of ERK 1/2, p38mapk and PKB/Akt signalling by H2O2 in vascular smooth muscle cells: potential involvement in vascular disease. *Int. J. Mol. Med.* **11**, 229–234

Borowicz, S., Van Scoyk, M., Avasarala, S., Karuppusamy Rathinam, M.K., Tauler, J., Bikkavilli, R.K. and Winn R.A. (2014) The Soft Agar Colony Formation Assay. *J. Vis. Exp.* **92**, e51998

Bradford, M.M. (1976) A Rapid and Sensitive Method for the Quantitation of Microgram Quantities of Protein Utilizing the Principle of Protein-Dye Binding. *Anal. Biochem.* **72**, 248–254

Bramhall, S., Noack, N., Wu, M. and Loewenberg, J.R. (1969) A simple colorimetric method for determination of protein. *Anal. Biochem.* **31**, 146–148

Brown, K.L., Darris, C., Rose, K.L., Sanchez, O.A., Madu, H., Avance, J., Brooks, N., Zhang, M.Z., Fogo, A., Harris, R., Hudson, B.G. and Voziyan, P. (2015) Hypohalous Acids Contribute to Renal Extracellular Matrix Damage in Experimental Diabetes. *Diabetes*. **64**, 2242–2253

Bryan, H.K., Olayanju, A., Goldring, C.E. and Park, B.K. (2013) The Nrf2 cell defence pathway: Keap1-dependent and -independent mechanisms of regulation. *Biochem. Pharmacol*. **85**, 705–717

Cannito, S., Novo, E., di Bonzo, L.V., Busletta, C., Colombatto, S. and Parola, M. (2010) Epithelial-mesenchymal transition: from molecular mechanisms, redox regulation to implications in human health and disease. *Antioxid. Redox Signal*. **12**, 1383–1430

Cano, A., Pérez-Moreno, M.A., Rodrigo, I., Locascio, A., Blanco, M.J., del Barrio, M.G., Portillo, F., Nieto, M.A. (2000) The transcription factor snail controls epithelial-mesenchymal transitions by repressing E-cadherin expression. *Nat. Cell Biol.* **2**, 76–83

Chade, A.R., Lerman, A. and Lerman, L.O. (2005) Kidney in early atherosclerosis. *Hypertension*. **45**, 1042–1049

Cheng, G., Li, H., Cao, Z., Qiu, X., McCormick, S., Thannickal, V.J. and Nauseef, W.M. (2011) Vascular Peroxidase-1 is Rapidly Secreted, Circulates in Plasma, and Supports Dityrosine Cross-Linking Reactions. *Free Radic. Biol. Med.* **51**, 1445–1453

Cheng, G., Salerno, J.C., Cao, Z., Pagano, P.J. and Lambeth, J.D. (2008) Identification and characterization of VPO1, a new animal heme-containing peroxidase. *Free Radic. Biol. Med.* **45**, 1682–1694

Cheng, K.Y. and Hao, M. (2017) Mammalian Target of Rapamycin (mTOR) Regulates Transforming Growth Factor-β1 (TGF-β1)-Induced Epithelial-Mesenchymal Transition via Decreased Pyruvate Kinase M2 (PKM2) Expression in Cervical Cancer Cells. *Med. Sci. Monit.* **27**, 2017–2028

Choi, A., Lao, R., Ling-Fung Tang, P., Wan, E., Mayer, W., Bardakjian, T., Shaw, G.M., Kwok, P.Y., Schneider, A. and Slavotinek, A. (2015) Novel mutations in *PXDN* cause microphthalmia and anterior segment dysgenesis. *Eur. J. Hum. Genet.* **23**, 337–341

Chorley, B.N., Campbell, M.R., Wang, X., Karaca, M., Sambandan, D., Bangura, F., Xue, P., Pi, J., Kleeberger, S.R. and Bell, D.A. (2012) Identification of novel NRF2-regulated genes by ChIP-Seq: influence on retinoid X receptor alpha. *Nucleic Acids Res.* **40**, 7416–7429

Cuff, S., Lewis, R.D., Chinje, E., Jaffar, M., Knox, R. and Weeks, I. (2018) An improved cell-permeable fluorogenic substrate as the basis for a highly sensitive test for NAD(P)H quinone oxidoreductase 1 (NQO1) in living cells. *Free Radic. Biol. Med.* **116**, In press

Davies, M.J., Hawkins, C.L., Pattison, D.I. and Rees, M.D. (2008) Mammalian heme peroxidases: from molecular mechanisms to health implications. *Antioxid. Redox Signal.* **10**, 1199–1234

Dinkova-Kostova, A.T., Holtzclaw, W.D., Cole, R.N., Itoh, K., Wakabayashi, N., Katoh, Y., Yamamoto, M. and Talalay, P. (2002) Direct evidence that sulfhydryl groups of Keap1 are the sensors regulating induction of phase 2 enzymes that protect against carcinogens and oxidants. *Proc. Natl. Acad. Sci. U.S.A.* **99**, 11908–11913

Dunnill, C., Patton, T., Brennan, J., Barrett, J., Dryden, M., Cooke, J., Leaper, D. and Georgopoulos, N.T. (2017) Reactive oxygen species (ROS) and wound healing: the

functional role of ROS and emerging ROS-modulating technologies for augmentation of the healing process. *Int. Wound J.* **14**, 89–96

Dyksterhuis, L.D., White, J.F., Hickey, M., Kirby, N., Mudie, S., Hawley, A., Vashi, A., Nigro, J., Werkmeister, J.A. and Ramshaw, J.A.M. (2011) Impact of Heparan Sulfate Chains and Sulfur-Mediated Bonds on the Mechanical Properties of Bovine Lens Capsule. *Biophys. J.* **100**, 2077–2083

Eble, J.A. and de Rezende, F.F. (2014) Redox-relevant aspects of the extracellular matrix and its cellular contacts via integrins. *Antioxid. Redox Signal.* **20**, 1977–1993

Ehrlich, H.P. and Hunt, T.K. (2012) Collagen Organisation Critical Role in Wound Contraction. *Adv. Wound Care.* **1**, 3–9

Eskandani, M., Hamishehkar, H. and Ezzati Nazhad Dolatabadi, J. (2014) Cytotoxicity and DNA damage properties of tert-butylhydroquinone (TBHQ) food additive. *Food Chem.* **153**, 315–320

Fabrizio, F.P., Costantini, M., Copetti, M., la Torre, A., Sparaneo, A., Fontana, A., Poeta, L., Gallucci, M., Sentinelli, S., Graziano, P., Parente, P., Pompeo, V., De Salvo, L., Simone, G., Papalia, R., Picardo, F., Balsamo, T., Flammia, G.P., Trombetta, D., Pantalone, A., Kok, K., Paranita, F., Muscarella, L.A. and Fazio, V.M. (2017) Keap1/Nrf2 pathway in kidney cancer: frequent methylation of KEAP1 gene promoter in clear renal cell carcinoma. *Oncotarget.* **8**, 11187–11198

Fadare, O., Reddy, H., Wang, J., Hileeto, D., Schwartz, P.E. and Zheng, W. (2005) E-cadherin and β-catenin expression in early stage cervical carcinoma: a tissue microarray study of 147 cases. *World J. Surg. Oncol.* **3**, 1–11

Fahey, J.W., Haristoy, X., Dolan, P.M., Kensler, T.W., Scholtus, I., Stephenson, K.K., Talalay, P. and Lozniewski, A. (2002) Sulforaphane inhibits extracellular, intracellular, and antibiotic-resistant strains of *Helicobacter pylori* and prevents benzo[a]pyrene-induced stomach tumours. *Proc. Natl. Acad. Sci. U. S. A.* **99**, 7610–7615

Fang, M., Yuan, J., Peng, C. and Li, Y. (2014) Collagen as a double-edged sword in tumour progression. *Tumour Biol.* **35**, 2871–2882

Fidler, A.L., Vanacore, R.M., Chetyrkin, S.V., Pedchenko, V.K., Bhave, G., Yin, V.P., Stothers, C.L., Rose, K.L., McDonald, W.H., Clark, T.A., Borza, D.B., Steele, R.E., Ivy, M.T., Aspirnauts, T., Hudson, J.K. and Hudson, B.G. (2014) A unique covalent bond in basement membrane is a primordial innovation for tissue evolution. *Proc. Natl. Acad. Sci. U. S. A.* **111**, 331–336

Filippova, M., Filippov, V., Williams, V.M., Zhang, K., Kokoza, A., Bashkirova, S. and Duerksen-Hughes, P. (2014) Cellular levels of oxidative stress affect the response of cervical cancer cells to chemotherapeutic agents. *Biomed. Res. Int.* **2014**, 1–14

Friedl, P. and Gilmour, D. (2009) Collective cell migration in morphogenesis, regeneration and cancer. *Nat. Rev. Mol. Cell Biol.* **10**, 445–457

Friedrichs, K., Baldus, S. and Klinke, A. (2012) Fibrosis in Atrial Fibrillation- Role of Reactive Species and MPO. *Front. Physiol.* **20**, 1–11

Furukawa, M. and Xiong, Y. (2005) BTB protein Keap1 targets antioxidant transcription factor Nrf2 for ubiquitination by the Cullin 3-Roc1 ligase. *Mol. Cell Biol.* **25**, 162–171

Gao, J., Zhu, Y., Nilsson, M. and Sundfeldt, K. (2014) TGF-β isoforms induce EMT independent migration of ovarian cancer cells. *Cancer Cell Int.* **14**, 1–10

Gaut, J.P., Yeh, G.C., Tran, H.D., Byun, J., Henderson, J.P., Richter, G.M., Brennan, M.L., Lusis, A.J., Belaaouaj, A., Hotchkiss, R.S. and Heinecke, J.W. (2001) Neutrophils employ the myeloperoxidase system to generate antimicrobial brominating and chlorinating oxidants during sepsis. *Proc. Natl. Acad. Sci. U. S. A.* **98**, 11961–11966

Giannelli, G., Bergamini, C., Fransvea, E., Marinosci, F., Quaranta, V. and Antonaci, S. (2001) Human hepatocellular carcinoma (HCC) cells require both α3β1 integrin and matrix metalloproteinases activity for migration and invasion. *Lab. Invest.* **81**, 613–627

Giannoni, E., Parri, M. and Chiarugi, P. (2012) EMT and Oxidative Stress: A Bidirectional Interplay Affecting Tumour Malignancy. *Antioxid. Redox Signal.* **16**, 1248–1263

Gill, J.G., Piskounova, E. and Morrison, S.J. (2016) Cancer, Oxidative Stress, and Metastasis. *Cold Spring Harb. Symp. Quant. Biol.* **81**, 163–175

Guérin, P., El Mouatassim, S. and Ménézo, Y. (2001) Oxidative stress and protection against reactive oxygen species in the pre-implantation embryo and its surroundings. *Hum. Reprod. Update*. **7**, 175–189

Gueron, G., De Siervi, A., Ferrando, M., Salierno, M., De Luca, P., Elguero, B., Meiss, R., Navone, N. and Vazquez, E.S. (2009) Critical role of endogenous Heme Oxygenase 1 as a tuner of the invasive potential of prostate cancer cells. *Mol. Cancer Res*. **7**, 1745–1755

Guo, Y. and Shen, L. (2017) Overexpression of NRF2 is correlated with prognoses of patients with malignancies: A meta-analysis. *Thorac. Cancer*. **8**, 558–564

Haass, N.K., Beaumont, K.A., Hill, D.S., Anfosso, A., Mrass, P., Munoz, M.A., Kinjyo, I. and Weninger, W. (2014) Real-time cell cycle imaging during melanoma growth, invasion, and drug response. *Pigment Cell Melanoma Res*. **27**, 764–776

Harvey, A.J., Kind, K.L. and Thompson, J.G. (2002) REDOX regulation of early embryo development. *Reproduction*. **123**, 479–486

Hayes, J.D. and Dinkova-Kostova, A.T. (2014) The Nrf2 regulatory network provides an interface between redox and intermediary metabolism. *Trends Biochem. Sci*. **39**, 199–218

Hecker, L., Vittal, R., Jones, T., Jagirdar, R., Luckhardt, T.R., Horowitz, J.C., Pennathur, S., Martinez, F.J. and Thannickal, V.J. (2009) NADPH oxidase-4 mediates myofibroblast activation and fibrogenic responses to lung injury. *Nat. Med*. **15**, 1077–1081

Heinecke, J.W., Li, W., Daehnke, H.L. 3rd and Goldstein, J.A. (1993) Dityrosine, a specific marker of oxidation, is synthesized by the myeloperoxidase-hydrogen peroxide system of human neutrophils and macrophages. *J. Biol. Chem*. **268**, 4069–4077

Holmström, K.M. and Finkel, T. (2014) Cellular mechanisms and physiological consequences of redox-dependent signalling. *Nat. Rev. Mol. Cell Biol*. **15**, 411–421

Homma, S., Ishii, Y., Morishima, Y., Yamadori, T., Matsuno, Y., Haraguchi, N., Kikuchi, N., Satoh, H., Sakamoto, T., Hizawa, N., Itoh, K. and Yamamoto, M. (2009) Nrf2 Enhances Cell Proliferation and Resistance to Anticancer Drugs in Human Lung Cancer. *Clin. Cancer Res*. **15**, 3423–3432

Hong, F., Freeman, M.L. and Liebler, D.C. (2005) Identification of sensor cysteines in human Keap1 modified by the cancer chemopreventive agent sulforaphane. *Chem. Res. Toxicol.* **18**, 1917–1926

Horikoshi, N., Cong, J., Kley, N. and Shenk, T. (1999) Isolation of Differentially Expressed cDNAs from p53-Dependent Apoptotic Cells: Activation of the Human Homologue of the *Drosophila* Peroxidasin Gene. *Biochem. Biophys. Res. Commun.* **261**, 864–869

Huang, H.C., Nguyen, T. and Pickett, C.B. (2002) Phosphorylation of Nrf2 at Ser-40 by Protein Kinase C Regulates Antioxidant Response Element-mediated Transcription. *J. Biol. Chem.* **277**, 42769–42774

Huang, R.Y., Guilford, P. and Thiery, J.P. (2012) Early events in cell adhesion and polarity during epithelial-mesenchymal transition. *J. Cell Sci.* **125**, 4417–4422

Humphries, M.J. (2009) Cell Adhesion assays. *Methods Mol. Biol.* **522**, 203–210

Imhoff, B.R. and Hansen, J.M. (2010) *tert*-butylhydroquinone induces mitochondrial oxidative stress causing Nrf2 activation. *Cell Biol. Toxicol.* **26**, 541–551

Ishikawa, K., Takenaga, K., Akimoto, M., Koshikawa, N., Yamaguchi, A., Imanishi, H., Nakada, K., Honma, Y. and Hayashi, J. (2008) ROS-generating mitochondrial DNA mutations can regulate tumor cell metastasis. *Science*. **320**, 661–664

Jayachandran, A., Prithviraj, P., Lo, P.H., Walkiewicz, M., Anaka, M., Woods, B.L., Tan, B., Behren, A., Cebon, J. and McKeown, S.J. (2016) Identifying and targeting determinants of melanoma cellular invasion. *Oncotarget*. **7**, 41186–41202

Jeong, Y., Hoang, N.T., Lovejoy, A., Stehr, H., Newman, A.M., Gentles, A.J., Kong, W., Truong, D., Martin, S., Chaudhuri, A., Heiser, D., Zhou, L., Say, C., Carter, J.N., Hiniker, S.M., Loo, B.W. Jr, West, R.B., Beachy, P., Alizadeh, A.A. and Diehn, M. (2017) Role of Keap1/NRF2 and TP53 Mutations in Lung Squamous Cell Carcinoma Development and Radiation Resistance. *Cancer Discov.* **7**, 86–101

Jiang, J., Wang, K., Chen, Y., Chen H., Nice, E.C. and Huang, C. (2017) Redox regulation in tumor cell epithelial-mesenchymal transition: molecular basis and therapeutic strategy. *Signal Transduct. Target. Ther.* **2**, 1–12

Jones-Paris, C.R., Paria, S., Berg, T., Saus, J., Bhave, G., Paria, B.C. and Hudson, B.G. (2017) Embryo implantation triggers dynamic spatiotemporal expression of the basement membrane toolkit during uterine reprogramming. *Matrix Biol*. **57–58**, 347–365

Jordan, N.V., Johnson, G.L. and Abell, A.N. (2011) Tracking the intermediate stages of epithelial-mesenchymal transition in epithelial stem cells and cancer. *Cell Cycle*. **10**, 2865–2873

Jung, B.J., Yoo, H.S., Shin, S., Park, Y.J. and Jeon, S.M. (2018) Dysregulation of NRF2 in Cancer: from Molecular Mechanisms to Therapeutic Opportunities. *Biomol*. *Ther*. **26**, 57–68

Kalluri, R. and Weinberg, R.A. (2009) The basics of epithelial-mesenchymal transition. *J*. *Clin*. *Invest*. **119**, 1420–1428

Karp, D.D., Lee, S.J., Keller, S.M., Wright, G.S., Aisner, S., Belinsky, S.A., Johnson, D.H., Johnston, M.R., Goodman, G., Clamon, G., Okawara, G., Marks, R., Frechette, E., McCaskill-Stevens, W., Lippman, S.M., Ruckdeschel, J. and Khuri, F.R. (2013) Randomized, double-blind, placebo-controlled, phase III chemoprevention trial of selenium supplementation in patients with resected stage I non-small-cell lung cancer: ECOG 5597. *J*. *Clin*. *Oncol*. **31**, 4179–4187

Kensler, T.W., Egner, P.A., Agyeman, A.S., Visvanathan, K., Groopman, J.D., Chen, J.G., Chen, T.Y., Fahey, J.W. and Talalay, P. (2013) Keap1-Nrf2 Signalling: A Target for Cancer Prevention by Sulforaphane. *Top*. *Curr*. *Chem*. **329**, 163–177

Kessenbrock, K., Plaks, V. and Werb, Z. (2010) Matrix metalloproteinases: regulators of the tumor microenvironment. *Cell*. **141**, 52–67

Khan, K., Rudkin, A., Parry, D.A., Burdon, K.P., McKibbin, M., Logan, C.V., Abdelhamed, Z.I.A., Muecke, J.S., Fernandez-Fuentes, N., Laurie, K.J., Shires, M., Fogarty, R., Carr, I.M., Poulter, J.A., Morgan, J.E., Mohamed, M.D., Jafri, H., Rasshid, Y., Meng, N., Piseth, H., Toomes, C., Casson, R.J., Taylor, G.R., Hammerton, M., Sheridan, E., Johnson, C.A., Inglehearn, C.F., Craig, J.E. and Ali, M. (2011) Homozygous Mutations in *PXDN* Cause Congenital Cataract, Corneal Opacity, and Developmental Glaucoma. *Am*. *J*. *Hum*. *Genet*. **89**, 464–473

Kim, W.D., Kim, Y.W., Cho, I.J., Lee, C.H. and Kim, S.G. (2012) E-cadherin inhibits nuclear accumulation of Nrf2: implications for chemoresistance of cancer cells. *J. Cell Sci.* **125**, 1284–1295

Kim, Y.R., Oh, J.E., Kim, M.S., Kang, M.R., Park, S.W., Han, J.Y., Eom, H.S., Yoo, N.J. and Lee, S.H. (2010) Oncogenic NRF2 mutations in squamous cell carcinomas of oesophagus and skin. *J. Pathol.* **220**, 446–451

Klebanoff, S.J. (2005) Myeloperoxidase: friend and foe. *J. Leukoc. Biol.* **77**, 598–625

Kumar, B., Koul, S., Khandrika, L., Meacham, R.B. and Koul, H.K. (2008) Oxidative stress is inherent in prostate cancer cells and is required for aggressive phenotype. *Cancer Res.* **68**, 1777–1785

Kuosmanen, S.M., Viitala, S., Laitinen, T., Peräkylä, M., Pölönen, P., Kansanen, E., Leinonen, H., Raju, S., Wienecke-Baldacchino, A., Närvänen, A., Poso, A., Heinäniemi, M., Heikkinen, S. and Levonen, A.L. (2016) The Effects of Sequence Variation on Genome-wide NRF2 Binding–New Target Genes and Regulatory SNPs. *Nucleic Acids Res.* **44**, 1760–1775

Kwak, M.K., Itoh, K., Yamamoto, M., Sutter, T.R. and Kensler, T.W. (2001) Role of Transcription Factor Nrf2 in the Induction of Hepatic Phase 2 and Antioxidative Enzymes in vivo by the Cancer Chemoprotective Agent, 3*H*-1, 2-Dithiole-3-thione. *Mol. Med.* **7**, 135–145

Lamouille, S., Xu, J. and Derynck, R. (2014) Molecular mechanisms of epithelial-mesenchymal transition. *Nat. Rev. Mol. Cell Biol.* **15**, 178–196

Lázár, E., Péterfi, Z., Sirokmány, G., Kovács, H.A., Klement, E., Medzihradszky, K.F. and Geiszt, M. (2015) Structure-function analysis of peroxidasin provides insight into the mechanism of collagen IV crosslinking. *Free Radic. Biol. Med.* **83**, 273–282

Lee, J.M. and Johnson, J.A. (2004) An Important Role of Nrf2-ARE Pathway in the Cellular Defense Mechanism. *J. Biochem. Mol. Biol.* **37**, 139–143

Lee, J.M., Moehlenkamp, J.D., Hanson, J.M. and Johnson, J.A. (2001) Nrf2-dependent activation of the antioxidant responsive element by *tert*-butylhydroquinone is independent of

oxidative stress in IMR-32 human neuroblastoma cells. *Biochem. Biophys. Res. Commun.* **280**, 286–292

Lévigne, D., Modarressi, A., Krause, K.H. and Pittet-Cuénod, B. (2016) NADPH oxidase 4 deficiency leads to impaired wound repair and reduced dityrosine-crosslinking, but does not affect myofibroblast formation. *Free Radic. Biol. Med.* **96**, 374–384

Li, D.J., Zhao, T., Xin, R.J., Wang, Y.Y., Fei, Y.B. and Shen, F.M. (2014) Activation of α7 nicotinic acetylcholine receptor protects against oxidant stress damage through reducing vascular peroxidase-1 in a JNK signalling-dependent manner in endothelial cells. *Cell. Physiol. Biochem.* **33**, 468–478

Li, H., Cao, Z., Moore, D.R., Jackson, P.L., Barnes, S., Lambeth, J.D., Thannickal, V.J. and Cheng, G. (2012) Microbial activity of Vascular Peroxidase 1 in human plasma via generation of hypochlorous acid. *Infect. Immun.* **80**, 2528–2537

Li, J., Johnson, D., Calkins, M., Wright, L., Svendsen, C. and Johnson, J. (2005) Stabilization of Nrf2 by tBHQ Confers Protection against Oxidative Stress-Induced Cell Death in Human Neural Stem Cells. *Toxicol. Sci.* **83**, 313–328

Lin, X., Yang, H., Zhou, L.C. and Guo, Z.M. (2011) Nrf2-Dependent Induction of NQO1 in Mouse Aortic Endothelial Cells Over expressing Catalase. *Free Radic. Biol. Med.* **51**, 97–106

Link, A.J. and LaBaer, J. (2011) Trichloroacetic acid (TCA) precipitation of proteins. *Cold Spring Harb. Protoc.* **2011**, 993–994

Lippman, S.M., Klein, E.A., Goodman, P.J., Lucia, M.S., Thompson, I.M., Ford, L.G., Parnes, H.L., Minasian, L.M., Gaziano, J.M., Hartline, J.A., Parsons, J.K., Bearden, J.D. 3rd, Crawford, E.D., Goodman, G.E., Claudio, J., Winquist, E., Cook, E.D., Karp, D.D., Walther, P., Lieber, M.M., Kristal, A.R., Darke, A.K., Arnold, K.B., Ganz, P.A., Santella, R.M., Albanes, D., Taylor, P.R., Probstfield, J.L., Jaqpal, T.J., Crowley, J.J., Meyskens, F.L. Jr., Baker, L.H. and Coltman C.A. Jr, (2009) Effect of selenium and vitamin E on risk of prostate cancer and other cancers: the Selenium and Vitamin E Cancer Prevention Trial (SELECT). *JAMA.* **301**, 39–51

Liu, B., Luo, X.J., Yang, Z.B., Zhang, J.J., Li, T.B., Zhang, X.J., Ma, Q.L., Zhang, G.G., Hu, C.P. and Peng, J. (2014) Inhibition of NOX/VPO1 pathway and inflammatory reaction by

trimethoxystilbene in prevention of cardiovascular remodelling in hypoxia-induced pulmonary hypertensive rats. *J. Cardiovasc. Pharmacol.* **63**, 567–576

Liu, X., Dai, R., Ke, M., Suheryani, I., Meng, W. and Deng, Y. (2017) Differential Proteomic Analysis of Dimethylnitrosamine (DMN)-Induced Liver Fibrosis. *Proteomics*. **17**, 1–13

Liu, X.F., Zhou, D.D., Xie, T., Malik, T.H., Lu, C.B., Li, H.J., Wang, F., Shu, C., Liu, C., Lu, C.W. and Hao, J.L. (2017) Nrf2, a Potential Therapeutic Target against Oxidative Stress in Corneal Diseases. *Oxid. Med. Cell. Longev.* **2017**, 1–9

Liu, X.M., Peyton, K.J., Ensenat, D., Wang, H., Hannink, M., Alam, J. and Durante, W. (2007) Nitric oxide stimulates heme oxygenase-1 gene transcription via the Nrf2/ARE complex to promote vascular smooth muscle cell survival. *Cardiovasc. Res.* **75**, 381–389

Liu, Y., Carson-Walter, E.B., Cooper, A., Winans, B.N., Johnson, M.D. and Walter, K.A. (2010) Vascular gene expression patterns are conserved in primary and metastatic brain tumours. *J. Neurooncol.* **99**, 13–24

Liu, Z., Liu, Y., Xu, Q., Peng, H., Tang, Y., Yang, T., Yu, Z., Cheng, G., Zhang, G. and Shi, R. (2017) Critical role of vascular peroxidase 1 in regulating endothelial nitric oxide synthase. *Redox Biol.* **12**, 226–232

Loboda, A., Damulewicz, M., Pyza, E., Jozkowicz, A. and Dulak, J. (2016) Role of Nrf2/HO-1 system in development, oxidative stress response and diseases: an evolutionarily conserved mechanism. *Cell. Mol. Life Sci.* **73**, 3221–3247

Long, M., de la Vega, M.R., Wen, Q., Bharara, M., Jiang, T., Zhang, R., Zhou, S., Wong, P.K., Wondrak, G.T., Zheng, H. and Zhang, D.D. (2016) An essential role of Nrf2 in Diabetic Wound Healing. *Diabetes*. **65**, 780–793

Ma, J.Q., Tuersun, H., Jiao, S.J., Zheng, J.H., Xiao, J.B. and Hasim, A. (2015) Functional Role of NRF2 in Cervical Carcinogenesis. *PLoS One*. **10**, e0133876

Ma, Q.L., Zhang, G.G. and Peng, J. (2013) Vascular peroxidase 1: A novel enzyme in promoting oxidative stress in cardiovascular system. *Trends Cardiovasc. Med.* **23**, 179–183

Mathelier, A., Fornes, O., Arenillas, D.J., Chen, C.Y., Denay, G., Lee, J., Shi, W., Shyr, C., Tan, G., Worsley-Hunt, R., Zhang, A.W., Parcy, F., Lenhard, B., Sandelin, A. and

Wasserman, W.W. (2016) JASPAR 2016: a major expansion and update of the open-access database of transcription factor binding profiles. *Nucleic Acids Res*. **44**, D110–D115

McCall, A.S., Cummings, C.F., Bhave, G., Vanacore, R., Page-McCaw, A. and Hudson, B.G. (2014) Bromine is an essential trace element for assembly of collagen IV scaffolds in tissue development and architecture. *Cell*. **157**, 1380–1392

McMahon, M., Itoh, K., Yamamoto, M., Chanas, S.A., Henderson, C.J., McLellan, L.I., Wolf, C.R., Cavin, C. and Hayes, J.D. (2001) The Cap 'n' Collar Basic Leucine Zipper Transcription Factor Nrf2 (NF-E2 p45-related Factor 2) Controls Both Constitutive and Inducible Expression of Intestinal Detoxification and Glutathione Biosynthetic Enzymes. *Cancer Res*. **61**, 3299–3307

Micheal, S., Siddiqui, S.N., Zafar, S.N., Iqbal, A., Khan, M.I. and den Hollander, A.I. (2016) Identification of Novel Variants in LTBP2 and PXDN Using Whole-Exome Sequencing in Developmental and Congenital Glaucoma. *PLoS One*. **11**, e0159259

Midwinter, R.G., Vissers, M.C.M. and Winterbourn, C.C. (2001) Hypochlorous Acid Stimulation of the Mitogen-Activated Protein Kinase Pathway Enhances Cell Survival. *Arch. Biochem. Biophys*. **394**, 13–20

Milkovic, L., Zarkovic, N. and Saso, L. (2017) Controversy about pharmacological modulation of Nrf2 for cancer therapy. *Redox Biol*. **12**, 727–732

Mitchell, M.S., Kan-Mitchell, J., Minev, B., Edman, C. and Deans, R.J. (2000) A Novel Melanoma Gene (*MG50*) Encoding the Interleukin 1 Receptor Antagonist and Six Epitopes Recognized by Human Cytolytic T Lymphocytes. *Cancer Res*. **60**, 6448–6456

Mitra, A., Mishra, L. and Li, S. (2015) EMT, CTCs and CSCs in tumor relapse and drug-resistance. *Oncotarget*. **6**, 10697–10711

Mori, K., Shibanuma, M. and Nose, K. (2004) Invasive potential induced under long-term oxidative stress in mammary epithelial cells. *Cancer Res*. **64**, 7464–7472

Moriguchi, T. (2016) Versatile activity of the master regulator of the antioxidant response in tumour initiation, progression and metastasis. *Cancer Cell Microenviron*. **3**, 1–5

Morry, J., Ngamcherdtrakul, W. and Yantasee, W. (2017) Oxidative stress in cancer and fibrosis: Opportunity for therapeutic intervention with antioxidant compounds, enzymes, and nanoparticles. *Redox Biol*. **11**, 240–253

Nakagami, Y. (2016) Nrf2 is an Attractive Therapeutic Target for Retinal Diseases. *Oxid. Med. Cell. Longev*. **2016**, 1–8

Nelson, R.E., Fessler, L.I., Takagi, Y., Blumberg, B., Keene, D.R., Olson, P.F., Parker, C.G. and Fessler, J.H. (1994) Peroxidasin: a novel enzyme-matrix protein of *Drosophila* development. *EMBO J*. **13**, 3438–3447

Nguyen, T., Sherratt, P.J., Huang, H.C., Yang, C.S. and Pickett, C.B. (2003) Increased protein stability as a mechanism that enhances Nrf2-mediated transcriptional activation of the antioxidant response element. Degradation of Nrf2 by the 26 S proteasome. *J. Biol. Chem.* **278**, 4536–4541

Ni, H.M., Woolbright, B.L., Williams, J., Copple, B., Cui, W., Luyendyk, J.P., Jaeschke, H. and Ding, W.X. (2014) Nrf2 promotes the development of fibrosis and tumorigenesis in mice with defective hepatic autophagy. *J. Hepatol*. **61**, 617–625

Nieto, M.A. (2002) The snail superfamily of zinc-finger transcription factors. *Nat. Rev. Mol. Cell Biol*. **3**, 155–166

Nieto, M.A., Huang, R.Y., Jackson, R.A. and Thiery, J.P. (2016) EMT: 2016. *Cell*. **166**, 21–45

Ohta, T., Lijima, K., Miyamoto, M., Nakahara, I., Tanaka, H., Ohtsuji, M., Suzuki, T., Kobayashi, A., Yokota, J., Sakiyama, T., Shibata, T., Yamamoto, M. and Hirohashi, S. (2008) Loss of Keap1 function activates Nrf2 and provides advantages for lung cancer cell growth. *Cancer Res*, **68**, 1303–1309

Okamura, D.M. and Pennathur, S. (2015) The balance of powers: Redox regulation of fibrogenic pathways in kidney injury. *Redox Biol*. **6**, 495–504

Osburn, W.O. and Kensler, T.W. (2008) Nrf2 signalling: An adaptive response pathway for protection against environmental toxic insults. *Mutat. Res*. **659**, 31–39

Paoli, P., Giannoni, E. and Chiarugi, P. (2013) Anoikis molecular pathways and its role in cancer progression. *Biochim. Biophys. Acta*. **1833**, 3481–3498

Pappa, G., Strathmann, J., Löwinger, M., Bartsch, H. and Gerhäuser, C. (2007) Quantitative combination effects between sulforaphane and 3,3′-diindolylmethane on proliferation of human colon cancer cells *in vitro*. *Carcinogenesis*. **28**, 1471–1477

Paumann-Page, M., Katz, R.S., Bellei, M., Schwartz, I., Edenhofer, E., Sevcnikar, B., Soudi, M., Hofbauer, S., Battistuzzi, G., Furtmüller, P.G. and Obinger, C. (2017) Pre-steady-state Kinetics Reveal the Substrate Specificity and Mechanism of Halide Oxidation of Truncated Human Peroxidasin 1. *J. Biol. Chem.* **292**, 4583–4592

Peinado, H., Quintanilla, M. and Cano, A. (2003) Transforming growth factor β-1 induces snail transcription factor in epithelial cell lines: mechanisms for epithelial mesenchymal transitions. *J. Biol. Chem*. **278**, 21113–2123

Péterfi, Z., Donkó, A., Orient, A., Sum, A., Prókai, A., Molnár, B., Veréb, Z., Rajnavölgyi, E., Kovács, K.J., Müller, V., Szabó, A.J., and Geiszt, M. (2009) Peroxidasin is secreted and incorporated into the Extracellular Matrix of myofibroblasts and fibrotic kidney. *Am. J. Pathol*. **175**, 725–735

Pi, J., Zhang, Q., Woods, C.G., Wong, V., Collins, S. and Anderson, M.E. (2008) Activation of Nrf2-mediated oxidative stress response in macrophages by hypochlorous acid. *Toxicol. Appl. Pharmacol*. **226**, 236–243

Piskounova, E., Agathocleous, M., Murphy, M.M., Hu, Z., Huddlestun, S.E., Zhao, Z., Leitch, A.M., Johnson, T.M., DeBerardinis, R.J. and Morrison, S.J. (2015) Oxidative stress inhibits distant metastasis by human melanoma cells. *Nature*. **527**, 186–191

Poillet-Perez, L., Despouy, G., Delage-Mourroux, R. and Boyer-Guittaut, M. (2015) Interplay between ROS and autophagy in cancer cells, from tumor initiation to cancer therapy. *Redox Biol*. **4**, 184–192

Porporato, P.E., Payen, V.L., Pérez-Escuredo, J., De Saedeleer, C.J., Danhier, P., Copetti, T., Dhup, S., Tardy, M., Vazeille, T., Bouzin, C., Feron, O., Michiels, C., Gallez, B. and Sonveaux, P. (2014) A mitochondrial switch promotes tumor metastasis. *Cell Rep*. **8**, 754–766

Promega Corporation (2013) Steady-Glo® Luciferase Assay System Technical Manual, viewed on 18 November 2017 from https://www.promega.com/resources/protocols/technical-manuals/0/steady-glo-luciferase-assay-system-protocol/

Pronk, T.E., van der Veen, J.W., Vandebriel, R.J., van Loveren, H., de Vink, E.O. and Pennings, J.L.A. (2014) Comparison of the molecular topologies of stress-activated transcription factors HSF1, AP-1, NRF2, and NF-κB in their induction kinetics of HMOX1. *BioSystems*. **124**, 75–85

Rachakonda, G., Sekhar, K.R., Jowhar, D., Samson, P.C., Wikswo, J.P., Beauchamp, R.D., Datta, P.K. and Freeman, M.L. (2010) Increased cell migration and plasticity in Nrf2-deficient cancer cell lines. *Oncogene*. **29**, 3703–3714

Radisky, D.C. (2005) Epithelial-mesenchymal transition. *J. Cell Sci*. **118**, 4325–4326

Rangasamy, T., Guo, J., Mitzner, W.A., Roman, J., Singh, A., Fryer, A.D., Yamamoto, M., Kensler, T.W., Tuder, R.M., Georas, S.N. and Biswal, S. (2005) Disruption of *Nrf2* enhances susceptibility to severe airway inflammation and asthma in mice. *J. Exp. Med*. **202**, 47–59

Reddy, N.M., Suryanarayana, V., Kalvakolanu, D.V., Yamamoto, M., Kensler, T.W., Hassoun, P.M., Kleeberger, S.R. and Reddy, S.P. (2009) Innate immunity against bacterial infection following hyperoxia exposure is impaired in Nrf2-deficient mice. *J. Immunol*. **183**, 4601–4608

Reuter, S., Gupta, S.C., Chaturvedi, M.M. and Aggarwal, B.B. (2010) Oxidative stress, inflammation, and cancer: how are they linked? *Free Radic. Biol. Med*. **49**, 1603–1616

Rochette, L., Lorin, J., Zeller, M., Guilland, J.C., Lorgis, L., Cottin, Y. and Vergely, C. (2013) Nitric oxide synthase inhibition and oxidative stress in cardiovascular diseases: possible therapeutic targets? *Pharmacol. Ther*. **140**, 239–257

Satoh, H., Moriguchi, T., Taguchi, K., Takai, J., Maher, J.M., Suzuki, T., Winnard, P.T. Jr., Raman, V., Ebina, M., Nukiwa, T. and Yamamoto, M. (2010) Nrf2-deficiency creates a responsive microenvironment for metastasis to the lung. *Carcinogenesis*. **31**, 1833–1843

Saw, C.L., Yang, A.Y., Huang, M.T., Liu, Y., Lee, J.H., Khor, T.O., Su, Z.Y., Shu, L., Lu, Y., Conney, A.H. and Kong, A.N. (2014) Nrf2 null enhances UVB-induced skin inflammation and extracellular matrix damages. *Cell Biosi*. **4**, 1–7

Shi, R., Hu, C., Yuan, Q., Yang, T., Peng, J., Li, Y., Bai, Y., Cao, Z., Cheng, G. and Zhang, G. (2011) Involvement of vascular peroxidase 1 in angiotensin II-induced vascular smooth muscle cell proliferation. *Cardiovasc*. *Res*. **91**, 27–36

Shin, D.H., Park, H.M., Jung, K.A., Choi, H.G., Kim, J.A., Kim, D.D., Kim, S.G., Kang, K.W., Ku, S.K., Kensler, T.W. and Kwak, M.K. (2010) The NRF2-heme oxygenase-1 system modulates cyclosporine A-induced epithelial-mesenchymal transition and renal fibrosis. *Free Radic*. *Biol*. *Med*. **48**, 1051–1063

Singh, A., Misra, V., Thimmulappa, R.K., Lee, H., Ames, S., Hoque, M.O., Herman, J.G., Baylin, S.B., Sidransky, D., Gabrielson, E., Brock, M.V. and Biswal, S. (2006) Dysfunctional KEAP1-NRF2 interaction in non-small-cell lung cancer. *PLoS Med*. **3**, 1865–1876

Sitole, B.N. and Mavri-Damelin, D. (2018) Peroxidasin is regulated by the epithelial-mesenchymal transition master transcription factor Snai1. *Gene*. **646**, 195–202

Soudi, M., Zamocky, M., Jakopitsch, C., Furtmüller, P.G. and Obinger, C. (2012) Molecular Evolution, Structure, and Function of Peroxidasins. *Chem*. *Biodivers*. **9**, 1776–1793

Stoneman, V.E.A. and Bennett, M.R. (2004) Role of apoptosis in atherosclerosis and its therapeutic implications. *Clin*. *Sci*. **107**, 343–354

Suarez-Carmona, M., Lesage, J., Cataldo, D. and Gilles, C. (2017) EMT and inflammation: inseparable actors of cancer progression. *Mol*. *Oncol*. **11**, 805–823

Surh, Y.J., Kundu, J.K. and Na, H.K. (2008) Nrf2 as a Master Redox Switch in Turning on the Cellular Signalling Involved in the Induction of Cytoprotective Genes by Some Chemopreventive Phytochemicals. *Planta*. *Med*. **74**, 1526–1539

Sykiotis, G.P. and Bohmann, D. (2010) Stress-Activated Cap'n'collar Transcription Factors in Aging and Human Disease. *Sci*. *Signal*. **3**, re3

Taguchi, K. and Yamamoto, M. (2017) The KEAP1-NRF2 System in Cancer. *Front*. *Oncol*. **7**, 1–11

Taguchi, K., Motohashi, H. and Yamamoto, M. (2011) Molecular mechanisms of Keap1-Nrf2 pathway in stress response and cancer evolution. *Genes Cells*. **16**, 123–140

Tahmasbpour, E., Ghanei, M., Qazvini, A., Vahedi, E. and Panahi, Y. (2016) Gene expression profile of oxidative stress and antioxidant defense in lung tissue of patients exposed to sulphur mustard. *Mutat*. *Res*. *Genet*. *Toxicol*. *Environ*. *Mutagen*. **800–801**, 12–21

Tan, Y., Ichikawa, T., Li, J. Si, Q., Yang, H., Chen, X., Goldblatt, C.S., Meyer, C.J., Li, X., Cai, L. and Cui, T. (2011) Diabetic downregulation of Nrf2 activity via ERK contributes to oxidative stress-induced insulin resistance in cardiac cells *in vitro* and *in vivo*. *Diabetes*. **60**, 625–633

Tang, Y., Xu, Q., Peng, H., Liu, Z., Yang, T., Yu, Z., Cheng, G., Li, X., Zhang, G. and Shi, R. (2015) The role of vascular peroxidase 1 in ox-LDL-induced vascular smooth muscle cell calcification. *Atherosclerosis*. **243**, 357–363

Tarin, D., Thompson, E.W. and Newgreen, D.F. (2005) The fallacy of epithelial mesenchymal transition in neoplasia. *Caner Res*. **65**, 5996–6000

Tauber, S., Jais, A., Jeitler, M., Haider, S., Husa, J., Lindroos, J., Knöfler, M., Mayerhofer, M., Pehamberger, H., Wagner, O. and Bilban, M. (2010) Transcriptome analysis of human cancer reveals a functional role of Heme Oxygenase-1 in tumour cell adhesion. *Mol*. *Cancer*. **9**, 200–216

Thiery, J.P., Acloque, H., Huang, R.Y. and Nieto, M.A. (2009) Epithelial-mesenchymal transitions in development and disease. *Cell*. **139**, 871–890

Thimmulappa, R.K., Lee, H., Rangasamy, T., Reddy, S.P., Yamamoto, M., Kensler, T.W. and Biswal, S. (2006) Nrf2 is a critical regulator of the innate immune response and survival during experimental sepsis. *J*. *Clin*. *Invest*. **116**, 984–995

Tschuch, C., Schulz, A., Pscherer, A., Werft, W., Benner, A., Hotz-Wagenblatt, A., Barrionuevo, L.S., Lichter, P. and Mertens, D. (2008) Off-target effects of siRNA specific for GFP. *BMC Mol*. *Biol*. **24**, 1–14

Ulrich, T.A., de Juan Pardo, E.M. and Kumar, S. (2009) The mechanical rigidity of the extracellular matrix regulates the structure, motility, and proliferation of gliomas cells. *Cancer Res*. **69**, 4167–4174

Vanacore, R., Ham, A.J.L., Voehler, M., Sanders, C.R., Conrads, T.P., Veenstra, T.D., Sharpless, K.B., Dawson, P.E. and Hudson, B.G. (2009) A sulfilimine Bond Identified in Collagen IV. *Science*. **325**, 1230–1234

Wagener, F.A.D.T.G., Volk, H.D., Willis, D., Abraham, N.G., Soares, M.P., Adema, G.J. and Figdor, C.G. (2003) Different Faces of the Heme-Heme Oxygenase System in Inflammation. *Pharmacol*. *Rev*. **55**, 551–571

Wakabayashi, N., Slocum, S.L., Skoko, J.J., Shin, S. and Kensler, T.W. (2010) When Nrf2 talks, who's listening? *Antioxid*. *Redox Signal*. **13**, 1649–1663

Wang, H., Liu, X., Long, M., Huang, Y., Zhang, L., Zhang, R., Zheng, Y., Liao, X., Wang, Y., Liao, Q., Li, W., Tang, Z., Tong, Q., Wang, X., Fang, F., Rojo de la Vega, M., Ouyang, Q., Zhang, D.D., Yu, S. and Zheng, H. (2016) NRF2 activation by antioxidant antidiabetic agents accelerates tumor metastasis. *Sci*. *Transl*. *Med*. **8**, 334ra51

Wang, X., Zhao, X., Yi, Z., Ma, B., Wang, H., Pu, Y., Wang, J. and Wang, S. (2018) WNT5A promotes migration and invasion of human osteosarcoma cells via SRC/ERK/MMP-14 pathway. *Cell Biol*. *Int*. **9999**, 1–10

Wang, Y., Rosen, H., Madtes, D.K., Shao, B., Martin, T.R., Heinecke, J.W. and Fu, X. (2007) Myeloperoxidase Inactivates TIMP-1 by Oxidising Its N-terminal Cysteine Residue: an Oxidative Mechanism for Regulating Proteolysis During Inflammation. *J*. *Biol*. *Chem*. **282**, 31826–31834

Weiss, S.J. (2012) Peroxidasin: tying the collagen-sulfilimine knot. *Nat*. *Chem*. *Biol*. **8**, 740–741

Willis, B.C. and Borok, Z. (2007) TGF-β-induced EMT: mechanisms and implications for fibrotic lung disease. *Am*. *J*. *Physiol*. *Lung Cell*. *Mol*. *Physiol*. **293**, L525–L534

Wu, J.M., Oraee, A., Doonan, B.B., Pinto, J.T. and Hsieh, T.C. (2016) Activation of NQO1 in NQO1*2 polymorphic human leukemic HL-60 cells by diet-derived sulforaphane. *Exp. Hematol. Oncol.* **5**, 1–9

Wyckoff, J.B., Wang, Y., Lin, E.Y., Li, J.F., Goswami, S., Stanley, E.R., Segall, J.E., Pollard, J.W. and Condeelis, J. (2007) Direct visualisation of macrophage-assisted tumour cell intravasation in mammary tumours. *Cancer Res.* **67**, 2649–2656

Yan, C., Grimm, W.A., Garner, W.L., Qin, L., Travis, T., Tan, N. and Han, Y.P. (2014) Epithelial to Mesenchymal Transition in Human Skin Wound Healing Is Induced by Tumor Necrosis Factor-α through Bone Morphogenic Protein-2. *Am. J. Pathol.* **176**, 2247–2258

Yan, X., Sabrautzki, S., Horsch, M., Fuchs, H., Gailus-Durner, V., Beckers, J., Hrabě de Angelis, M. and Graw, J. (2014) Peroxidasin is essential for eye development in the mouse. *Hum. Mol. Genet.* **23**, 5597–5614

Yang, J. and Weinberg, R.A. (2008) Epithelial-Mesenchymal Transition: At the Crossroads of Development and Tumor Metastasis. *Dev. Cell.* **14**, 818–829

Yang, Y., Cao, Z., Tian, L., Garvey, W.T. and Cheng, G. (2013) VPO1 mediates ApoE oxidation and impairs the clearance of plasma lipids. *PLoS One.* **8**, e57571

Yang, Y., Pan, X., Lei, W., Wang, J. and Song, J. (2006) Transforming growth factor-β1 induces epithelial-to-mesenchymal transition and apoptosis via a cell-cycle-dependent mechanism. *Oncogene.* **25**, 7235–7244

You, B., Liu, Y., Chen, J., Huang, X., Peng, H., Liu, Z., Tang, Y., Zhang, K., Xu, Q., Li, X., Cheng, G., Shi, R. and Zhang, G. (2018) Vascular peroxidase 1 mediates hypoxia-induced pulmonary artery smooth muscle cell proliferation, apoptosis resistance and migration. *Cardiovasc. Res.* **114**, 188–199

Young, C.D., Zimmerman, L.J., Hoshino, D., Formisano, L., Hanker, A.B., Gatza, M.L., Morrison, M.M., Moore, P.D., Whitwell, C.A., Dave, B., Stricker, T., Bhola, N.E., Silva, G.O., Patel, P., Brantley-Sieders, D.M., Levin, M., Horiates, M., Palma, N.A., Wang, K., Stephens, P.J., Perou, C.M., Weaver, A.M., O'Shaughnessy, J.A., Chang, J.C., Park, B.H., Liebler, D.C., Cook, R.S. and Arteaga, C.L. (2015) Activating *PIK3CA* Mutations Induce an

Epidermal Growth Factor Receptor (EGFR)/Extracellular Signal-regulated Kinase (ERK) Paracrine Signaling Axis in Basal-like Breast Cancer. *Mol. Cell. Proteomics*. **14**, 1959–1976

Zavadil, J. and Böttinger, E.P. (2005) TGF-β and epithelial-to-mesenchymal transitions. *Oncogene*. **24**, 5764–5774

Zhang, Y., Wen, G., Shao, G., Wang, C., Lin, C., Fang, H., Balajee, A.S., Bhagat, G., Hei, T.K. and Zhao, Y. (2009) *TGFβI* Deficiency Predisposes Mice to Spontaneous Tumor Development. *Cancer Res*. **69**, 37–44

Zhang, Y.S., He, L., Liu, B., Li, N.S., Luo, X.J., Hu, C.P., Ma, Q.L., Zhang, G.G., Li, Y.J. and Peng, J. (2012) A novel pathway of NADPH oxidase/vascular peroxidase 1 in mediating oxidative injury following ischemia-reperfusion. *Basic Res. Cardiol*. **107**, 1–19

Zucker, S.N., Fink, E.E., Bagati, A., Mannava, S., Bianchi-Smiraglia, A., Bogner, P.N., Wawrzyniak, J.A., Foley, C., Leonova, K.I., Grimm, M.J., Moparthy, K., Ionov, Y., Wang, J., Liu, S., Sexton, S., Kandel, E.S., Bakin, A.V., Zhang, Y., Kaminski, N., Segal, B.H. and Nikiforov, M.A. (2014) Nrf2 amplifies oxidative stress via induction of Klf9. *Mol. Cell*. **53**, 916–928

Appendix A

Table A1: Buffer and solution recipes required for experiments.

Buffer/ solution	Recipe
1X PBS	137 mM NaCl, 2.7 mM KCl, 8.1 mM Na_2HPO_4•$12H_2O$, 1.8 mM KH_2PO_4, pH 7.2, autoclaved
Trypan Blue	0.2% (w/v) Trypan blue in 1X PBS, filter sterilised
1X RIPA buffer	50 mM Tris-HCl pH 8.0, 150 mM NaCl, 0.1% (w/v) SDS, 1% (v/v) Triton X-100, 0.5% (w/v) sodium deoxycholate, 1 mM PMSF, 10 μM leupeptin
Native lysis buffer	25 mM Tris-HCl pH 8.0, 75 mM NaCl, 0.5% (v/v) Triton X-100, 1 mM PMSF, 10 μM leupeptin
5X Bradford reagent	117 μM Coomassie Brilliant Blue G-250, 4.75% (v/v) 95% (v/v) methanol, 8.5% (v/v) 85% (v/v) phosphoric acid, filtered with grade 1 Whatman™ filter paper
Coomassie blue dye	3 mM Coomassie Brilliant Blue G-250, 50% (v/v) methanol, 10% (v/v) glacial acetic acid
Destain solution	12% (v/v) Glacial acetic acid, 10% (v/v) methanol
Elution buffer	66% (v/v) Methanol, 1% (v/v) 25% (v/v) ammonia
4X protein loading buffer	240 mM Tris-HCl pH 6.8, 8% (w/v) SDS, 0.04% (w/v) bromophenol blue, 5% (v/v) β-mercaptoethanol, 40% (v/v) glycerol
SDS-PAGE Running Buffer	3.5 mM SDS, 192 mM glycine, 25 mM Tris, pH 8.8
Transfer buffer	192 mM Glycine, 25 mM Tris, 20% (v/v) methanol, pH 8.3
1X TBS/T	20 mM Tris-HCl pH 7.6, 137 mM NaCl, 0.1% (v/v) Tween-20
Blocking buffer	5% (w/v) Fat-free milk, 1X TBS/T
Developer	6.4 M Metol, 0.6 M sodium sulphite, 80 mM hydroquinone, 45 mM sodium carbonate, 34 mM potassium bromide
Fixer	0.8 M Sodium thiosulphate, 0.2 M sodium metasulphite
1X TAE	40 mM Tris-HCl pH 8, 0.11% (v/v) glacial acetic acid, 1 mM EDTA pH 8.0
6X DNA loading dye	30% (v/v) Glycerol, 3.7 mM bromophenol blue
IP buffer	20 mM Tris-HCl pH 8.0, 150 mM NaCl, 0.5% (v/v) Triton X-100, 1 mM PMSF, 10 μM leupeptin
ChIP IP buffer	20 mM Tris-HCl pH 8.0, 2 mM EDTA pH 8.0, 150 mM NaCl, 1% (v/v) Triton X-100, 1 mM PMSF, 10 μM leupeptin
ChIP wash buffer	20 mM Tris-HCl pH 8.0, 2 mM EDTA pH 8.0, 150 mM NaCl, 1% (v/v) Triton X-100, 0.1% (v/v) SDS
ChIP final wash buffer	20 mM Tris-HCl pH 8.0, 2 mM EDTA pH 8.0, 500 mM NaCl, 1% (v/v) Triton X-100, 0.1% (v/v) SDS
ChIP elution buffer	1% (v/v) SDS, 100 mM $NaHCO_3$
SOC broth	2% (w/v) LB broth, 10 mM $MgCl_2$
Solution A	25 mM Tris-HCl, 10 mM EDTA, pH 8.0
Solution B	0.4 M NaOH, 2% (v/v) SDS
Crystal violet	0.2% (w/v) Crystal violet powder, 20% (v/v) ethanol
2X cell culture medium	1.5% (w/v) DMEM and 0.5% (w/v) F12 (3:1), 0.4% (w/v) $NaHCO_3$, 10% (v/v) FBS, 0.1% (v/v) penicillin/streptomycin, filter sterilised

Buffer recipes requiring protease inhibitors had phenylmethanesulfonyl fluoride (PMSF) and leupeptin added just before use.

Table A2: Forward and reverse primer sequences and thermocycling conditions for all PCR experiments.

Primer	Forward primer (5' to 3')	Reverse primer (5' to 3')	PCR Thermocycling conditions (T, t, C)				
			Initiation	Denaturation	Annealing	Extension	Finalisation
GAPDH^{mRNA}	CAAGGTCATCCATGACAACTTTG	GTCCACCACCCTGTTGCTGTAG	95, 120, 1	95, 30, 30	53, 30, 30	72, 45, 30	72, 120, 1
PXDN^{mRNA}	TATTGAGGGCCAGACCGTGGATTT	ATCATTTGGAGAACGAGGACGGCT	95, 120, 1	95, 30, 35	59, 30, 35	72, 50, 35	72, 120, 1
PXDN^{Nt2+}	GTTTGCGACGGGAACACGCC	AAAGCCCCTCATTCCTTTTGAGGA	95, 180, 1	98, 20, 40	61, 15, 40	72, 50, 40	72, 300, 1
PXDN^{Nt2-}	CAGACTCCCTTGCTGTGCGCTTTG	AGCTGTGCACATGCGCGAGGCT	95, 180, 1	98, 20, 35	59, 15, 35	72, 50, 35	72, 300, 1
*NQO1^{Nt2+}	CCCTTTTAGCCTTGGCACGAAA	TGCACCCAGGGAAGTGTGTTGTAT	95, 180, 1	98, 20, 35	57, 15, 35	72, 30, 35	72, 300, 1
*NQO1^{Nt2-}	TAAAAAGTAGAGTGGTTGGAGTGATGACG	TCTCAGTTTTTGCCCTTATTTAATCCC	95, 180, 1	98, 20, 35	57, 15, 35	72, 30, 35	72, 300, 1
PXDN^{Full}	TTCTGTGTTGTACTCTCATTCTCT	ATAGATATCAGCTGTGCACATGCGCCGAGGCT	95, 180, 1	98, 20, 30	61, 15, 30	72, 80, 30	72, 300, 1
REPXDN^{Nt2+}	ATAGCTAGCGTTTGCGACGGGAACACGCC	AAAGATATCAAAGCCCCTCATTCCTTTTGAGGA	95, 180, 1	98, 20, 40	61, 15, 40	72, 50, 40	72, 300, 1
REPXDN^{Nt2-}	ATAGCTAGCCAGACTCCCTTGCTGTGCGCTTT	ATAGATATCAGCTGTGCACATGCGCCGAGGCT	95, 180, 1	98, 20, 40	61, 15, 40	72, 50, 40	72, 300, 1
RENQO1^{Nt2+}	ATAGCTAGCCCCTTTTAGCCTTGGCACGAAA	ATTGATATCTGCACCCAGGGAAGTGTGTTGT	95, 180, 1	98, 20, 35	60, 15, 35	72, 30, 35	72, 300, 1
RENQO1^{Nt2-}	AATGCTAGCTAAAAAGTAGAGTGGTTGGAGT	ATTGATATCTCTCAGTTTTTGCCCTTATTTA	95, 180, 1	98, 20, 35	60, 15, 35	72, 30, 35	72, 300, 1
RENQO1^{WNt2+}	AAAGCTAGCCAAGTGCAGAATCTGAATCTTGC	ATTGATATCTTTGTTTCTTCCTTTGCAAGATTCA	95, 180, 1	98, 20, 35	60, 15, 35	72, 15, 35	72, 300, 1
REPXDN^{WNt2+}	ATAGCTAGCCCATGCTGTGCCTCTGAATCTGGC	ATAGATATCCAGGGTGACGGTGCCAGATTCA	95, 180, 1	98, 20, 35	62, 15, 35	72, 15, 35	72, 300, 1
RENQO1^{MtNt2+}	AAAGCTAGCCAAGTGCAGAATCCTGATCTCAC	ATTGATATCTTTGTTTCTTCCTTTGTGAGATCAG	95, 180, 1	98, 20, 35	60, 15, 35	72, 15, 35	72, 300, 1
REPXDN^{MtNt2+}	ATAGCTAGCCCCATGCTGTGCCTCGATATCTAGC	ATAGATATCCAGGGTGACGGTGCTAGATATC	95, 180, 1	98, 20, 35	62, 15, 35	72, 15, 35	72, 300, 1
REPXDN^{M2Nt2+}	ATAGCTAGCCCATGCTGTGCCTCCAGATCTAGC	ATAGATATCCAGGGTGACGGTGCTAGATCTG	95, 180, 1	98, 20, 35	62, 15, 35	72, 15, 35	72, 300, 1
pGL4.10	CTAGCAAAATAGGCTGTCCC	TTCATGGCTTTGTGCAGCT	95, 120, 1	95, 30, 30	60, 30, 30	72, 50-60, 30	72, 120, 1

Underlined regions of primers show restriction enzyme binding sites for NheI (forward primers) and EcoRV (reverse primers). *Primer sequences from Chorley *et al*. (2012). For thermocycling conditions: T is the temperature (°C), t is time (s) and C is the number of cycles.

Appendix B

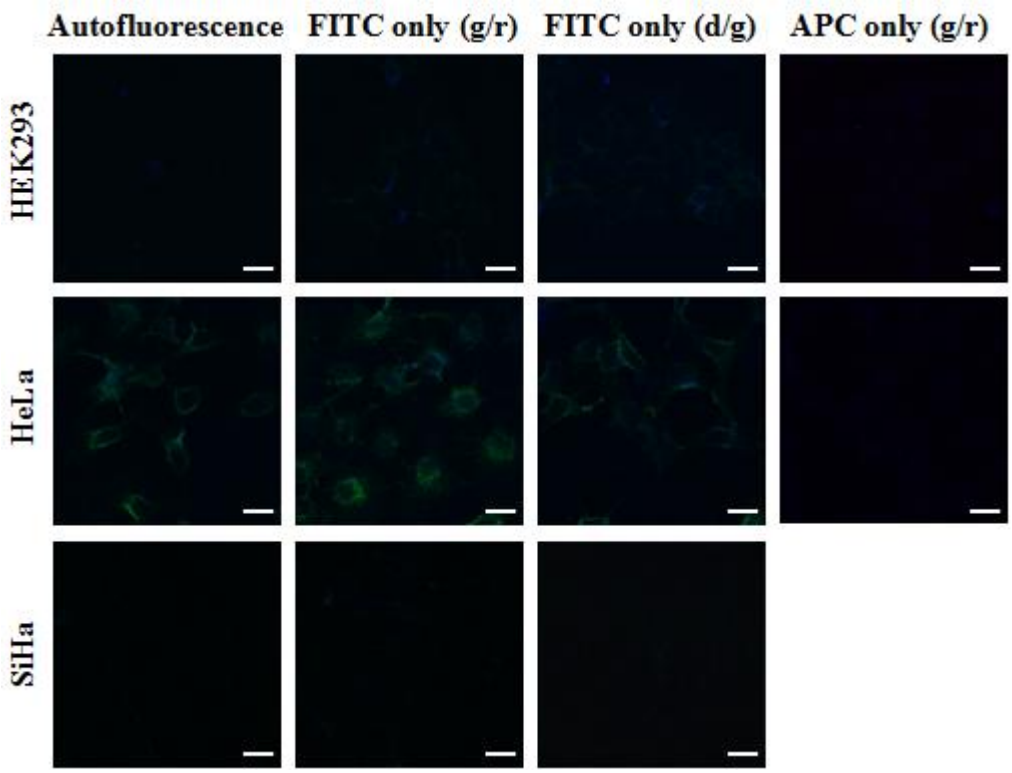

Figure B1: Autofluorescence and secondary antibody only controls for IF microscopy. Autofluorescence and secondary antibody only controls for IF confocal microscopy were performed on HEK293, HeLa and SiHa cells. Secondary antibodies included: FITC goat anti-rabbit (g/r), FITC donkey anti-goat (d/g) and APC goat anti-rabbit (g/r). Minimal fluorescence was detected in all of the above controls (63X magnification; scale bar = 20 μm).

Table B1: Pearson correlation coefficients for Nrf2 colocalisation with DAPI-stained nuclei in Figures 2.2 and 2.3.

	Treatment		
Cell line	**Unt**	**3 h H_2O_2**	**18 h H_2O_2**
HEK293	0.72 ± 0.01	0.83 ± 0.01; *P*<0.0001	0.87 ± 0.01; *P*<0.0001
HeLa	0.72 ± 0.02	0.85 ± 0.01; *P*<0.0001	0.88 ± 0.02; *P*<0.0001

Cells were treated with 100 μM H_2O_2 and IF microscopy performed. Coefficients were determined using Image-Pro (Ver. 10.0) software (n = 6 independent cells; mean ± SD).

Table B2: Pearson correlation coefficients for Nrf2 colocalisation with DAPI-stained nuclei in Figures 2.5 and 2.6.

	Treatment		
Cell line	**Unt**	**24 h SFN**	**24 h tBHQ**
HEK293	0.74 ± 0.02	0.88 ± 0.01; *P*<0.0001	0.85 ± 0.02; *P*<0.0001
HeLa	0.76 ± 0.02	0.87 ± 0.01; *P*<0.0001	0.88 ± 0.02; *P*<0.0001

Cells were treated with 5 μM SFN or 40 μM tBHQ and IF microscopy performed. Coefficients were determined using Image-Pro (Ver. 10.0) software (n = 6 independent cells; mean ± SD).

Table B3: Pearson correlation coefficients for Nrf2 colocalisation with DAPI-stained nuclei in Figure 2.8.

		Treatment	
Cell line	**Protein**	**Control**	**+Nrf2**
HEK293	NQO1	0.41 ± 0.01	0.71 ± 0.01; *P*<0.0001
	PXDN	0.38 ± 0.02	0.67 ± 0.02; *P*<0.0001
HeLa	NQO1	0.32 ± 0.01	0.61 ± 0.01; *P*<0.0001
	PXDN	0.34 ± 0.02	0.67 ± 0.01; *P*<0.0001

Cells were treated with transfection reagent only (control) or transfected with the pcDNA3-EGFP-C4-Nrf2 over-expression vector (+Nrf2) for 24 h and IF microscopy performed. Coefficients were determined using Image-Pro (Ver. 10.0) software (n = 6 independent cells; mean ± SD).

Table B4: Pearson correlation coefficients for Snai1 colocalisation with DAPI-stained nuclei in Figure 3.6.

	Treatment		
Cell line	**Unt**	**24 h H_2O_2**	**24 h TGF-β1**
HeLa	0.79 ± 0.03	0.71 ± 0.01; *P*=0.002	0.86 ± 0.01; *P*=0.0008
SiHa	0.63 ± 0.02	0.55 ± 0.03; *P*=0.0009	0.71 ± 0.01; *P*=0.0001

Cells were treated with 100 μM H_2O_2 or 5 ng/ml TGF-β1 and IF microscopy performed. Coefficients were determined using Image-Pro (Ver. 10.0) software (n = 6 independent cells; mean ± SD).